Experimental and Modelling of Emulsified Oil Adsorption Using Functionalized Magnetic Nanoparticles

By

©Hamideh Hamedi

A thesis submitted to the school of Graduate Studies in partial fulfilment of the requirement for the degree of

Doctor of Philosophy

Faculty of Engineering & Applied Science

Memorial University of Newfoundland

February 2024

St. John's, Newfoundland and Labrador

Canada

ABSTRACT

Conventional oil-water separation techniques have limited effectiveness in separating emulsified oil separation from wastewater due to the high stability of oil-in-water (o/w) emulsions. Magnetic nanoparticles (MNPs) application for emulsified oil separation from wastewater is becoming more popular, despite their inherent instability due to their high chemical activity. Thereby, their tendency to agglomerate, precipitate, and oxidize by air, results in decreasing magnetism and dispersibility. Stabilization of MNPs is needed by generating a protective coating layer on their surfaces to prevent their agglomeration and enable MNPs to disperse properly in the aqueous content through changing their functionality. Functionalizing MNPs using amphiphilic compounds, featuring both hydrophilic and oleophilic properties, improves their dispersivity, which is required for an efficient demulsification.

This research aims to study demulsification performance of functionalized MNPs using surfactants, as amphiphilic compounds, for capturing emulsified oil droplets from nanoemulsions. To this end, different sizes of Fe_3O_4 nanoparticles are functionalized using sodium dodecyl sulfate (SDS) as an anionic surfactant, and cetyltrimethylammonium bromide (CTAB) as a cationic surfactant. The functionalized particles are characterized using Transmission Electron Microscopy (TEM), Scanning Electron Microscopy (SEM), Energy Dispersive X-ray (EDX), contact angle (CA), hydrodynamic diameter, and zeta potential measurement. We study the effect of size and concentration of MNPs, coating materials, and surfactant to MNPs mass ratio on demulsification performance to find the optimum MNP feature with the highest oil separation efficiency (SE), which is measured via Gas Chromatography equipped with Flame Ionization Detector (GC-FID) analysis. The demulsification performance of the functionalized MNPs is tested for oil adsorption from 1000 ppm dodecane-in-water nanoemulsion, containing ultra-small droplets (almost 300

nm). The oil-water separation results reveal the superior performance of 0.5 g/l smaller size CTAB-coated particles (MNP-S@CTAB) with lower CTAB to MNP mass ratio of 0.4 (SE = 99.80%), compared to the bare MNPs, and MNP-S@SDS that achieve SE around 57.46% and 86.1%, respectively. This high SE is attributed to (i) the more positive surface charge density on CTAB-coated particles compared to bare and SDS-coated ones, which is verified through zeta potential measurements; (ii) more hydrophilicity of the CTAB-coated MNPs (compared to SDS-coated ones) as evidenced by the WCA analysis; and (iii) less aggregation of MNP@CTAB in the aqueous phase as illustrated in the SEM and TEM images. Moreover, better performance of smaller functionalized particles compared to the larger ones is attributed to their higher surface energy and charge density. The reusability test indicates an excellent cycling stability of MNP-S@CTAB after ten cycles.

In the modelling phase of the research, to obtain a better understanding of the oil capturing behavior and the rate of adsorption, systematic investigations about isotherm and kinetic models are conducted. To this end, we employ three adsorption isotherms, including Langmuir, Freundlich, Temkin, and three kinetic models, including pseudo-first-order (PFO), pseudo-second-order (PSO), and intra-particle diffusion (IPD). The oil adsorption equilibrium data is estimated by oil adsorption capacity measurements using GC-FID. It is found that the Freundlich isotherm and PFO kinetic models are the best fit to the experimental equilibrium data, verifying a multilayer heterogeneous physical adsorption of oil onto MNPs. Moreover, optimization of the oil adsorption process using the functionalized MNPs is investigated to achieve a higher oil adsorption capacity. To this end, smart models based on artificial intelligence (AI) strategies such as least squares support vector machines (LSSVM) hybridized with the coupled simulated annealing (CSA) algorithm, adaptive network-based fuzzy inference system (ANFIS), and gene expression

programming (GEP) are applied to assess the non-linear relationships of effective input and output variables. Oil adsorption capacity is considered as the target variable, and the oil concentration, mixing time, and MNP dosage are selected as the input variables. After conducting experiments, 149 data points are obtained, divided into two parts; 80% for the training process and the remaining 20% for the testing step of modelling. Detailed smart model evaluation and error analysis indicate that the LSSVM-CSA model predicts better than ANFIS and GEP in terms of accuracy, with the highest R^2 of 0.9921 and a very small MAPE of 3.7597% based on the entire dataset. Moreover, the relative importance analysis using Pearson's and Spearman's correlation coefficients shows that the oil concentration and MNP dosage are the most influential variables in oil adsorption capacity predictions with direct and indirect relationships, respectively.

ACKNOWLEDGEMENTS

I would like to express my sincere gratitude to my supervisor, Dr. Sohrab Zendehboudi for his unconditional support, valuable advice, guidance, and encouragement throughout my PhD journey. His expertise and insightful feedback have played a pivotal role in shaping this thesis. I would also like to extend my appreciation to my co-supervisor, Dr. Nima Rezaei for his valuable contribution, mentorship, and collaborative efforts. I am truly fortunate to have had the opportunity to work under the supervision of them. Their dedication, patience, and unwavering belief in my abilities have inspired and motivated me to overcome challenges and strive for excellence.

I would like to acknowledge my supportive dissertation committee members, Dr. Helen Zhang, and Dr. Noori Saady for their valuable comments and suggestions have shaped the final appearance of this work. Special thanks to Dr. Helen Zhang and Dr. Christina Bottaro for their generously permission to use their laboratory facilities during certain stages of my experiments. Their kind support has greatly contributed to the successful completion of my research.

I am extremely grateful to Memorial University (NL, Canada), the Natural Science and Engineering Research Council of Canada (NSERC), Suncor Energy, and Terra Nova Young Innovator Award for their financial support.

Most importantly, I would like to express my heartfelt appreciation to my parents for their love, faithful support, and constant inspiration in all my endeavors. And most of all for my beloved husband and my adorable baby, Soren. Your presence has reminded me of the legacy I want to create for our family and the importance of pursuing my passion. This achievement would not have been possible without you both by my side.

Table of Content

LIST OF TABLES

LIST OF FIGURES

1. CHAPTER ONE

Introduction and Overview

1.1. Background and Research Gap

Oily wastewater is commonly generated in various industrial processes, including textile, food, leather, oil and gas production, metal processing, petrochemical, and mining industries. Additionally, frequent oil spill incidents can occur during oil extraction, production, refining, and transportation processes [1]. Proper management of oily wastewater is essential to protect environment, maintain water quality, ensure sustainable water resource management, and facilitate oil recovery. Oily wastewater can be categorized based on the size of oil droplets into free oil (>150 μ), dispersed oil (20–150 μ), and emulsified oil (<20 μ) [2]. Each category requires specific treatment methods for effective removal and remediation of the oily wastewater. Separating emulsified oil contamination is the most challenging one due to the inherent emulsion stability resulted from oil droplets with small size [3].

There are some practical and technical challenges in oily wastewater treatment that need to be considered. The different composition of oily wastewater, including various oil types and concentrations, complicates the design of effective treatment strategies. Additionally, the large volumes of wastewater generated by industries such as petroleum refining, mining, and manufacturing pose challenges in terms of capacity and efficiency of treatment systems [4]. Regulatory standards for wastewater discharge are becoming stricter, requiring industries to invest in advanced treatment technologies to meet compliance. More importantly, after separation, the recovered oil and solid residual need to be managed and disposed, which can be expensive and environmentally challenging [5]. Conventional techniques for separating oil and water such as using dispersants, skimmers, floatation, and coagulation have some challenges, including long separation time, large space, high energy consumption, complex recycling process, and the potential for generating secondary contaminants [6]. These techniques are particularly less

effective for treatment of wastewater streams with dispersed and emulsified oil phases. Addressing these challenges requires innovative solutions to efficiently remove oil from emulsified oily wastewater and balance efficiency, sustainability, and regulatory compliance. Advanced separation techniques such as centrifuges and membrane filtration have shown promise in breaking emulsions and enhancing separation efficiency. Chemical treatments, biological methods, and adsorption techniques offer diverse solutions/mechanisms to tackle different types of contaminants [7].

Continued research and development will likely lead to more efficient and sustainable separation methods, reducing energy consumption and increasing separation efficiency. Integration of smart monitoring and sensors will enable real-time process optimization. Moreover, the concept of the circular economy will drive innovations in recovering valuable resources from oily wastewater, aligning with environmental and economic goals. As regulations evolve, industries will need to adopt more advanced treatment methods to ensure both compliance and environmental responsibility [5].

Effective demulsification relies on enhancing the rates of flocculation and coalescence to disrupt the interfacial forces between the oil and water phases, allowing for the separation and recovery of the individual components [8]. To this end, several demulsification techniques have been developed, including heat treatment, electrical methods, chemical additives, and mechanical processes. The chemical demulsification has been conventionally used for oil capturing from oily wastewater streams. Some of the chemical demulsifiers contain hazardous or toxic substances that can pose risks to the environment and human health [9]. In this respect, developing non-toxic and cost-effective demulsifiers to successfully capture oil from emulsified oily wastewater is required [10]. Recently, applying magnetic nanoparticles (MNPs) has attracted great interest as a nano

adsorbent for oil capturing based on magnetic removal mechanisms [11, 12]. Iron oxide (Fe_3O_4) is a common MNPs with promising demulsification performance due to their superparamagnetic properties, low toxicity, high adsorption capacity, and recyclability [13, 14]. However, their application is limited due to their intrinsic instability and agglomeration resulting from their high chemical activity. Therefore, the stabilization of MNPs through surface modification is crucial to enhance their capability in oil adsorption applications and address the challenges associated with their chemical reactivity [14].

In this regard, using organic and inorganic materials to form a protecting layer on the surface of MNPs has been of great interest for researchers to improve particle stability and dispersivity in continuous phase of emulsion, leading to a higher oil removal effectiveness [15, 16]. Based on the literature, amphiphilic compounds due to featuring both hydrophilic and hydrophobic characteristics at the same time can enhance oil adsorption capacity through providing better dispersivity of particles in the aqueous phase of emulsion, which is crucial for demulsification [17]. For instance, Xu et al. [18] developed an amphiphilic magnetically responsive demulsifier using diatomite, which effectively removed oil from oil-in-water emulsions. The incorporation of grafted Fe_3O_4 particles resulted in improved demulsification performance. In another study, hydrophilic/oleophilic magnetic Janus particles were developed by Song et al. [19] for stabilizing emulsions. They demonstrated the efficiency of these amphiphilic particles in removing oil from o/w emulsions owing to their high interfacial activity, facilitating rapid adsorption onto the oil-water interface.

Prior research studies have used MNPs to separate oil droplets from water when the oil droplets are of micrometer size range. In this study, we aim to demulsify O/W using functionalized MNPs for oil droplets of nanometer size that are more stable in the continuous phase. We also study the

effect of MNPs size on demulsification that is found controversial in the literature [28] by considering two different sizes of Fe_3O_4 nanoparticles and also mass ratios of coating-to-MNPs. Moreover, to the best of our knowledge, no study investigated the optimization of emulsified oil adsorption process using MNPs. To this end, we employ three advanced machine learning approaches, to optimize the emulsified oil adsorption using functionalized MNPs.

This product holds significant potential for diverse industries facing oil-water separation challenges, including offshore operations, food industries, and restaurants, as it efficiently captures fat, oil, and grease. Nevertheless, further research is required to explore the feasibility of implementing these particles on a large scale.

1.2. Research Objectives and Approach

The main contributions/phases of this research thesis are given below:

Experimental Phase:

- Most of studies in the literature on demulsification with MNPs deal with separating micrometer oil droplets from the water, while in this research, we aim to demulsify nanoemulsion which is more challenging due to more stability of nanometer oil droplets in the emulsion systems.
- Demulsification performance of functionalized MNPs using both cationic and anionic surfactants, as amphiphilic compounds, is assessed to achieve a better understanding of oil adsorption mechanisms in terms of electrostatic interaction between oil droplets and functionalized MNPs.
- The effect of size of MNPs on their demulsification performance is investigated which is controversial in the previous studies. Therefore, different sizes of Fe_3O_4 nanoparticles are coated using sodium dodecyl sulfate (SDS) as an anionic surfactant, and

cetyltrimethylammonium bromide (CTAB) as a cationic surfactant with different mass ratios of surfactant-to-MNPs (e.g., 0.4 and 0.8). The optimum MNPs features such as size, coating chemistry, and surfactant-to-MNPs mass ratio are achievable by comparing the results of oil separation efficiency for various scenarios via gas chromatography equipped with flame ionization detector (GC-FID).

Modelling Phase:

- Adsorption isotherm aspect is investigated using three adsorption isotherms, including Langmuir, Freundlich, and Temkin to assess oil adsorption mechanisms, and interactions between oil molecules as the adsorbate and MNP as the adsorbent.
- For kinetic modelling study, we employ pseudo-first-order (PFO), pseudo-second-order (PSO), and intra-particle diffusion (IPD) to determine the rate of adsorption over time by measuring oil adsorption capacity at specific time interval.
- Oil adsorption process using MNPs is affected by various factors such as MNPs size and concentration, type and concentration of oil, contact time, and operational conditions. Thus, optimization of the process is required to achieve higher oil adsorption capacity. To the best of our knowledge, no previous studies have investigated the optimization of emulsified oil adsorption onto MNPs using machine-learning approach, yet. To this end, three advanced smart tools based on artificial intelligence (AI) approaches, including adaptive network-based fuzzy inference system (ANFIS), least square support vector machine (LSSVM), and gene expression programming (GEP) are applied. The performance of these models is examined and compared based on statistical criteria such as coefficient of determination (R^2), mean percentage error (MPE), and mean absolute percentage error (MAPE) to introduce the most reliable and precise model. A systematic

sensitivity analysis is performed to assess the relative importance of input variables affecting the oil adsorption capacity as the target using the most accurate model.

1.3. Thesis Structure

This thesis consists of six chapters as follows:

Chapter One presents an overview and contributions of the study and provides the structure of the thesis.

Chapter Two has been published in the Journal of Cleaner Production. The manuscript provides a comprehensive literature review on the demulsification using functionalized magnetic nanoparticles (MNPs) where various processes such as emulsion stability and demulsification techniques are discussed. This review consists of recent advancements in the development and application of functionalized MNPs for demulsification, considering both oil-in-water and water-in-oil emulsions.

Chapter Three has been published in the Langmuir Journal, ACS publications. Demulsification performance of both sizes of functionalized MNPs using SDS and CTAB is investigated to find the optimum MNP features (e.g., size, dosage, coating type and concentration), achieving the highest separation efficiency. The results of oil separation from o/w nanoemulsion are analyzed via GC-FID.

Chapter Four focuses on the adsorption isotherm and kinetic aspects of emulsified oil adsorption onto functionalized MNPs, which has been published in the journal of Energies. This manuscript is going to provide a better understanding of the adsorption process behavior and interaction between the adsorbate and adsorbent.

Chapter Five is optimization of oil adsorption capacity on functionalized MNPs using machine learning approach, which has been published in the Molecular Liquid journal. In this phase of our

research, we introduce smart connectionist models to predict oil adsorption capacity as our target by assessing non-linear relationships of the effective variables.

Chapter Six contains a summary, conclusions, and recommendations for future work.

References

[1] Ali N, Zaman H, Bilal M, Shah A-u-HA, Nazir MS, Iqbal HMN. Environmental perspectives of interfacially active and magnetically recoverable composite materials – A review. Sci Total Environ. 2019;670:523-38.

[2] Faisal W, Almomani F. A critical review of the development and demulsification processes applied for oil recovery from oil in water emulsions. Chemosphere. 2022;291:133099.

[3] Issaka S, Nour A, Yunus RbM. Review on the Fundamental Aspects of Petroleum Oil Emulsions and Techniques of Demulsification. Journal of Petroleum & Environmental Biotechnology. 2015;6:1-15.

[4] Jamaly S, Giwa A, Hasan SW. Recent improvements in oily wastewater treatment: Progress, challenges, and future opportunities. Journal of Environmental Sciences. 2015;37:15-30.

[5] Abuhasel K, Kchaou M, Alquraish M, Manusamy Y, Yong TJ. Oily Wastewater Treatment: Overview of Conventional and Modern Methods, Challenges, and Future Opportunities. Water. 2021;13:980.

[6] McClements DJ, Jafari SM. Improving emulsion formation, stability and performance using mixed emulsifiers: A review. Adv Colloid Interface Sci. 2018;251:55-79.

[7] Medeiros AD, Silva Junior CJ, Amorim JD, Durval IJ, Costa AF, Sarubbo LA. Oily Wastewater Treatment: Methods, Challenges, and Trends. Processes2022.

[8] Goodarzi F, Zendehboudi S. A Comprehensive Review on Emulsions and Emulsion Stability in Chemical and Energy Industries. The Canadian Journal of Chemical Engineering. 2019;97:281-309.

[9] Hamedi H, Rezaei N, Zendehboudi S. A comprehensive review on demulsification using functionalized magnetic nanoparticles. Journal of Cleaner Production. 2022;380:134868.

[10] Mohammed L, Gomaa HG, Ragab D, Zhu J. Magnetic nanoparticles for environmental and biomedical applications: A review. Particuology. 2017;30:1-14.

[11] Su C. Environmental implications and applications of engineered nanoscale magnetite and its hybrid nanocomposites: A review of recent literature. J Hazard Mater. 2017;322:48-84.

[12] Zhou K, Zhou X, Liu J, Huang Z. Application of magnetic nanoparticles in petroleum industry: A review. Journal of Petroleum Science and Engineering. 2020;188:106943.

[13] Simonsen G, Strand M, Øye G. Potential applications of magnetic nanoparticles within separation in the petroleum industry. Journal of Petroleum Science and Engineering. 2018;165:488-95.

[14] Qiao K, Tian W, Bai J, Wang L, Zhao J, Du Z, et al. Application of magnetic adsorbents based on iron oxide nanoparticles for oil spill remediation: A review. Journal of the Taiwan Institute of Chemical Engineers. 2019;97:227-36.

[15] Abdullah MMS, Al-Lohedan HA. Fabrication of Environmental-Friendly Magnetite Nanoparticle Surface Coatings for the Efficient Collection of Oil Spill. Nanomaterials (Basel, Switzerland). 2021;11.

[16] Kharissova OV, Dias HVR, Kharisov BI. Magnetic adsorbents based on micro- and nano-structured materials. RSC Advances. 2015;5:6695-719.

[17] Elmobarak WF, Almomani F. Functionalization of silica-coated magnetic nanoparticles as powerful demulsifier to recover oil from oil-in-water emulsion. Chemosphere. 2021;279:130360.

[18] Xu H, Wang J, Ren S. Removal of Oil from a Crude Oil-in-Water Emulsion by a Magnetically Recyclable Diatomite Demulsifier. Energy & Fuels. 2019;33:11574-83.

[19] Song Y, Zhou J, Fan J-B, Zhai W, Meng J, Wang S. Hydrophilic/Oleophilic Magnetic Janus Particles for the Rapid and Efficient Oil–Water Separation. Adv Funct Mater. 2018;28:1802493.

2. CHAPTER TWO

Literature Review: A Comprehensive Review on Demulsification Using Functionalized Magnetic Nanoparticles

Preface

A version of this chapter has been published in the Journal of Cleaner Production, 380 (2022) 134868. As the primary author of this paper, I conducted most of the literature, data collection and the comparison of demulsification performance of different functionalized magnetic nanoparticles. I drafted the first version of the manuscript and subsequently made revisions based on the feedback from my co-authors, Nima Rezaei and Sohrab Zendehboudi as well as the comments received from the peer review process. The co-authors contributed through providing the manuscript's outlines, comments on different sections of the paper, and technical critiques and insights on earlier studies in the relevant field. They also assisted with reviewing and revising the manuscript.

2.1. Introduction

Conventional oil-water separation methods, using dispersants, skimmers, floatation, and coagulation have limitations such as low selectivity, high energy consumption, long separation time, large land requirements, complicated recycling, and secondary contaminant production (Deng et al., 2013). These methods are even less efficient in separating fine emulsions. Researchers have used surfaces with tailored wettability to increase the selectivity and efficiency of oil-water separation (Rasouli et al., 2021a, b; Zhang et al., 2013); however, their effectiveness in emulsion systems is challenged by the emulsified droplet size and the emulsion stability. A successful demulsification requires increased flocculation and coalescence rates that can be achieved by increasing temperature or oil-water interfacial tension (IFT), decreasing viscosity, and neutralizing the electric charge on the dispersed droplets. Therefore, several demulsification techniques have been developed based on these treatment methods, including chemical, thermal, microwave, and electrical treatments. In the literature, the chemical demulsification has been conventionally used, which is economically viable.

Along recent advances in smart oil-absorbing materials with engineered wettability and morphology and ease of recycling, the use of iron oxide based magnetic nanoparticles (MNPs) has attracted a great interest for demulsification application. The first attempt in adsorbing oil contaminants using magnetic removal mechanism was made by Turbeville (Turbeville, 1973). Magnetic responsiveness of the MNPs allows them to be manipulated in a switchable magnetic field. The MNPs also feature high oil adsorption capacity, reusability, easy separation and recovery, dispersivity without settling, non-toxicity, and low degradability without producing secondary pollutants (Simonsen et al., 2018). However, pristine iron oxide MNPs have a high chemical activity with a limited long-time stability and are susceptible to oxidation by air that

causes loss of magnetism and dispersivity; also, they tend to agglomerate, resulting in settling. Therefore, developing protective and functional layers on the surface of MNPs is suggested to improve their demulsification effectiveness (Qiao et al., 2019). In the literature, different stabilization and functionalization approaches are used, including core-shell, matrix-dispersed, Janus, shell-core-shell, and dendritic (Zhou et al., 2020). The core shell materials can add features such as pH responsiveness to alter the interfacial activities for improved demulsification (Wang, X. et al., 2015). The main challenge in stabilization of the MNPs is limitations in chemical, thermal, and mechanical stability of the coating material. For example, polymers have good chemical resistance but are unstable at higher temperatures; silica based coatings have excellent temperature resistance but are reactive under alkali condition; carbon-based coatings have high chemical and thermal stability, but have limited dispersivity in the aqueous phase (Lü et al., 2017). MNPs with dendritic hierarchical structures have shown to have a higher demulsification efficiency because of larger exposed surface area (compared to non-dendritic MNPs); however, they are more challenging to be separated and reused (Wang et al., 2018). Recently, Janus particles have gained great attention due to their amphiphilic properties and high interfacial activity.

Most of studies in the literature on demulsification with MNPs deal with oil-in-water emulsion (o/w) systems. In the systems, the dispersed oil droplets and MNPs interact through electrostatic and hydrophobic interactions (Lü et al., 2018a). Commonly the oil droplets are negatively charged in an o/w system. Therefore, using MNPs with cationic functional groups facilitates the emulsification process (Zhang et al., 2017). Also, because of water being the continuous phase in o/w, the presence of amphiphilic functional groups on MNPs improves their dispersity, which is required for an efficient demulsification. Depending on the amount of emulsified oil and droplet size, researchers have used MNPs with different coatings and dosage range (0.01 g/L to 400 g/L);

high demulsification efficiency (commonly in the range 90% to 99.9%) has been observed for demulsification of o/w. The demulsification process by MNPs was found to be vulnerable to conditions such as surfactant-stabilized emulsions (Shao, 2019), high viscosity emulsions (Ichikawa et al., 2004), and high pH emulsions (Zhao et al., 2019). Under strong alkali conditions, the electrostatic charge on MNPs can alter from positive to negative, causing the MNPs to be repelled from negatively charged oil droplets (in o/w systems); the induced repulsion decreases the o/w demulsification efficiency. A systematic stability and recyclability analysis of the used MNPs is required in future studies to enable assessing the demulsification process by MNPs at a larger scale. Most of the studies that used MNPs for demulsification did not investigate the MNP recyclability. For the remaining investigations, the recyclability was tested from 4 cycles (Xu et al., 2019) to a maximum of 10 cycles (Zhao et al., 2019). A better recyclability is desired for economic viability at a large-scale. Finally, one aspect that requires attention is the effect of MNP size (and size distribution) for a given emulsion size distribution; this is missing from the literature to the best of our knowledge.

Despite significant efforts to review the potential applications of MNPs (Ali et al., 2020; Ali et al., 2019; Campos et al., 2015; Mohammed et al., 2017; Su, 2017), a comprehensive literature review on the performance of functionalized MNPs in demulsification is missing. Here, we review recent research progresses in development and application of functionalized MNPs for demulsification. We cover both the o/w and w/o emulsions. Compared to the previous studies, the main contribution of the current review is to provide a comprehensive analysis of emulsion stability, demulsification methods, and MNPs application for demulsification performance. The main challenges, advantages, and disadvantages of various techniques are discussed. Different structures of functionalized MNPs and their performance in demulsification are covered. In addition, we discuss

challenges and future prospects of MNPs application in demulsification, following a summary and remarks.

2.2. Emulsification and Demulsification Processes

2.2.1. Emulsification

In its simplest form, an emulsion is a colloidal solution of two immiscible liquids, of which one forms spherical droplets as the dispersed phase and the other liquid forms the continuous phase. For a water-oil system, there are simple and multiple emulsion types possible, as shown in Figure 2. 1. The simple emulsion includes water droplets in continuous oil phase (w/o), or oil droplets in continuous water phase (o/w). In this review paper, we will consistently use o/w for oil-in-water emulsions and w/o for water-in-oil-emulsions. Multiple emulsions are obtained by the successive presence of droplets of one phase in another. For example, double emulsions can be categorized to oil in water in oil emulsions (o/w/o) where the continuous phase is the non-dispersed oil phase, and water in oil in water emulsions (w/o/w) where the continuous phase is the non-dispersed water phase (McClements, 2007).

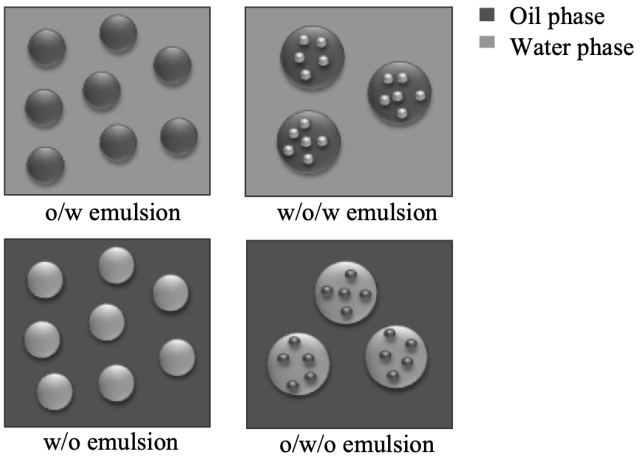

Figure 2. 1. Common types of emulsions in water/oil systems.

2.2.2. Emulsion Characterization and Stability

Stable emulsions resist physiochemical interactions over a long time and challenge separating the emulsified oil contaminations (o/w or w/o). Emulsions are only kinetically stable over a period of time while thermodynamically unstable due to their natural tendency to minimize the interfacial interactions between the two immiscible liquids (McClements and Jafari, 2018).

Figure 2. 2**Error! Reference source not found.** shows different destabilization mechanisms in emulsion systems from density difference between the dispersed and continuous phases, including, gravitational separation (creaming and sedimentation); flocculation; coalescence; and phase separation. Flocculation and coalescence are two major steps contributing significantly to the demulsification. Coalescence is an irreversible process in which the oil droplets colloid, following flocculation that form larger droplets through interfacial film rupture between the two phases (Kokal, 2005). Film drainage and rupture of interfacial films after a droplet collision can merge droplets into a larger droplet.

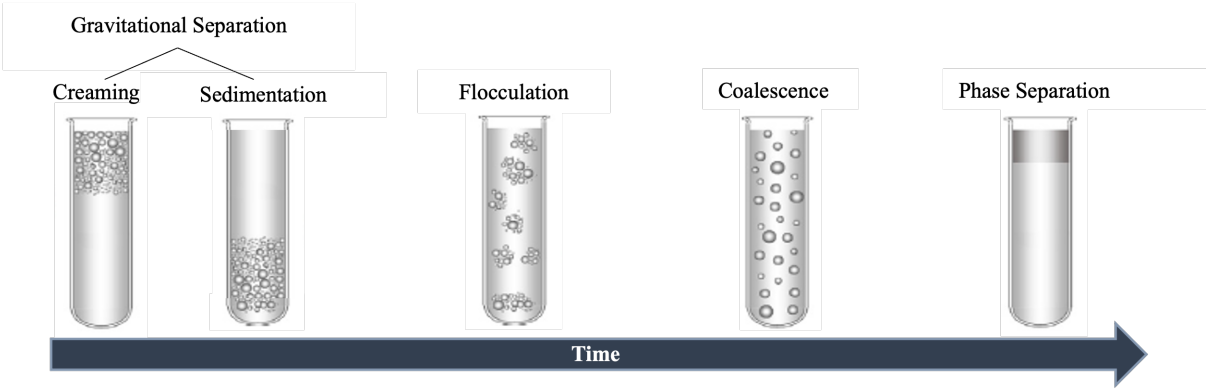

Figure 2. 2. Demulsification mechanism with time. The processes follow chronologically from left to right.

The rate of droplet collisions is one of the influential demulsification parameters, which depends on the dispersed phase concentration and size, and their relative motions compared to the

continuous phase. In the following, we discuss important variables that control emulsion stability and methods to quantify their impact on stability.

Droplet Size. Smaller droplets coalesce less frequently because of smaller interfacial area and less energy exchange. In addition, smaller droplets are more stable due to their internal pressure (Laplace pressure) developing from the oil-water interfacial tension. The droplet size is one of the most important criteria, controlling the emulsion stability (Tadros, 2009).

The size of emulsion droplet can be analyzed with different techniques, including dynamic light scattering (DLS), nuclear magnetic resonance (NMR), ultrasonic spectroscopy, and electrical pulse counting. These techniques differ considerably based on their underlying physical principles. The DLS is based on the fluctuations in the light scattering caused by droplets over time as the droplets move due to Brownian motion. The NMR technique is based on signal attenuation, resulting from the droplets' random movements when the sample is imposed to two magnetic fields (Goodarzi and Zendehboudi, 2019). The ultrasonic spectroscopy is based on ultrasonic attenuation, which is suitable for online analysis of optically opaque emulsions. The electric pulse counting method measures the electrical conductivity changes after emulsion sample is filled between two electrodes (McClements and Jafari, 2018). Table 2. 1 screens each technique for analyzing emulsion samples.

Table 2. 1. The criteria of different particle sizing instruments (McClements, 2007).

Technique	Droplet Size	Droplet Concentration (wt%)	Sample Transparency
DLS	3 nm – 5 μm	0.001 – 10	Transparent
NMR	200 nm – 100μm	1 – 80	Opaque to dark
Ultrasonic Spectroscopy	10 nm – 1000μm	1 – 50	Opaque
Electrical Pulse Counting	0.4 μm – 1200μm	< 0.1	Transparent

Zeta Potential. Generally, the oil droplets are negatively charged. One of the limiting factors in coalesce is to overcome the electrical double layer barrier around each droplet. As illustrated in Figure 2. 3, the electrical double layer contains a first rigid layer of the positive charge (immobile stern layer) and a second layer of positive and negative charges surrounding the stern layer (mobile diffuse layer). The boundary domain around the diffuse layer is called slipping plane. The strength of this double layer is called zeta potential, which is a qualitative measure of the emulsion stability as shown in Table 2. 2 (Stachurski and Michálek, 1996). The magnitude of zeta potential shows the degree of electrostatic repulsion between adjacent droplets. Lower zeta potential values imply a lower droplet repulsion, resulting in rapid flocculation and coalescence, and consequently demulsification.

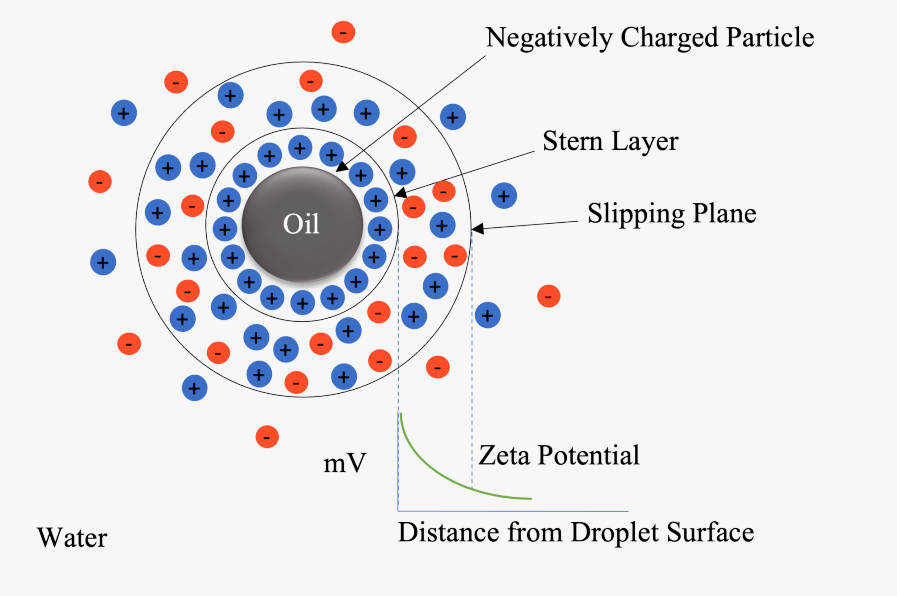

Figure 2. 3. Electrical double layer configuration.

Table 2. 2. Emulsion stability for different zeta potential values.

Zeta potential (mV)	Stability status
0 to ±5	Rapid flocculation and coagulation
±10 to ±30	Initial instability
±30 to ±40	Moderated stability
±40 to ±60	Good stability
> ±60	Excellent stability

Micro-electrophoresis and electroacoustic instruments can be used to measure zeta potential. The micro-electrophoresis technique applies electrical field to measure the velocity and direction of the charged droplets from which the charge magnitude and sign are obtained, respectively. The signals are then correlated to zeta potential (McClements, 2007).

Oil-Water Interfacial Film Properties. The surface of the oil-water interfacial film possesses surface tension. The molecules in the bulk are subject to interactions equally in every direction. However, on the surface, these interactions are not present from all sides, developing a net attractive force at the surface of a liquid. By increasing the similarities between the intramolecular forces of the oil and water phases, the interfacial tension (IFT) value decreases. Decreasing the IFT reduces the rate of droplet coalescence and enhances the emulsion stability. Also, a stabilizing film on the oil-water interfacial limits the rate of droplet coalescence. Therefore, the thickness and rigidity of the interfacial film control the emulsion stability. A thicker interfacial film increases the film drainage time and reduces the rate of demulsification (Ali et al., 2019).

Surfactants are surface active agents with amphiphilic features that include a hydrophilic head and a hydrophobic tail. Surfactants reduce the IFT because the interactions between the hydrophobic tails of surfactant-oil and the hydrophilic head of surfactant-water are much stronger than the oil-

water interactions (Milton, 2012). Griffin (Griffin, 1949) developed a semi-empirical criterion to select a surfactant using hydrophilic-lipophilic balance (HLB) number, that is based on the relative percentages of the hydrophilic head to lipophilic (hydrophobic) tail in the surfactant molecule. The HLB ranges depend on the oil nature and can be used to predict the type of emulsions for different applications (Table 2. 3). Some researchers have attempted to relate the HLB numbers to selective coalescence rate and emulsion stability without a success because the emulsion stability depends on various other factors, such as droplet size distribution, pH, temperature, and elastic and viscous modulus. Thus, the HLB number can only be used as a criterion to choose the surfactant (Tadros, 2009).

Table 2. 3. Summary of HLB ranges of surfactants (Tadros, 2009).

HLB Range	Applications
3–6	w/o emulsifier
7–9	wetting agent
8–18	o/w emulsifier
13–15	detergent
15–18	solubilizer

In addition to lowering IFT followed by droplet size reduction, surfactants can change the interfacial film elasticity. Higher surfactant concentration increases the elasticity and therefore enhances the emulsion stability up to a critical concentration known as critical micelle concentration (CMC). The addition of surfactant beyond the CMC threshold no longer reduces the IFT (and consequently, droplet size).

The rheology of emulsions plays a key role in the emulsion stability and droplet morphology through parameters and variables such as viscosity, elasticity, and shear stress. There are

dimensionless numbers employed to assess the emulsion stability. When shear stress (ratio of force to area) is applied to a droplet, it causes droplet deformation from spherical to ellipsoidal and eventually break-up. The shear stress can be applied in a laminar or turbulent flow regime, depending on the magnitude of Reynolds number (Re, ratio of inertia to viscous forces); the shear stress and the fluid flow regime both affect the droplet size (Tadros, 2009). The inertia force is related to the fluid momentum affected by the fluid velocity and density; a denser fluid having a higher velocity exhibits more inertia force. Viscous forces are the ratio of shear stress to shear strain that can cause droplet deformation (Goodarzi and Zendehboudi, 2019). When the turbulent eddies are larger and smaller than the droplets, the shear stress is applied on the droplets by the eddies and inertia force, respectively, to deform the droplets. In the emulsion systems under laminar flow regime ($Re < 1000$), the viscous forces are greater than inertia forces, whereas under the turbulent flow regime ($Re > 2000$), the viscous forces are less than inertia forces. Thus, increasing Re leads to stronger droplet deformation through increasing inertia force, which in turn transfers the stress to the interfacial layer, affecting the droplet stability. Droplets can be more stable in either the viscous flow where the interfacial forces are balanced by the viscous forces, or in the inertial flow where the inertial forces are dominant or in balance with the interfacial forces. The viscosity of dispersed phase greatly impacts the droplet deformation time and a higher viscosity prolongs the droplet deformation (Tadros, 2009).

Two other important dimensionless numbers that are relevant to the emulsion systems are Weber number (We) and capillary number (Ca). In a single emulsion system (o/w or w/o), Ca for the continuous phase and We for the dispersed phase are typically low. Thus, the emulsion stability can be assessed by critical values of Ca and We numbers, which depend on the ratio of the viscosities of the dispersed and continuous phases (Li et al., 2018).

2.2.3. Demulsification Processes

Currently, several techniques are being used to separate emulsified mixtures of oil and water. These methods can be used as standalone or hybrid to achieve a better demulsification performance in terms of efficiency and costs. Emulsion breaking can be enhanced by increasing flocculation rate, IFT, temperature, and the demulsifier contact time, or by decreasing viscosity and applied shear. Current demulsification techniques are summarized in Table 2. 4 and include thermal, microwave irradiation, electrical, mechanical (centrifugation), and chemical methods.

Table 2. 4. A summary of different demulsification techniques with their advantages and disadvantages.

Demulsification Methods	Mechanisms	Advantages	Disadvantages
Thermal	• interfacial viscosity reduction • flocculation/coalescence rate increase (He, 2020)	• no chemical contamination of emulsions	• high energy demand • expensive • demulsification of finer droplets is not possible (Kokal, 2005)
Microwave	• viscosity reduction (dispersed phase) • droplet surface charge reduction by microwave-induced rotation of emulsified molecules • internal pressure increase (dispersed phase), reducing interfacial film thickness by droplet expansion (Fortuny et al., 2007; Issaka et al., 2015)	• no need for chemical additives • no secondary pollution production • more uniform heating compared to thermal method and excellent demulsification efficiency. • electromagnetic waves can neutralize the electric repulsion between droplets, causing zeta potential reduction and aggregation (Abdulbari et al., 2011)	• high capital and operational costs • uncertainty in scale up potentials (Mutyala et al., 2010) • might require adding chemical demulsifier to achieve the desired separation efficiency (Zolfaghari et al., 2016)
Centrifuge	• demulsification acceleration due to density difference and increased	• no chemical contamination of emulsions	• not cost-effective due to being labor and energy intensive.

	gravity acceleration (Issaka et al., 2015)		• complete demulsification not possible using only the centrifuge method; to be applied in conjunction with other techniques.
Electrical	• droplet contact increase, due to increased droplet motion, resulting in coalescence (Eow et al., 2001) • polar molecules rearrangements and double layer thickness reduction, weakening the interfacial film rigidity, increasing droplet coalescence (Issaka et al., 2015)	• no chemical contamination of emulsions • lower energy cost than thermal and centrifuge (Zolfaghari et al., 2016)	• high energy demand, • usually applied in combination with thermal and chemical demulsification techniques (Ichikawa et al., 2004)
Chemical	• interfacial tension increase • mechanical strength reduction, elasticity, interfacial film thickness, and increasing flocculation and coalescence rates (Simonsen et al., 2018)	• highly efficient • convenient • economical	• secondary pollution production • some demulsifies (e.g., ethyl cellulose) cannot be recycled even if they are biodegradable and non-toxic; therefore, causing low reusability and sustainability (Su, 2017).

Chemical demulsification is a conventional and economical technique, which generally includes surface-active amphiphilic compounds with special wettability (Kokal, 2005). Chemical demulsifier cause droplet coalescence due to: 1) increasing IFT, 2) reducing elasticity and viscosity of droplets, and 3) decreasing the interfacial film thickness through film drainage/shrinking that decreases the mechanical strength of droplets (Simonsen et al., 2018). An essential step in the chemical demulsification process is to choose the demulsifier chemical composition, containing solvent, surfactants, flocculants, and wetting agents. Adding demulsifiers leads to emulsion destabilization by decreasing the elasticity/viscosity of the film. Generally, low- and high molecular-weight polymeric surfactants are commercially available as demulsification chemicals (Feng et al., 2009). Low-molecular-weight polymeric demulsifiers feature high interfacial activity that can break the emulsions through irreversibly adsorbing onto the oil-water interface, destroying the interfacial film. In contrast, high-molecular-weight demulsifiers lead to emulsion destabilization by droplet flocculation based on the bridging effect (Peña et al., 2005). Polymeric demulsifiers with intermediate molecular weight result in effective demulsification due to flocculation/coalescence mechanisms (Wang, X. et al., 2015; Wu et al., 2003).

Simple vial test is effective in screening a wide range of demulsifiers at various concentration and composition levels. The bottles are shaken to disperse the demulsifiers, and then the phase separations are visually investigated. The vial tests can be conducted under dynamic conditions to analyze different parameters such as demulsifier concentration, settling/retention time, and temperature (Adeyanju and Oyekunle, 2019). Generally, the efficiency of the chemical demulsifiers depends on their adsorptions at the oil-water interface. Other important factors influencing are the oil composition, pH, salinity, and temperature. Despite the success of the chemical demulsification in breaking emulsions, they produce secondary pollutions that needs

treatment prior to disposal or recycling (Liang et al., 2018). Thus, designing an eco-friendly and economic demulsifier with the highest efficiency is critical. MNPs are considered as a chemical demulsifier with high oil adsorption capacity and suitable reusability and recovery, which can effectively break stable emulsions without generating a secondary waste stream (Grein-Iankovski and Loh, 2020; Liu et al., 2012).

2.3. Magnetic Nanoparticles Synthesis and Characterization as Demulsifiers

Pristine MNPs have a limited intrinsic stability that cause particles to agglomeration. The bare particles are chemically reactive and are easily oxidized in the air (Simonsen et al., 2018), leading to loss of magnetism and dispersity. To prevent aggregation and oxidation, the MNPs are commonly coated or grafted with a protection layer which improves effectiveness in aqueous solutions (Campos et al., 2015; Lü et al., 2018a). Therefore, for demulsification application, the MNPs larger than 100 nm consist of three layers, including a magnetic core (e.g., Fe, Ni, Co, or their oxides), a stabilizing shell layer, and a functional layer, containing polymers and metal ions. In Figure 2. 4, we show various types of MNPs structures based on different coating techniques, to obtain core-shell, shell-core-shell, Janus, and dendritic/hyperbranched structures.

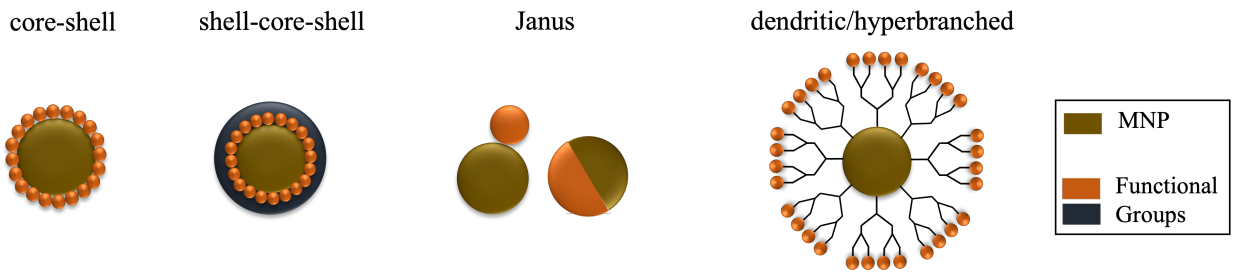

Figure 2. 4. Different structure of functionalized MNPs

The size and morphology of functionalized MNPs, and the chemical compositions of different layers affect their physio-chemical, thermal, and mechanical properties (Lu et al., 2007).

In the magnetic core of the MNPs, iron oxides (such as γ-Fe_2O_3 and Fe_3O_4), spinel ferromagnets ($MgFe_2O_4$, $MnFe_2O_4$, or $CoFe_2O_4$), and pure metals (Fe and Co) are commonly used (Simonsen et al., 2018). The iron oxide nanoparticles are the most common choices as they feature superparamagnetic and biocompatibility properties with a low agglomeration potential (compared to other MNPs) that leave zero residual magnetization after removing the external magnetic field (Mohammed et al., 2017). The MNP features such as structural, thermal, electrical, optical, and magnetic are mainly related to their size. Surface and interfacial effects become more pronounced in smaller MNPs which is because of larger exposed surface area per MNP loading unit; however, the magnetization decreases by decreasing the size of MNPs. The magnetic particles perform best when their size is smaller than a critical value that is typically around 10–20 nm, depending on the material (Lu et al., 2007).

2.3.1. Synthesis of Magnetic Nanoparticles for Demulsification

Different synthesis methods are developed to produce functionalized MNPs with different compositions and shapes, using top-down or bottom-up approaches. In the top-down strategy, the size of materials is reduced through high pressure homogenization or milling. In contrast, self-assembly and precipitation methods are used to develop MNPs, in the bottom-up approach (Petschacher et al., 2013). The most common MNP synthesis methods include co-precipitation, thermal decomposition, hydrothermal, and microemulsion routes (Ali et al., 2019). The biggest challenge in the synthesis of MNPs is to control the structural properties such as size, shape, morphology, porosity, crystallinity, and polydispersity (Campos et al., 2015).

Co-precipitation. It is a conventional method to prepare the MNPs from iron oxides such as γ-Fe_2O_3 and Fe_3O_4 through chemical reactions of iron salts (Fe^{2+}/Fe^{3+} salts) in a highly basic aqueous medium. MNPs with dimensions of 5–20 nm can be synthesized by this method (Campos et al.,

2015). Generally, the properties of the formed particles such as size, shape, and composition are highly influenced by the type of iron salts, ratio of Fe^{2+}: Fe^{3+}, reaction temperature, pH, and ionic strength (Lu et al., 2007). One drawback of the co-precipitation technique is that the high pH during the synthetic and purification processes can adversely affect the uniformity of the MNPs (Qiao et al., 2019), leading to polydisperse MNPs (Su, 2017).

Thermal Decomposition. The thermal decomposition of organometallic compounds at the boiling point (100–300°C) is a conventional method to synthesize small, high quality, and monodispersed MNPs. The as prepared monodispersed MNPs have a narrow size distribution and are only dispersible in nonpolar solvents (Qiao et al., 2019). Annealing temperature, duration of reaction, and ageing period can be adjusted during the synthesis to control the size and size distribution of the MNPs (Yang et al., 2017). Also, the composition of mixture, containing organometallic compounds, surfactant, and solvent effectively control the synthesis process (Lu et al., 2007).

Hydrothermal. The synthesis process is conducted under hydrothermal conditions where chemical reactions occur at a high temperature (130–250 °C) in aqueous solution, and at a high vapor pressure (0.3–4 MPa) (Qiao et al., 2019). The concentration of iron-based precursors and the reaction time affect the size and shape of the MNPs. For instance, spherical particles are obtained using a higher concentration of precursors, whereas monodispersed particles are synthesized using shorter reaction times (Yang et al., 2017). Moreover, increasing the hydrothermal temperature increases the saturation magnetization (Attallah et al., 2016; Bhavani et al., 2017).

Microemulsion. In this method, the MNPs are formed using w/o microemulsion where the nanodroplets surrounded by a monolayer surfactant are dispersed in the continuous oil phase (Ali et al., 2019). The MNPs are formed after adding a precipitating agent to the microemulsion containing an aqueous solution with iron salt precursors and surfactant. The emulsion droplet size

can vary by the ratio of water-to-surfactant which can eventually control the shape and size distribution of the MNPs. Other experimental variables such as reaction temperature and pH value are also influential (Qiao et al., 2019).

Electrochemical. This process is based on the reduction/oxidation using an iron-based electrode immersed in an electrolyte. In the anode, the metallic electrode is oxidized into ions that under an electric field are reduced onto the cathode in metal (Niculescu et al., 2022). The synthesized MNPs characteristics depend on the current density, applied cell potential, electrochemical cell geometry, electrode separation, electrolyte and electrodes' composition, and temperature (Lozano et al., 2017). For instance, by adjusting the applied current density, the particle size of the MNPs can be controlled (Cabrera et al., 2008).

Various MNPs synthesis methods are summarized in Table 2. 5. Among various techniques, hydrothermal is relatively less exploited despite the high quality of synthesized MNPs (Lu et al., 2007). The microemulsion method can produce a variety of morphologies for monodispersed MNPs with precise control of their size and size distribution (Campos et al., 2015). However, this technique requires a large quantity of solvents that limits its large scale production (Yang et al., 2017). Commonly, co-precipitation and thermal decomposition methods are favored for the MNP synthesis. Co-precipitation is the simplest synthesis method for MNP synthesis, while thermal decomposition provides a better control on the size and morphology of the MNPs (Ali et al., 2019). Electrochemical synthesis method is considered as a green technique with no need of additives, scalability, short time reaction, and flexibility to control the morphology and size. Only the electrochemical method can produce larger MNPs (≥ 20 nm), that is required in applications such as hypothermia and separation processes (Cabrera et al., 2008). However, the low production rate

and complex design of the electrochemical method can be considered as important drawbacks (Rahimdad et al., 2019).

Table 2. 5. Summary comparison of the synthesis methods (Ali et al., 2019).

Methods	Process	Reaction temperature (°C)	Reaction time	Solvent	Size distribution
Co-precipitation	Simple, ambient conditions	20–90	Minutes	Water	Narrow
Thermal decomposition	Complex, inert environment	100–300	Hours	Organic	Very narrow
Hydrothermal	Simple, high pressure	130–250	Hours	Water/ethanol	Very narrow
Microemulsion	Complex, ambient conditions	20–50	Hours	Organic	Narrow
Electrochemical	Complex, ambient conditions	Room temperature	Minute	Water	Very narrow

2.3.2. Characterization of Magnetic Nanoparticles

Different physio-chemical properties of the MNPs are analyzed using various characterization techniques. Microscopic and spectroscopic methods can characterize the morphological and structural features of the MNP sample, respectively while physical adsorption tests relate to the particle size and surface area.

Morphological Characterization Using Microscopic Techniques. Morphology is an important property of the MNPs. Microscopic characterization techniques such as polarized optical

microscopy (POM), scanning electron microscopy (SEM), and transmission electron microscopy (TEM) are commonly used to characterize the morphology of the MNPs. The microstructure of functionalized MNPs such as crystallinity and amorphous areas of the MNPs can be analyzed through POM (Lin et al., 2017). SEM is widely used to study the morphology and distribution of the nanoparticles in the bulk. Similarly, TEM uses particle beams of electrons to visualize the MNPs. As illustrated in Figure 2. 5, SEM provides information about the surface structure of the particles in a 3D image, while TEM gives information about the core material, and crystallization in a 2D image at a higher resolution (Khan et al., 2019).

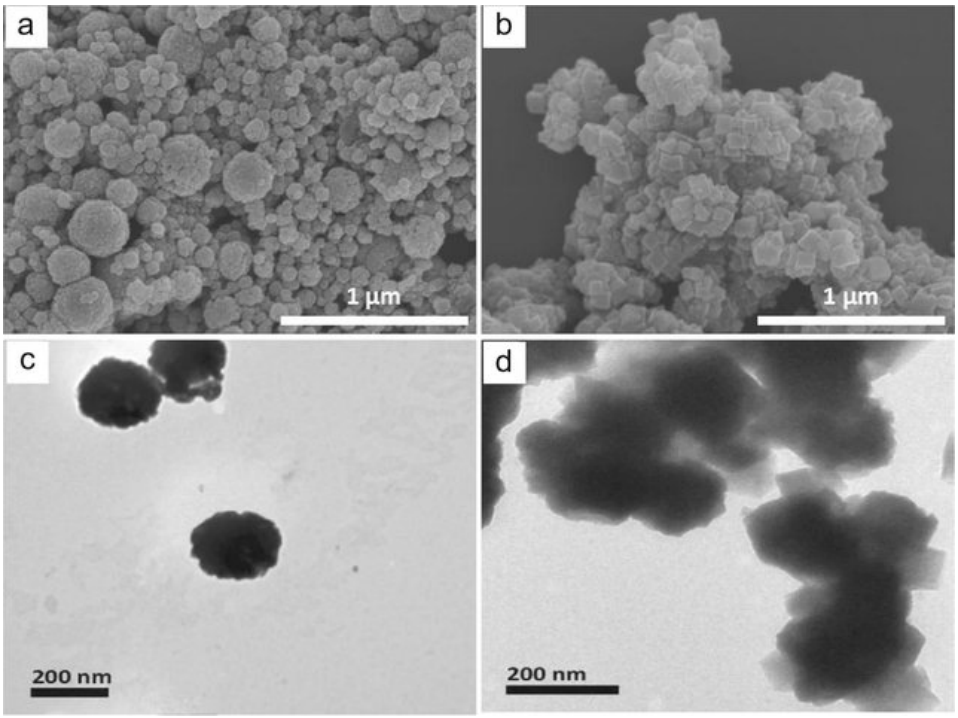

Figure 2. 5. SEM (a,b) and TEM (c,d) images of MNPs (Li et al., 2019).

Structural Characterization Using Spectroscopic Techniques. Spectroscopic techniques provide additional information about the structure of the MNPs by studying the chemical composition and nature of bonding materials through Fourier transform infrared spectroscopy (FTIR) and X-ray diffraction (XRD) as shown in Figure 2. 6 (Khan et al., 2019). In addition to XRD and FTIR,

energy dispersive X-ray (EDX) and X-ray photoelectron spectroscopy (XPS) are other important analytical techniques to identify the structure of the MNPs (Lesiak et al., 2019). XRD provides information about the crystallinity and phase of the particles in single- and multi-phase systems (Ingham, 2015). Also, XRD can estimate the particle size through the Debye Scherer formula (Rahmawati et al., 2017). EDX is an X-ray technique to determine the elemental compositions of the MNPs. Nanoparticles contain elements that emit X-ray radiation through electron beam irradiation. The intensity of the X-ray emissions is proportional to the concentration of the elements, and can be analyzed by EDX (Khan et al., 2019). XPS is a surface sensitive electron spectroscopy for the chemical analysis based on photoelectric effect. It can be used to identify the elemental composition and bonding nature of the elements in nanoparticles. XPS can also provide information about the overall elemental composition and its topological changes with depth or across the surface (Tayefeh et al., 2019). FTIR is an analytical technique to study the characteristic functional groups, including organic, polymeric, and in some cases, inorganic materials that are coated on the surface of the MNPs (Silva et al., 2013).

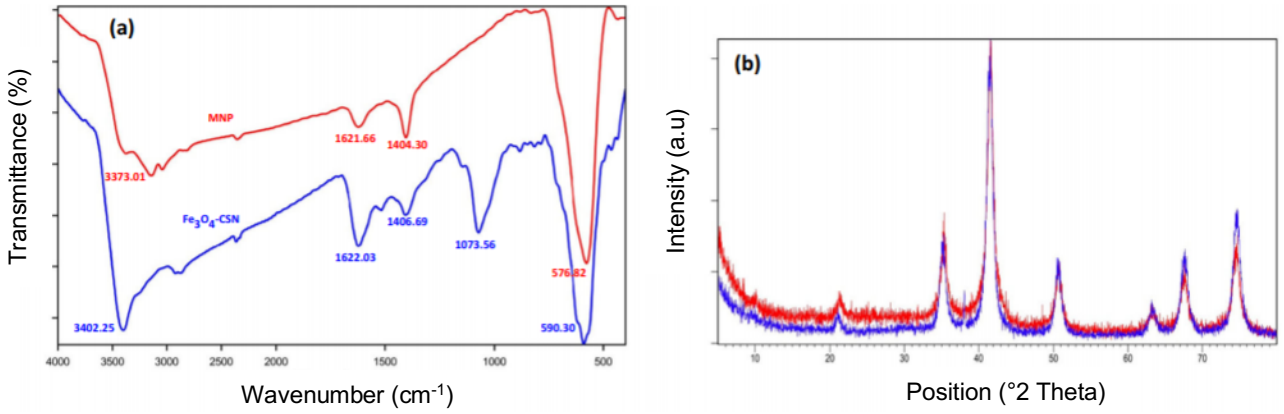

Figure 2. 6. FTIR Spectra (a), and XRD Patterns (b) of MNPs (Omidinasab et al., 2018).

Physical Adsorption Characterization. The physical adsorption onto the MNPs is affected by their morphological and structural properties such as surface area, pore size, and shape. Particle size

and surface area characterization can be conducted through different techniques, including SEM, TEM, XRD, and atomic force microscope (AFM). Also, dynamic light scattering (DLS) can give information about MNPs sizes at an extremely low level based on zeta potential size analyzer (Khan et al., 2019). Brunauer-Emmet-Teller (BET) technique is a widely utilized analytical method to obtain the specific surface area of the MNPs based on adsorption and desorption processes at a low temperature (Chen et al., 2017). For instance, the pore size, shape, and size distribution can be obtained from the desorption isotherms from Barrett, Joyner, and Halenda (BJH) model (Asthana et al., 2016). Nanoparticle tracking analysis (NTA) is a relatively new technique to visualize and analyze the nanoparticles in the solution phase based on the rate of Brownian motion to particle size (Shipunova et al., 2018). The rate of particles' movement only depends on the emulsion viscosity and temperature; not affected by the particles features such as density. Therefore, NTA can be used to directly count nanoparticles to obtain absolute number count and accurate size distribution of MNPs (Zhang et al., 2020).

2.4. Experimental Demulsification Studies Using Magnetic Nanoparticles

Without any surface coating, the MNPs are hydrophobic with a large surface area to volume ratio. In addition to the flocculation due to van der Waals force, the MNPs particles tend to agglomerate through hydrophobic interactions and strong magnetic dipole-dipole attractions (Gupta and Gupta, 2005). Adding MNPs to the emulsion creates Pickering emulsion with the oil or water droplets engulfed by the MNPs. Subsequently, droplets coalescence and are separated after applying an external magnetic field (Simonsen et al., 2018). The main mechanism to separate the oil-water mixtures is electrostatic attractions between the negatively charged oil droplets and the positively charged MNPs. The oil adsorbed between the agglomerated MNPs can be easily collected by applying an external magnetic field (Ko et al., 2016). For an effective driving force to recover most

of the MNPs, the external magnetic force should exceed the total drag and gravitational forces (Lü et al., 2020). To achieve excellent demulsification efficiency, the MNPs should be dispersible in the continuous phase, which later allow them to be transferred onto the oil-water interface. Therefore, it is required to change the surface wettability of the MNPs through surface coating/chemical grafting, as it changes the physio-chemical properties of the MNPs (Zhang et al., 2016; Zhou et al., 2020). Using functional materials, as a protective shell eliminates the MNPs agglomeration by stabilization which leads to wettability alteration of the MNPs that significantly affect the demulsification mechanism. The majority of the MNPs are functionalized as amphiphilic particles with both hydrophilic and oleophilic properties. In the case of o/w, the MNPs can be easily dispersed in the continuous water phase and transferred to the surface of emulsified oil droplets. The amphiphilic MNPs can facilitate demulsification process due to high interfacial activity between the oil droplets and functionalized MNPs, which is an important mechanism in controlling the demulsification performance (Lü et al., 2018c). In addition to the MNP coating, emulsion properties such as pH and salinity can also affect the interfacial interactions. For instance, the adsorption of oil onto the surface of MNPs can occur under acidic and neutral conditions due to both electrostatic attraction and hydrophobic interactions. Under alkaline conditions, due to the repulsion between negatively charged MNPs and oil droplets, the hydrophobic interactions can be considered as the only mechanism for adsorption (Lü et al., 2018a).

2.4.1. Effect of MNP Functionalization Chemistry and Morphology

The MNP stabilization is required because of the tendency of the pristine MNPs to form aggregates and their potential to be oxidized in the air. Different coating materials are used in the literature to functionalize MNPs with various structures for demulsification applications (Table 2. 6). The functional groups and surface-active agents can alter the physio-chemical properties of MNPs to

add a desired functionality (Zhou et al., 2020). In the following section, we review literature studies on MNP coating chemistry and structures, using organic and inorganic materials.

MNPs with a superparamagnetic core and polymeric shell are desirable in oil-water separation application. The core-shell MNPs were used in demulsification by Wang et al. (Wang, C. et al., 2015) where a magnetite core of Fe_3O_4 was coated with a polymer shell of PDMAEMA as a pH-responsive polymer. The functionalized MNPs exhibited dual stimuli-responsiveness to both external magnetic fields and environmental pH. Their results showed that the polymer stabilized the MNPs and engulfed the oil droplets to form stable Pickering emulsions. The dual responsive MNPs could quickly form and break the Pickering emulsions by increasing and decreasing the solution pH, respectively. Lu et al. (Lü et al., 2018a) examined the performance of core-shell MNPs coated with AEAPFS for demulsification of diesel-in-water (o/w) emulsions. The AEAPFS chemical has an extra aminoethyl group than 3-aminopropyltriethoxysilane (APTES); thus, the AEAPFS molecules with additional positive charges could be utilized as a more surface-active coating. According to the results, water transmittance > 95% was obtained by adding 650, 740, and 800 mg/L MNPs to the emulsion system at pH levels 4, 7, and 10, respectively.

Hyperbranched polyamidoamine-graphene oxide (GO) MNPs were used by Chen et al. (Chen et al., 2019) to separate crude-in-water (o/w) emulsions. The GO MNPs are not suitable for demulsification of o/w where the average oil droplet size < 2 μm; however, the hyperbranched polyamidoamine provided a better demulsification performance for smaller emulsion droplet size because of the hyperbranched structure. Although both GO and hyperbranched polyamidoamine achieved good demulsification efficiencies, they could not be recycled. They studied the effects of MNPs dosage, temperature, and pH on the demulsification efficiency. The maximum demulsification performance (99.1%) was obtained by employing 20 mg/L of coated MNPs at

40°C, and pH 6. The demulsification efficiency decreased to 97% after seven cycles. A core-shell MNP with a magnetic core and hydrophobic shell was utilized by Wang et al. (Wang et al., 2020) to separate o/w. They synthesized mesoporous silica shell with a dendritic structure through stabilizing Fe_3O_4 nanoparticles by oleic acid (OA), grafting with CTAB and NaSal, and adding a 1:8 ratio of ODMS to TEOS to increase the MNP dispersivity. Their synthesized MNPs with dendritic structures achieved > 98.1% demulsification efficiency. Chen et al. (Chen et al., 2018) compared the separation efficiency of o/w by applying three types of magnetic microparticles, including spiky-ODTMS, smooth-ODTMS, and smooth-ODTMS/CTAB. The results revealed that the spiky-ODTMS iron oxide nanoparticles coated with ZnO nano spikes have a higher demulsification efficiency than the smooth-ODTMS and smooth-ODTMS/CTAB because of the superhydrophobicity and superoleophilicity of the spiky-ODTMS and larger effective surface area. The lower efficiency of the smooth-ODTMS and smooth-ODTMS/CTAB with surfactant was due to decreased hydrophobicity and decreased external surface area, resulting in less particle-oil contact. However, dendrimer MNPs are more difficult to be efficiently collected and recycled (Wang et al., 2018).

Recently, Janus particles have been considered as an attractive option in demulsification because of their high interfacial activity and amphiphilic properties. The effectiveness of the Janus MNPs for demulsification of toluene-in-water (o/w) was analyzed by Song et al. (Song et al., 2018). The MNPs were synthesized by emulsion interfacial polymerization through applying hydrophilic acrylic acid (AA) and oleophilic styrene/divinylbenzene (St/DVB) to Fe_3O_4 particles. The prepared MNPs with amphiphilic properties exhibited an excellent demulsification performance with a separation efficiency of > 99% within 120 s. They tested different oils, including hexane, petroleum ether, diesel, and gasoline droplets in water were effectively separated within 120 s.

Functionalized MNPs with Organic Compounds. Organic compounds such as surfactants and polymers can chemically or physically interact with the MNPs and create steric repulsive, to balance the magnetic and van der Waals attractive forces exerted on the MNPs. Generally, the electrostatic and steric repulsion can be used to enhance the dispersivity of the MNPs in a suspension by stabilizing them in a stable colloidal state. Functional groups composed of organic materials provide nanoscale networks with a larger surface area on the MNPs surfaces to increase their applications as sorbents. For instance, functional materials with a strong affinity for oil provide a higher oil removal efficiency (Qiao et al., 2019).

Fatty acid-based: The application of fatty acids as surfactants such as oleic acid (OA), citric acid (CA), elaidic acid (EA), humic acid (HA), stearic acid (SA), myristic acid (MA), and palmitic acid (PA) for stabilization of MNPs are investigated in various studies (Cao et al., 2014; Liang et al., 2014; Munjal and Khare, 2017). OA is an excellent surfactant to functionalize MNPs during the synthesis of MNPs and through chemical precipitation. For instance, Liang et al. (Liang et al., 2015) examined the performance of single-layer OA-coated Fe_3O_4 in demulsification of cyclohexane-diluted crude o/w nanoemulsions under external magnetic field. The -COOH groups in OA have a high affinity for the Fe atoms in iron oxide and provide a non-polar shell with the outward hydrophobic tails. The maximum separation efficiency of 97% was achieved with 100 g/L coated Fe_3O_4 with a water contact angle of 90°. The SE was stable at acidic pH, while it gradually decreased in basic environment when the pH was increased from 8 to 11. The recyclability of the coated MNPs indicated no significant changes to SE over five cycles. Munjal and Khare (Munjal and Khare, 2017) synthesized cobalt ferrite ($CoFe_2O_4$) nanoparticles and coated them with OA and CA. The results showed that the prepared hydrophobic OA-cobalt ferrite (CFO) and hydrophilic CA-CFO have excellent performances in effectively demulsifying o/w and w/o

emulsions, respectively. Fossati et al. (Fossati et al., 2019) used covalently functionalized MNPs with a styrene-maleic acid copolymer for oil removal of crude oil emulsions. OA coated iron oxide NPs were dissolved in an acid solution and were then functionalized with acrylic ester of γ-mercaptopropyltriethoxysilane (SPS), styrene, and maleic acid. Oil removal > 95% was achieved by 0.1 mg/L of functionalized MNPs due to their amphiphilic nature. The synthesized MNPs exhibited a good dispersivity in water, while their lipophilic core simultaneously provided a superior oil capture potential from the emulsions. In another study, fast demulsification of heavy oil in water emulsions (SE 99%) was achieved by employing poly(methyl methacrylate-acrylic acid-divinylbenzene)/iron oxide magnetic composite nanoparticles due to the amphiphilic properties of the composite MNPs. The poly(MMA-AA-DVB)/Fe_3O_4 MNPs, which were prepared by solvothermal processes, exhibited an excellent demulsification efficiency for five cycles (Ali et al., 2015).

Amine-based: These types of polymers have a wide range of applications as emulsifiers, pharmaceutical ingredient, cation exchange resin, and drug delivery. Kaang et al. (Kwon Kaang et al., 2018) developed magnetic amphiprotic catalyst (MAC) with amin-based functional polymers for demulsification application. Their MNPs were coated stepwise with polydopamine (PDA), polyethyleneimine (PEI), octadecylamine (ODA), and Au nanoparticles. The fabricated MACs were normally dispersed in the oil phase and forced into the water phase to decompose the aqueous pollutants by applying an external magnetic field. Without imposing the magnetic field, the MACs naturally returned to the hydrophobic phase to remove the non-aqueous contaminants. Therefore, the synthesized MACs showed an excellent demulsification performance for both SDS-stabilized w/o and CTAB-stabilized diesel-in-water (o/w) emulsions. Mao et al. (Mao et al., 2019) studied demulsification of w/o using functionalized Fe_3O_4@PDA with poly[3-dimethyl (2-

methacryloyloxyethyl) ammonium propane sulfonate] (PDMAPS). The synthesized MNPs exhibited a high demulsification performance for asphaltene-stabilized w/o under an external magnetic field which was due to their superhydrophilic zwitterionic polyelectrolyte shells. The increase in the IFT at the water-oil interface upon using the functionalized MNPs caused instability of the water droplets, resulting in increased coalescence.

In another study conducted by Lu et al. (Lü et al., 2018b), demulsification efficiencies of different emulsified oils, including diesel, toluene, olive, and soybean oils, were analyzed under neutral pH conditions by employing fabricated PEI coated Fe_3O_4. The results showed water transmittance > 95% in all cases using 60 mg/L MNPs as the demulsifier; for soybean oil emulsions, MNP dosage of 100 mg/L was used. The same coating was employed to functionalize MNPs in a study conducted by Zhao et al. (Zhao et al., 2019), for demulsification of SDS-stabilized soybean oil-in-water emulsions. The synthesized MNPs demonstrated an outstanding demulsification performance with water transmittance around 90% within 30 s under magnetic field.

Separation of fine oil droplets from hexadecane-in-water emulsions was investigated by Mi et al. (Mi et al., 2020) using functionalized Fe_3O_4@HA@poly(dimethyldiallylammonium chloride) (PDDA), where HA with a variety of functional groups were used for coating. Fe_3O_4@HA NPs showed a significant performance in wastewater treatment. However, they were not suitable for demulsification of o/w due to the negative charges of both Fe_3O_4@HA and oil droplets. The cationic polyelectrolyte PDDA with substantial quaternary ammonium groups was employed on the MNP surface to modify the surface potential and hydrophilicity properties of the Fe_3O_4@HA. The results demonstrated an excellent demulsification efficiency (around 100%) at a low dosage of the functionalized MNPs (375 mg/L). In addition to electrostatic attractions, the interfacial

activity related to the hydrophobic aromatic rings and alkyl chains played an important role in the high demulsification efficiency.

The demulsification performance of functionalized MNPs with other polymers such as polyvinylpyrrolidone (PVP) was investigated by Shao et al. (Shao, 2019) for demulsification of diesel and soybean o/w. The results showed that both the emulsified oil droplets and PVP-MNPs were negatively charged; hence, there was a repulsive electrostatic interaction between them. The amphiphilic nature of the PVP molecules provided a good MNPs dispersivity and resulted in a higher demulsification efficiency. A water transmittance of 85% (equivalent to 99% oil removal) was obtained by employing 400 mg/L of PVP-MNPs. However, the demulsification efficiency decreased significantly by increasing the pH and surfactant concentration levels.

Cellulose is a natural and biodegradable polymer with low solubility in water. Carboxymethyl cellulose (CMC) is a cellulose derivative with multiple anionic carboxylic acid functional groups that can be adsorbed onto MNPs. Liang et al. (Liang et al., 2018) investigated demulsification of process water-in-diluted bitumen emulsions by applying functionalized Fe_3O_4 with sodium CMC followed by ethyl cellulose (EC). CMC was used to improve the chemical stability of MNPs and to increase the EC adsorption (onto the MNPs). The oil-water separation tests showed > 90% dewatering by adding mg/L synthesized Fe_3O_4-CMC-EC.

Functionalized MNPs with Inorganic and Hybrid Compounds. Combining MNPs with inorganic materials such as carbon (Nazifa et al., 2018), silica (Lu et al., 2002; Tago et al., 2002), precious metals or their oxides (Hong et al., 2008; Li et al., 2007) can enhance the MNPs stability, providing them with a wider applications. Inorganic compounds have a higher chemical and thermal stability, featuring a higher resistance against oxidation and acid leaching. Silica is the most common inorganic compound used in MNP functionalization to protect from oxidation by air and

agglomeration formation. Lu et al. (Lü et al., 2017) synthesized Fe_3O_4 MNPs coated with aminopropyl-functionalized silica (APFS) to graft chitosan molecular chains. Chitosan is the second most abundant natural biopolymer after cellulose, which has attracted great interests as a biological adsorbent without negative environmental impacts. This renewable adsorbent has desired properties such as nontoxicity, biocompatibility, biodegradability, and antibacterial activities. The free amine groups on chitosan (as its hydrophobic domains) lead to binding with negatively charged surfaces and provide a cross-linked polymeric network to improve the mechanical properties. In demulsification tests, chitosan grafted MNPs exhibited a strong magnetic response to a magnetic field and outstanding demulsification performance. The water transmittance increased by increasing the concentration of MNPs and decreased by increasing pH. Yang et al. (Yang et al., 2018) investigated demulsification of Pickering emulsion, stabilized by APTES coated MNPs. APTES is an aminosilane, which is frequently used in silanization processes for surface functionalization through covalent bonding. The results illustrated excellent emulsion stability for up to 12 days, following complete demulsification in a few minutes by applying an external magnetic field. Using different 0.1, 0.2, and 0.4 wt% coated MNPs, complete demulsification was achieved after 2, 8, and 18 min, respectively. Lu et al (Lü et al., 2018b) revealed that demulsification efficiency of the APTES coated MNPs is less than expected, especially under alkaline conditions because of the repulsion between the negatively charged MNPs and oil droplets. Moreover, alkaline solution containing active OH^- ions attacked the O-Si bonds, resulting in removal of functional groups (Murray, 2014). The hydrophobic driving force of aminopropyl did not overcome the electrostatic repulsion and the intensity of cationic charge of APTES decreased with increasing pH. Therefore, Lu et al. (Lü et al., 2018c) applied a highly cationic polyelectrolyte quaternized chitosan (QC)-grafted MNPs followed by surface coating with

silica (SiO_2) and APTES for demulsification of diesel o/w emulsions. The results revealed that MNPs with a higher grafting ratio led to a higher demulsification efficiency, while pH did not significantly affect the separation performance; a high demulsification efficiency was achieved under different pH values. Excellent demulsification performance with water transmittance > 95% was observed, using 15, 17, and 19 mg/L Fe_3O_4@SiO_2-QC under acidic, neutral, and alkaline conditions, respectively. The results showed significant phase separation was even without applying a magnetic field, due to the flocculation performance of the synthesized MNPs.

Zhang et al. (Zhang et al., 2017) coated Fe_3O_4@SiO_2-APTES with QC. The coated MNPs showed an excellent demulsification efficiency at different pH conditions; the separation efficiency reduced slightly under alkaline conditions for which a higher concentration of coated MNPs was required.

The amine-functionalized MNPs (NH_2-MNPs) followed by APTES coating were used by Wang et al. (Wang et al., 2018) to effectively demulsify a crude oil-in-water emulsion containing natural surfactants. According to their results, electrostatic attraction between the positive charge on NH_2 functional groups and the negative charge of oil droplets resulted in an effective demulsification. In another study, Ko et al. (Ko et al., 2016) investigated the performance of amine-functionalized MNPs using 3-APTES followed by grafting polyacrylic acid (PAA) for crude oil-in-water emulsion, which was stabilized with alkaline soap. Crude oils with different total acid numbers (0.15, 0.29, and 4.5) were tested as the oil phases. The results showed a separation efficiency of 99.9% in 5 min, using positively charged A-MNPs which confirmed electrostatic attraction as the main separate mechanism. Demulsification efficiency of diatomite (DM) was assessed by Xu et al. (Xu et al., 2019) for a crude oil-in-water emulsion. DM is a natural inorganic clay that mainly contains amorphous silica and is considered an ecofriendly natural adsorbent with high porosity

and high stability. DM was modified with APTES, followed by grafting Fe_3O_4 nanoparticles, then assembled with PEI to obtain amino-rich MNPs. Vial tests were used to investigate the demulsification performance of the prepared demulsifier. The results exhibited a superior performance of the synthesized MNPs at various pH levels. The electrostatic attraction and hydrogen-bond interaction between the MNPs and asphaltenes in the crude oil (as the main component in the interfacial film) lead to increased coalescence of oil droplets, resulting in demulsification.

The above-mentioned coatings cause the production of secondary pollutions due to using organic solvents to recycle the functionalized MNPs. To address this challenge, stimuli-responsive MNPs (e.g., temperature and/or pH-sensitive MNPs) are of great interest, because the oil adsorption and desorption can be adjusted by changing pH and temperature without using organic solvents. Lu et al. (Lü et al., 2020) synthesized pH and temperature responsive MNPs through coating $Fe_3O_4@SiO_2$ followed by grafting co-polymers of 2,2-Azobis[2-(2-imidazolin-2-yl) propane] Dihydrochloride (AIBI) to separate diesel-in-water emulsions. The separation results exhibited water transmittance of 75% and oil removal of 98%. The demulsification efficiency was reduced with increasing pH, and also, when the system temperature was exceeded the lower critical solution temperature. They proposed three different approaches for the recovery of the synthesized MNPs, including rinsing with alkaline water, hot water (70 °C), and room temperature DI water, respectively, instead of washing with any organic solvents. Based on these methods, the synthesized MNPs could be reused for at least five cycles without a significant loss in the separation efficiency.

Table 2. 6. Magnetic nanoparticles applications for demulsification of o/w and w/o systems.

Emulsion		Dispersed Phase			MNPs					Results			Analytical methods	Ref.
Type	Stabilization	Type	Concentration	Droplet size (μm)	Type	Coating	Bare (coated) size (nm)	Loading	Magnetization (emu/g) (MFS in T)	Coalescence time (min)	Separation (%)	Recyclability (cycle)		
o/w	Tween 60 (10 wt%)	Crude/ Cyclohexane	3.2 (vol%)	0.07 6	Fe_3O_4	OA	13 (11)	100 (g/L)	_	2	97	5	UV-vis, OCA, TEM	(Liang et al., 2015)
o/w	_	Diesel oil	2.5 (vol%)	>10	Fe_3O_4	SiO_2 (NP), PDMAEMA	20 (110)	400 (g/L)	75.1	_	_	6	DLS, OM, TEM, SQUID	(Wang, X. et al., 2015)
o/w (P-EM)	_	Silicon oil	2, 5 (wt%)	1–10	$Fe(CO)_5$	$CuSO_4$, HCl	500−5000	1 (g/g)	_	_	_	7	OM, OCA, SEM, EDX, XRD, FTIR, VSM	(Duan et al., 2015)
w/o (P-EM)	_	DI water (in nC_{12})	25 (g/L)	600–1500	(γ)Fe_2O_3 Fe_3O_4	GO	10 (200–400)	_	11.4	_	_	_	OM, SEM, EDX, TEM, XRD, FTIR, Raman, XRD, SQUID, VSM	(Lin et al., 2015)
w/o	Natural	Heavy crude	1:1 (vol:vol)	<10	Fe_3O_4	*p*(MMA-AA-DVB)	n/a (250)	500 (ppm)	< 25	60	99	5	DLS, TEM, FTIR, XRD, TGA, VSM	(Ali et al., 2015)
o/w	Alkaline soap	Crude	5 (wt%)	0.2–10	Fe_3O_4	3-APTES	10 (66)	0.04 (wt%)	90 (0.44–0.76)	5	99.9	_	OM (also Fluorescence M), DLS, TEM	(Ko et al., 2016)
o/w w/o	SDS	nC_{14}, nC_{16}	1:4	<20	Fe_3O_4	SiO_2 (NP), APTES, cyclodextrin	_	0.3–0.5 mL	_	0.5	_	8	OM, FTIR, TGA, SEM, TEM, XRD, OCA	(Zhang et al., 2016)

			(vol:vol)											
o/w	_	Diesel	0.2 (wt%)	_	Fe_3O_4	SiO_2 (NP), APTES, QC	12	34 (mg/L)	_	1/3	98	8	DLS, UV-vis, TEM, SEM, XRD, FTIR, TGA	(Zhang et al., 2017)
o/w (P-EM)	Eggshell (25 g/L)	Toluene	_	75	Fe_3O_4	_	_	50 (g/L)	1.336	_	_	_	FTIR, SEM, OCA, VSM	(Zhu et al., 2016)
o/w	SDS (0.1 g/L)	Toluene	1 (vol%)	_	$CoFe_2O_4$	OA	9 (10.6)	40 (g/L)	53 (0.052)	_	_	_	AGM, TEM, XRD, OCA, FTIR	(Munjal and Khare, 2017)
w/o	Span 80 (1 g/L)	Water	1 (vol%)	_	$CoFe_2O_4$	CA	9 (10.1)	40 (g/L)	49 (0.048)	_	_	_	TEM, XRD, FTIR, AGM, OCA	(Munjal and Khare, 2017)
o/w	SDS (4 wt%) Span 80 (1%)	nC_6/C_3H_8O	4 (wt%)	_	Fe_2O_3	_	5–20	6400 (ppm)	_	_	85.2	_	Optical tensiometer, DLS, TEM	(Hu et al., 2017)
o/w	_	Diesel	0.2 (wt%)	<6	Fe_3O_4	APFS, chitosan	250 (300)	0.5, 0.73 (g/L)	30.5	0.5	88	7	PPMS, DLS, UV–vis, OM, TEM, XRD, FTIR, TGA	(Lü et al., 2017)
o/w w/o	CTAB (o/w) SDS (w/o)	Diesel DI (in nC_6)	_	_	Fe_3O_4	PDA, PEI, ODA, Au (NP)	215 (366)	_	_	_	_	_	UV-vis, DLS, PSA, FE-TEM, SEM, EDX, FTIR, XRD, TGA	(Kwon Kaang et al., 2018)
o/w	_	Corn oil	2 (vol%)	<10	Iron oxide	ZnO (nano-spikes), ODTMS	<10 (1000)	40 mg/ml	_	_	_	_	OM, TEM, SEM, OCA	(Chen et al., 2018)
o/w	_	Diesel	0.2 (wt%)	<5	Fe_3O_4	SiO_2 (NP), APTES, QC	n/a (296)	15, 17 (mg/L)	25.4	1/3	>95	7	UV-vis, OM, EA, DLS, TEM, XRD, FTIR, PPMS	(Lü et al., 2018c)

o/w	_	Diesel, Toluene, Olive oil	1000 (ppm)	<5	Fe_3O_4	PEI	10	60 (mg/L)	67	1/3	>95	6	UV-vis, DLS, TEM, XRD, FTIR, TGA, BET, OCA, PPMS	(Lü et al., 2018b)
w/o	Solid (5 wt%)	Water (naphtha+ bitumen)	5 (wt%)	44–90	Fe_3O_4	CMC, EC	<100	150 mg	84	5	>90	_	DLS, FE-SEM, FTIR, ATM, TGA, OCA, PPMS	(Liang et al., 2018)
o/w	_	Diesel	1000 (ppm)	0.07–7	Fe_3O_4	AEAPFS	315 (360)	650, 740, 800 (mg/L)	69	1/6	99.9	5	UV-vis, OM, EA, TEM, XRD, FTIR, TGA, OCA, PPMS	(Lü et al., 2018a)
o/w	_	Toluene	1 (vol%)	<5	Janus Fe_3O_4	AA, St/DVB	6	25 (g/L)	_	2	>99	5	OM, SEM, EDX, TEM, OCA	(Song et al., 2018)
o/w (P-EM)	_	_	_	_	Fe_3O_4	APTES	10–20	0.1, 0.2, 0.4 (wt%)	56	2, 8, 18	_	5	FTIR, TEM, TGA, XPS	(Yang et al., 2018)
o/w	Natural (naphthenic A)	Crude	5 (vol%)	0.402	Fe_3O_4	APTES	n/a (102)	5 (g/L)	55	_	99.7	6	DLS, BET, OM, FTIR, TEM, TGA, SQUID	(Wang et al., 2018)
o/w	SDS	Soybean oil	1000 (ppm)	<6	Fe_3O_4	PEI	259 (177)	180, 480, 820 (mg/L)	77	0.5	90	10	DLS, UV-vis, OM, FTIR, FE-SEM, PPMS	(Zhao et al., 2019)
o/w	Natural	Crude	1 (wt%)	_	Fe_3O_4	DM-APTES-PEI	n/a (100–200)	450 (mg/L)	36.6	1	95.3	4	OM, UV-vis, FTIR, TEM, TGA, XPS, XRD, EDX, OCA, VSM	(Xu et al., 2019)
o/w	SDS	Diesel, Soybean oil	2700 (ppm)	<10	Fe_3O_4	PVP	<30 (90–410)	400 (mg/L)	71.4	_	99	5	DLS, OM, UV-vis, FTIR, TEM, TGA, XRD, PPMS	(Shao, 2019)
o/w	Natural	Crude	30 (ppm)	_	Fe_3O_4	OA, acrylic ester of SPS,	7.5 (9.5)	0.1 (g/L)	39	_	95	5	UV-vis, XRD, TEM, OCA, VSM	(Fossati et al., 2019)

						styrene-maleic acid								
o/w	Natural	Crude	5 (wt%)	<2	Fe_3O_4	polyamidoamine-GO	_	20 (mg/L)	10.8	_	97.7	7	UV-vis, FTIR, TEM, VSM	(Chen et al., 2019)
w/o	Asphaltene	DI water (in syn. oil)	20 (vol%)	_	Fe_3O_4	PDA, PDMAPS	200 (216)	3 (g/L)	51	1200	_	_	AFM, XRD, TEM, XPS, GPC, PPMS	(Mao et al., 2019)
o/w	Triton X-100, SDS (1:1)	Bilge mix #4	1000 (ppm)	_	Fe_3O_4 γFe_2O_3	_	15–20	_	50 (0.47)	5	_	_	SEM, EDX, XRD, VSM	(Waller et al., 2019)
o/w w/o	SDS J. Fe3O4	Toluene, Naphtha, Wat in bitumen	5–10 (%)	_	Fe_3O_4 Janus Fe_3O_4	M-CMC-EC M-CMC-EC-CMC	50–100 (145)	_	69.7,71	5	85.2 –95	5	DLS, TEM, FE-SEM, BET, FTIR, TGA, OCA, PPMS	(He et al., 2019)
o/w (P-EM)	_	Toluene	0.2, 0.5, 0.8 (v:v)	2.7, 6	Fe_3O_4	A binary of PEO & PMMA	8.6 (217)	0.1 (wt%)	58.4 (0.3)	_	_	_	DLS, OM, FTIR, XRD, TEM, XPS, TGA, SAXS, OCA, VSM	(Grein-Iankovski and Loh, 2020)
o/w	_	Cyclohexane, P. ether, nC_6, nC_8	1 (vol%)	_	Fe_3O_4	OA, ODMS, TEOS NaSal	10 (302)	4 (g/L)	0.73	_	>98. 1	5	UV-vis, SEM, FTIR, TEM, TGA, XPS, XRD, ICP, OCA, VSM	(Wang et al., 2020)
o/w (P-EM)	Pristine MNP	_	_	_	Fe_3O_4	PDMAEMA	_	_	29.22	_	_	6	DLS, UV-vis, OM, FE-SEM, FTIR, TGA, STEM, OCA, VSM	(Low et al., 2020)
o/w	_	Diesel	1000 (ppm)	_	Fe_3O_4	SiO_2 (NP), AIBI	200	800 (mg/L)	42.9	_	98	5	TEM, FTIR, XRD, TGA	(Lü et al., 2020)
o/w	_	nC_{16}	2 (vol%)	0.24 7	Fe_3O_4	HA, PDDA	30.6 (105)	375 (mg/L)	51.8	180	100	9	DLS, UV-vis, NZS, XRD, FTIR, SEM, TEM, OCA, VSM	(Mi et al., 2020)

Generally, a wide range of coating materials has been used in the synthesis of functionalized MNPs for demulsification application. However, some of these materials are toxic and expensive, and lack chemical stability under harsh conditions. For instance, polymer coated MNPs are not stable at high temperatures; silica coated MNPs experience difficulties to result a dense nonporous shell and show low stability under basic environments. Although carbon-coated MNPs show a remarkable stability under harsh conditions, their dispersity in o/w is challenging (Lü et al., 2017). These carbon coated MNPs are only dispersible in organic solvents and mostly non-dispersible in an aqueous phase. Therefore, MNP dispersivity in water and using inexpensive and eco-friendly materials such as surfactants provides an excellent option. Employing different types of surfactants (e.g., cationic, anionic, and non-ionic) for demulsification application can provide a better understanding of the oil adsorption mechanisms in terms of electrostatic interactions.

Thus, there is still a need to develop stable and robust MNPs that can withstand harsh conditions and obtain a detailed understanding of the adsorption mechanisms onto MNPs surfaces.

2.4.2. Effect of Process Operating Conditions

The operating conditions that significantly affect the demulsification efficiency include temperature, mixing time, and magnetic field strength. Temperature is of the most critical parameters affecting the demulsification performance (Ali et al., 2015). Xu et al. (Xu et al., 2019) studied removal of oil from crude oil-in-water emulsion using magnetic diatomite demulsifier showed that an increase in temperature leads to a better separation efficiency due to a decrease in emulsion stability Figure 2. 7. At a higher temperature, movement of interfacial molecules increases, while the interfacial viscosity decreases. Therefore, the adsorption of MNPs at the oil-water interface is easier, eventually resulting in a higher demulsification efficiency.

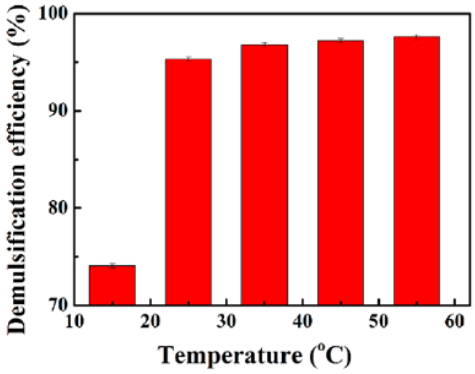

Figure 2. 7. The effect of temperature on demulsification efficiency (Xu et al., 2019).

The mixing time between emulsion and added MNP is another important factor governing the demulsification performance because a minimum contact time is required for the MNPs to attach to the oil droplets. Wang et al. (Wang et al., 2018) used MNPs with loading concentration 1.25 mg/mL to 7.5 mg/mL to separate crude oil-in-water emulsions (see Figure 2. 8). Although the ultimate demulsification efficiency was consistently high for all concentration levels, increasing the MNP concentration decreased the mixing time to achieve the ultimate separation efficiency. The probability of collisions between the MNPs and oil droplets increases at a higher MNP concentration, resulting in more aggregation and shorter demulsification time (Ko et al., 2016).

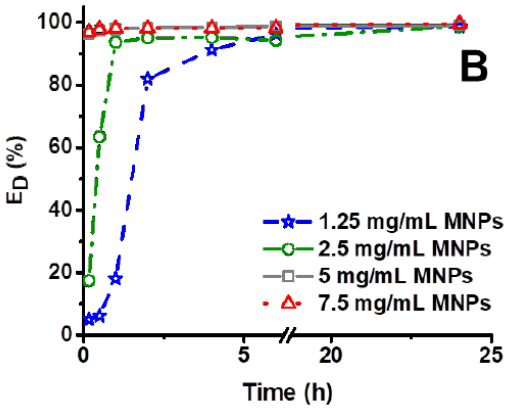

Figure 2. 8. The effect of mixing time on demulsification efficiency (Wang et al., 2018).

Based on Figure 2. 9, increasing the MNPs dosage enhances the demulsification efficiency before reaching a plateau. Increasing the MNPs concentration beyond this threshold value does not further improve the demulsification efficiency (Xu et al., 2019). Therefore, an optimal MNP dosage should be used for demulsification. The optimal MNPs concentration gives the lowest dosage at which the maximum demulsification is achieved (Wang et al., 2018). Ko et al. (Ko et al., 2014) found that adding MNPs beyond the optimum concentration can adversely affect the adsorption of oil droplets in o/w systems, due to the possibility of affinity between cationic MNPs and anionic surfactants rather than the oil droplets.

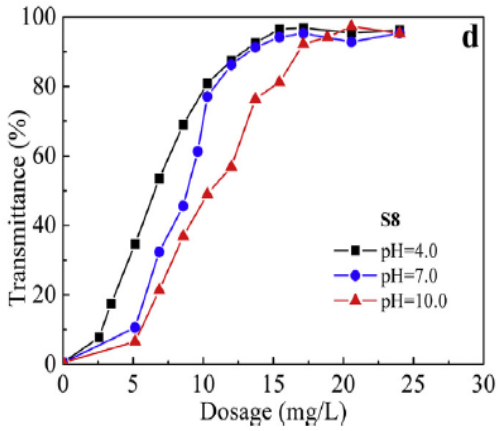

Figure 2. 9. The effect of MNPs dosage on demulsification performance (Lü et al., 2018c).

2.4.3. Effect of Emulsion Fluid Physical Properties

The emulsion characteristics such as pH, salinity, viscosity, interfacial rigidity, size of droplets, surfactant concentration, and the content of emulsion phases are considered as the critical parameters influencing demulsification performance. For instance, the interaction between the MNPs and emulsified droplets is highly affected by pH, which impacts the surface charge of MNPs in the emulsion system (Xu et al., 2019). Generally, an increase in the emulsion pH decreases zeta potential; in some cases, the surface charge on the MNPs is changed from positive to negative in

emulsion systems Figure 2. 10. The attachment of the MNPs onto the emulsified droplets becomes more difficult upon strong electrostatic repulsion, leading to a decline in demulsification efficiency (Shao, 2019; Zhao et al., 2019).

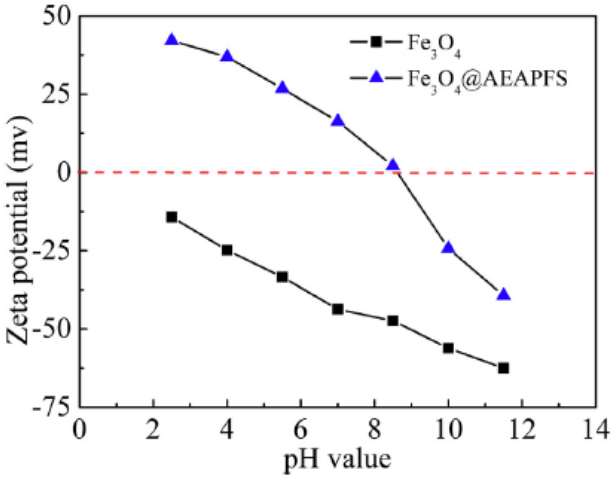

Figure 2. 10. Zeta potential of naked and coated MNPs at various pH values (Lü et al., 2018a).

In a series of studies by Lu et al. (Lü et al., 2017; Lü et al., 2018a; Lü et al., 2018b), the o/w demulsification efficiency was considerably increased under both acidic and neutral conditions (at pH values of 4 and 7), because the coated MNPs were positively charged, resulting in electrostatic attraction to the negatively charged oil droplets. However, under alkaline conditions, the emulsified oil droplets could not be effectively removed because the coated MNPs and oil droplets were both negatively charged at higher pH values that caused a strong electrostatic repulsion (Lü et al., 2017; Shao, 2019). In this case, the attachment of coated MNPs to the oil droplets was only possible through hydrophobic effect (Mirshahghassemi et al., 2016) where the hydrophobic forces compensated the electrostatic repulsion, facilitating the MNPs sorption onto oil droplet surfaces. However, in another study (Lü et al., 2018c), demulsification performance decreased slightly at a higher pH value (Figure 2. 11) using MNPs coated with SiO_2-QC that give positive surface

charges. Therefore, the MNPs could be easily adsorbed onto the negatively charged emulsified oil droplets via electrostatic attraction. Therefore, both electrostatic attraction and interfacial activity affect the sorption of MNPs onto oil droplets. As Lu et al. (Lü et al., 2018b) observed, even under acidic conditions, the pristine MNPs with positive surface charge could not be effectively adsorbed onto the negatively charged oil droplets, indicating that charge attraction is not a sufficient condition for efficient demulsification performance. Indeed, the demulsification performance could be highly attributed to the types of coating rather than pH conditions.

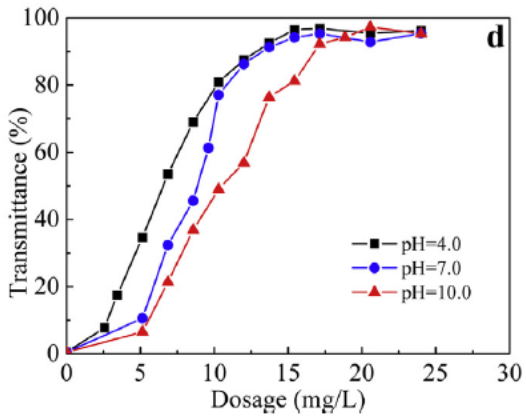

Figure 2. 11. Demulsification performance of Fe_3O_4@SiO_2-QC at different pH values (Lü et al., 2018c).

Because surface-active substances usually exist in oily wastewater either naturally or as an additive, the effect of surfactant concentration on emulsion stability should be assessed. As illustrated in Figure 2. 12, the emulsion becomes more stable by increasing the surfactant concentration, reducing the demulsification efficiency (Ko et al., 2014). For example, Zhao et al. (Zhao et al., 2019) observed that adding a higher concentration of SDS surfactant to the o/w resulted in a poor adsorption of MNPs at the oil-water interface. The adsorption of SDS molecules onto the oil droplet occurred through the oleophilic tail while the hydrophilic head was placed in the continuous phase making the oil droplet surfaces relatively hydrophilic. Some SDS molecules were desorbed from the oil droplets and attached to the MNPs, the electrostatic repulsion between

the oil droplets and MNPs could increase, resulting in a remarkable decrease in the demulsification efficiency (Shao, 2019; Zhang et al., 2012).

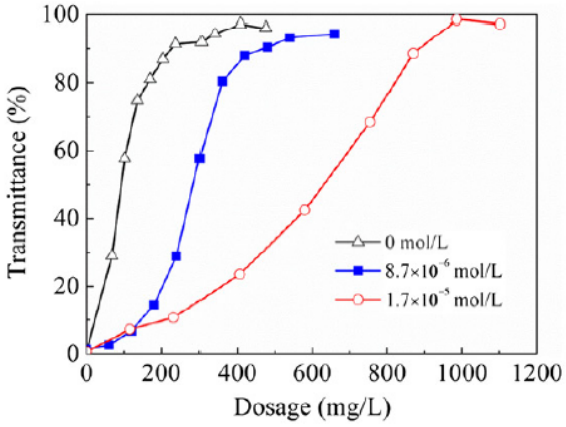

Figure 2. 12. The effect of SDS concentration on the demulsification efficiency (Zhao et al., 2019).

Emulsified oily wastewater commonly contains various types of salts; hence, it is essential to evaluate the influence of salinity/ionic strength on the demulsification efficiency. With salt addition, demulsification performance improves due to the electrostatic screening effect (Lü et al., 2018b) where the electrostatic repulsion between the MNPs and emulsified oil droplets reduces. Also, the hydration of salts enhances the hydrophobicity of the functionalized MNPs, favoring the adsorption of MNPs at the oil droplet surfaces (Mirshahghassemi et al., 2016). The mono- or divalent cations could neutralize the negative charge of the emulsified oil droplets in the emulsion, reducing the emulsion stability (Xu et al., 2019). Zhao et al. (Zhao et al., 2019) concluded that the effect of $CaCl_2$ on demulsification performance is more significant than that of NaCl (Figure 2. 13). The reason was that the electrostatic screening and hydration effects are more dominant for Ca^{2+} compared to Na^{+}.

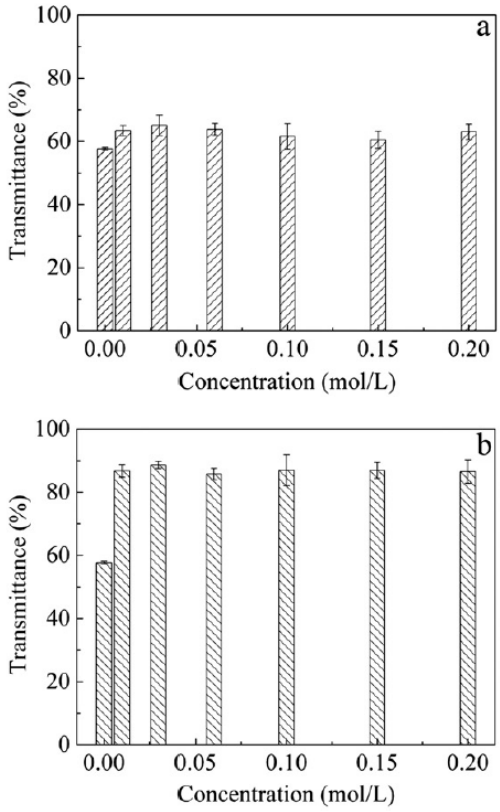

Figure 2. 13. The effect of NaCl (a) and $CaCl_2$ (b) concentration on the demulsification performance (Zhao et al., 2019).

The oil and water content of an emulsion affects the demulsification efficiency, since the electrostatic interaction at the oil-water interface depends on the pressure of both phases (Ali et al., 2015). For instance, in w/o, by increasing the water content, the internal pressure of the water phase is higher than that of the oil phase. So, increasing the water content decreases the demulsification time, leading to rapid demulsification. According to Figure 2. 14, the emulsion with a lower water content (w/o ratio of 5:5) features a better emulsion stability and interfacial film rigidity (Al-Sabagh et al., 2002). Wang et al. (Wang et al., 2018) observed that at a lower oil content in o/w systems, demulsification efficiency decreased due to higher external water pressure causing emulsion stability.

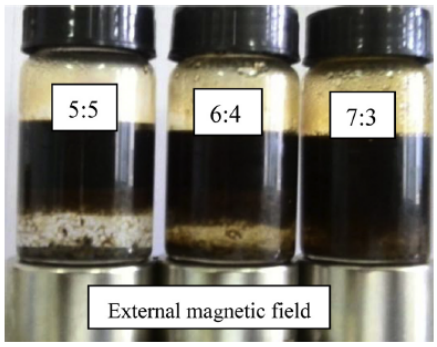

Figure 2. 14. Demulsification performance for different w/o ratios of 5:5, 6:4, and 7:3 (Ali et al., 2015).

2.4.4. Effect of MNP Properties

The characteristics of MNPs including size, concentration/dosage, wettability, and coating play critical roles in demulsification performance. Smaller MNPs have a larger contact surface area with the dispersed oil droplets (for o/w emulsion), which considerably influence the demulsification efficiency for a unit mass of MNPs (Lü et al., 2018a). However, the higher settling velocity of larger MNPs would be beneficial for improvement of separation efficiency (Ge et al., 2015). To the best of our knowledge, the effect of MNP size on the demulsification efficiency has not been analyzed.

The wettability state of MNPs is imposed by the coatings which significantly influence the demulsification performance (Zhang et al., 2017). Because the emulsified oil droplets in o/w are negatively charged, coatings with cationic functional groups are desirable. Munjal and Khare (Munjal and Khare, 2017) investigated the performance of functionalized cobalt ferrite ($CoFe_2O_4$) nanoparticles with hydrophobic OA and hydrophilic CA for demulsification of o/w and w/o, respectively. It was concluded that the hydrophobicity of the OA-CFO nanoparticles (with a water contact angle of 145°) could be attributed to the presence of -CH_3 groups in OA. The oleophilic OA-CFO nanoparticles containing -CH_3 exhibited an excellent separation efficiency for o/w by

maximizing the interfacial activity of nanoparticles. In contrary, the hydrophilic behavior of CA because of -COO^- functional group made the CA-CFO nanoparticles oleophobic and hydrophilic (with a water contact angle of 8°). This led to an excellent performance for MNPs to effectively separate w/o emulsion.

Although hydrophobic coatings on MNPs demonstrate a better demulsification performance in o/w systems, superhydrophobic MNPs are not suitable due to their poor dispersivity in the aqueous phase. To achieve efficient demulsification, the MNPs should have excellent dispersivity in water that can accumulate on the emulsified oil droplets (Lü et al., 2020; Lü et al., 2018c).

Liang et al. (Liang et al., 2014) studied the effect of MNP wettability on demulsification of cyclohexane-in-water nano-emulsion by using different amounts of OA to form a single layer on Fe_3O_4 nanoparticles. The hydrophobicity of the Fe_3O_4@OA increased by increasing the concentration of OA in the coating solution. As depicted in Figure 2. 15, by increasing the hydrophobicity of MNPs, demulsification efficiency initially increased and reached the highest amount at a contact angle of around 95° and then decreased. Hence, to achieve a higher demulsification efficiency for o/w, amphiphilic wetting conditions is desired to provide good dispersivity in the continuous phase and to allow their transfer to the oil droplet interfacial area (Lü et al., 2020).

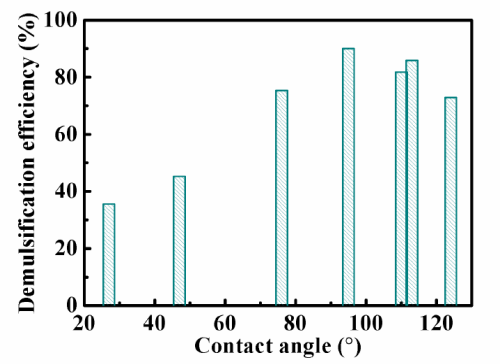

Figure 2. 15. The effect of wettability of Fe_3O_4@OA on cyclohexane-in-water demulsification (Liang et al., 2014).

The main factors affecting demulsification efficiency of MNPs are summarized in Table 2. 7.

Table 2. 7. Factors affecting MNP performance for demulsification.

Parameters		Impact on Demulsification Performance
Operational Conditions	Temperature	Increasing temperature improves demulsification performance for o/w and w/o because of • increased thermodynamic movement of interfacial molecules, • decreased interfacial viscosity, and • increased MNPs adsorption in the oil-water interface.
	Mixing time	Increasing mixing time improves demulsification performance for o/w and w/o because of • increased collision of MNPs and oil droplets, • increased particle aggregation, and • decreased demulsification time.

Fluid Properties	pH	Acidic and neutral conditions improve demulsification performance for o/w and w/o because of electrostatic attraction of the positively charged MNPs. Alkaline conditions decrease the separation efficiency because of strong electrostatic repulsion due to the negatively charged MNPs and zeta potential reduction.
	Salinity	Increasing salinity improves demulsification performance of o/w because of • reduced emulsion stability by neutralizing negatively charged oil droplets due to mono or divalent cations, • decreased electrostatic repulsion between MNPs and emulsified oil droplets, and • increased hydrophobicity of coated MNPs due to hydration of salts.
	Surfactant concentration	Increasing surfactant concentration decrease demulsification efficiency through IFT reduction, increased emulsion stability.
MNPs Features	Size	The effect of MNP size on emulsion stability is controversial.
	Concentration/ dosage	Increasing MNP dosage increases demulsification performance for both o/w and w/o up to a plateau/saturation.
	Wettability	Increasing MNP hydrophobicity improves demulsification efficiency of o/w and reaches its optimum performance at a contact angle of around 90°. The desirable wettability of MNPs for o/w emulsion is amphiphilic to provide a good dispersivity of MNPs in aqueous phase.

2.5. Challenges and Future Prospects of MNPs Application in Demulsification

The MNPs have a great potential to separate oil from emulsified oil-water mixtures. However, there are practical challenges in MNPs demulsification applications that need to be considered. For instance, the optimality of MNP synthesis method, loading, and magnetic field strength need to be further studied; recyclability, degradation, and regeneration efficiency of the MNPs are important factors that affect the sustainability of the process; and finally, toxicity is an important health hazard that need more attention (Zhang et al., 2013).

Despite significant technological advancements in MNPs synthesis, exploring a cost-efficient and eco-friendly methodology to develop desirable functionalized MNPs with promising and tunable features still remain an attractive research area. The optimal MNPs synthesis route needs to be developed to control the shape and size distribution of MNPs for attaining desirable physio-chemical properties. Furthermore, there are still challenges to engineer appropriate MNP coating chemistry and morphologies that provide high dispersivity, and long-term stability in harsh environments. For instance, the polymer- and silica-coated MNPs are not stable at high temperatures and under basic environment, respectively. Carbon coated MNPs show a high stability under harsh environments, but their dispersivity in o/w systems is a limiting factor.

Functionalized MNPs are only dispersible in organic solvents and are mostly non-dispersible in aqueous phases. Therefore, synthesis of functionalized MNPs with water dispersivity and using cheap eco-friendly materials such as surfactants would be an excellent option to overcome the dispersivity problems.

Most of the MNPs applications for demulsification are conducted at the laboratory scale; thus, their performance should be scaled up to pilot or industrial scales to assess their effectiveness for large-scale implementation. Parametric sensitivity analysis at a smaller scale is required to

minimize the practical challenges such as the optimum MNPs dosage or the feasibility of the MNPs recovery at larger scales. Cost-effective and facile synthesis of MNPs with environment-friendly functionalized materials is required for industrial applications to facilitate the recovery of MNPs at a larger scale. Reusability is an important factor for industrial applications that govern the sustainability and economy of the process. Thus, MNPs should be recycled for several cycles without significant changes to their structures and wetting characteristics to be able to maintain their performance.

One of the major concerns with using pristine MNPs is their low chemical resistance, resulting in oxidation, reduction, and/or dissolution. Also, there are environmental concerns with undesired release of the MNPs in the waste stream. Thus, the fate, toxicity, and degradability of the pristine and functionalized MNPs still need further investigations. Health and safety measures and evaluation (theoretical and practical) should be considered in a more effective manner. Biodegradable compounds with no harmful effects on the environment will be promising options to functionalize MNPs for future demulsification applications.

2.6. Summary

With increasing demand and consumption of oil in industrial and municipal activities, the volumes of oil-in-water emulsions (o/w) and water-in-oil emulsions (w/o) released to the environment have been increasing, resulting in environmental issues. Recently, a considerable attention has been focused on using magnetic nanoparticles (MNPs) with a high interfacial activity for demulsification. Large surface area, magnetic responsiveness, high adsorption capacity, economic aspect, low toxicity, thermal and chemical stabilities, and recovery/reusability are among features that make MNPs suitable options for separating emulsified contaminations. This literature review reveals excellent adsorption performance of MNPs in demulsification of both o/w and w/o

emulsions. The theory and background on MNPs, recent advancements in the synthesis of surface modified MNPs and their applications, and oil-water separation mechanisms are discussed in detail. The key concluding remarks of this review are as follows:

- The emulsion stability is highly affected by different variables such as droplet size, zeta potential, and oil-water interfacial film properties. Among these, droplet size is the most important criterion in controlling emulsion stability.
- Smaller interfacial area and less energy exchange of smaller droplets result in less flocculation and coalescence of droplets and increase the emulsion stability. Moreover, more stability of smaller emulsion droplets is because of the higher internal (Laplace) pressure developing from the oil-water interfacial tension (IFT).
- The thickness and rigidity of the interfacial film control the emulsion stability; a thicker interfacial film enhances the film drainage time and decreases the rate of demulsification. IFT reduction by increasing the similarities between intramolecular forces of the oil and water phases reduces the rate of droplet flocculation and coalescence.
- Lower zeta potential values imply less emulsion stability, resulting from decreasing electrostatic repulsion between adjacent droplets and consequently increasing flocculation rate.
- Demulsification occurs through enhancing flocculation rate, IFT, temperature, and the contact time, or reducing viscosity and applied shear stress.
- Chemical demulsifiers cause demulsification through increasing IFT, decreasing elasticity and viscosity of droplets, and reducing interfacial film thickness due to film drainage. Despite the success of the chemical demulsifiers in breaking emulsions, they generate secondary pollution. MNPs are considered as a chemical demulsifier with high oil

adsorption capacity and suitable reusability and recovery, without producing secondary contaminants.

- MNPs should have a good dispersivity in the continuous phase to be effectively recycled by applying the external magnetic force, which is required to be stronger than the other competing forces of drag and gravity. Therefore, alteration of the MNP surface wettability through coating is required. More importantly, a protective coating layer is required to overcome the intrinsic instability of MNPs, and to prevent their agglomeration, precipitation, oxidation, and thereby loss of magnetism.
- The functional groups can improve the physio-chemical properties of MNPs by changing the surface wettability of MNPs. Various types of MNPs structures are developed through surface coating/chemical grafting such as core-shell, shell-core-shell, Janus, and dendritic/hyperbranched structures. The latter exhibits higher oil adsorption capacity, while the dendrimers with adsorbed oil droplets show a difficulty in being effectively collected and recycled.
- The demulsification mechanisms in using MNPs are based on physical and chemical adsorption through the electrostatic attraction and interfacial activity between the oil droplets and MNPs. However, the electrostatic attractions between the negatively charged oil droplets and the positively charged MNPs are considered as the main mechanism. Indeed, interfacial activity is considered as the significant driving force for oil-water separation when electrostatic force is rarely involved.
- The electrostatic attraction applies through strong magnetic dipole-dipole attraction along with van der Waals interactions between the negatively charged oil droplets and positively charged MNPs. Therefore, applying cationic surfactant with a positive surface charge

results in a higher demulsification efficiency compared to anionic surfactant with negative surface charge.

- Interfacial activities or surface interactions between the oil droplets and functionalized MNPs increase the rate of oil separation. These interactions are attributed to the MNPs wettability resulted from MNPs coating using different compounds.
- The desirable MNPs wettability to be used in demulsification is amphiphilic with both hydrophilic and oleophilic properties to provide a good dispersibility of MNPs in the continuous phase. The amphiphilic MNPs provide high interfacial activity between the oil droplets and coated MNPs, leading to higher demulsification efficiency.
- Demulsification efficiency using MNPs is directly affected by temperature, mixing time, and salt concentration/content of the fluid, while it is inversely impacted by the pH and surfactant concentration in the emulsions.
- Improved demulsification performance at a higher temperature is due to increased movement of interfacial molecules and decreased interfacial viscosity. More mixing time provides greater collisions of MNPs and oil droplets, thereby increasing the oil adsorption efficiency. Higher salinity leads to lowering emulsion stability and electrostatic attraction between the MNPs and oil droplets through neutralizing negatively charged oil droplets, respectively.
- Emulsion pH impacts the surface charge of MNPs by changing zeta potential. Increasing emulsion pH decreases zeta potential of MNPs, results in changing the surface charge of MNPs from positive to negative, thereby it reduces demulsification efficiency. However, acidic and neutral conditions improve demulsification performance due to electrostatic attraction of positively charged MNPs.

- The effect of MNPs size is controversial as the larger size of MNPs with a higher settling velocity can increase the separation efficiency. In contrast, the smaller MNPs can achieve a better performance by providing a larger contact area with oil droplets. However, the MNPs features such as surface and interfacial effects become more pronounced in smaller MNPs because of exposure to a larger surface area per MNP loading unit. The magnetic particles perform best when their size is smaller than a critical value that is typically around 10–20 nm, depending on the type of material.
- The MNPs dosage directly affects demulsification efficiency to reach a plateau/saturation. Indeed, an optimum MNP concentration should be used for demulsification. Hence, an excessive MNPs concentration may adversely affect the oil/water separation performance.

Declaration of competing interest

The authors declare that they have no known competing financial interests or personal relationships that could have appeared to influence the work reported in this paper.

Data availability

No data was used for the research described in the article.

ACKNOWLEDGEMENTS

The financial support of Suncor Energy Inc. /Terra Nova Young Innovator, Memorial University (Canada), and the Natural Sciences and Engineering Research Council of Canada (NSERC) is acknowledged.

NOMENCLATURES

Acronyms

AA	-	Acrylic Acid

AEAPFS	-	N-(aminoethyl)-aminopropyl Functionalized Silica
AFM	-	Atomic Force Microscope
AGM	-	Alternating Gradient Magnetometer
AI	-	Artificial Intelligence
AIBI	-	2,2-Azobis[2-(2-imidazolin-2-yl) propane] Dihydrochloride
ANN	-	Artificial Neural Network
APFS	-	Aminopropyl-functionalized Silica
APTES	-	3-aminopropyltriethoxysilane
BET	-	Brunauer-Emmet-Teller
BJH	-	Barrett, Joyner and Halenda
BTEX	-	Benzene, Toluene, Ethylbenzene, Xylene
CA	-	Citric Acid
Ca	-	Capillary Number
CFO	-	Cobalt Ferrite
CMC	-	Carboxymethyl Cellulose
CMC	-	Critical Micelle Concentration
CO	-	Carbon Monoxide
CTAB	-	Cetyltrimethylammonium Bromide
DLS	-	Dynamic Light Scattering
DM	-	Diatomite
DSC	-	Differential Scanning Calorimetry
EA	-	Elemental Analyzer
EA	-	Elaidic Acid
EC	-	Ethyl Cellulose
EDX	-	Energy Dispersive X-ray
EM	-	Emulsion
FESEM	-	Fieal Emission Scanning Electron Microscopy
FTIR	-	Fourier Transform Infrared Spectroscopy

GO	-	Graphene Oxide
GA	-	Genetic Algorithm
GPC	-	Gel permeation chromatography
HA	-	Humic Acid
HLB	-	Hydrophilic-lipophilic Balance
ICP	-	Inductively Coupled Plasma
IFT	-	Interfacial Tension
LSSVM	-	Least Squares Support Vector Machines
MA	-	Myristic Acid
MAC	-	Magnetic Amphiprotic Catalyst
MD	-	Molecular Dynamic
MFS	-	Magnetic Field Strength
MNPs	-	Magnetic Nanoparticles
MPS	-	3- (trimethoxysilyl) Propyl Methacrylate
MS	-	Magnetic Saturation
NaSal	-	Natrium Salicylicum
NMR	-	Nuclear Magnetic Resonance
NTA	-	Nanoparticle Tracking Analysis
NZS	-	Nano Zetasizer
o/w	-	Oil in Water
OA	-	Oleic Acid
OCA	-	Optical Contact Angle
ODA	-	Octadecylamine
ODMS	-	Octadecyl Trimethoxysilane
ODTMS	-	Organic Tethers, Trimethoxy(octadecyl)silane
OM	-	Optical Microscope
OR	-	Oil Recovery
OTS	-	Trichloro(octadecyl)silane

P(MMA-AA-DVB)	-	Poly (methylmethacrylate-acrylicacid-divinylbenzene)
PA	-	Palmitic Acid
PAA	-	polyacrylic acid
PDA	-	Polydopamine
PDDA	-	Poly dimethyldiallylammonium Chloride
PDMAEMA	-	Poly[2-(dimethylamino) ethyl methacrylate]
PDMAPS	-	Poly[[3-[dimethyl(2-methacryloyloxyethyl) ammonio] propanesulfonate]]
PEI	-	Polyethyleneimine
P-EM	-	Pickering Emulsion
PEO	-	Poly(ethylene oxide)
PMMA	-	Poly(methyl methacrylate)
POM	-	Polarized Optical Microscopy
PPMS	-	Physical Property Measurement System
PSA	-	Particle Size Analyzer
PSO	-	Particle Swarm Optimization
PVP	-	Polyvinylpyrrolidone
QC	-	Quaternized Chitosan
Re	-	Reynolds Number
RSM	-	Response Surface Methodology
SA	-	Stearic Acid
SAXS	-	Small-angle X-ray Scattering
SEM	-	Scanning Electron Microscopy
SDS	-	Sodium Dodecyl Sulfate
SPS	-	γ-mercaptopropyltriethoxysilane
SQUID	-	Superconducting quantum interference device
St/DVB	-	Styrene/divinyl Benzene
STEM	-	Scanning Transmission Electron Microscopy
TEM	-	Transmission Electron Microscopy

TEOS	-	Tetraethylorthosilicate
TGA	-	Thermogravimetric Analysis
VSM	-	Vibrating sample Magnetometer
We	-	Weber Number
w/o	-	Water in Oil
WT	-	Water Transmittance
XPS	-	X-ray Photoelectron Spectroscopy
XRD	-	X-ray Diffraction

References

Abdulbari, H., Nour, A., Rosli, Y., Mahmood, W., Nour, A., 2011. Demulsification of petroleum emulsions Using microwave separation method. International Journal of the Physical Sciences 0.66.

Adeyanju, O.A., Oyekunle, L.O., 2019. Optimization of chemical demulsifications of water in crude oil emulsions. Egyptian Journal of Petroleum 28(4), 349-353.

Al-Sabagh, A.M., Badawi, A.M., Noor El-Den, M.R., 2002. BREAKING WATER-IN-CRUDE OIL EMULSIONS BY NOVEL DEMULSIFIERS BASED ON MALEIC ANHYDRIDE–OLEIC ACID ADDUCT. Petroleum Science and Technology 20(9-10), 887-914.

Ali, N., Bilal, M., Khan, A., Ali, F., Yang, Y., Khan, M., Adil, S.F., Iqbal, H.M.N., 2020. Dynamics of oil-water interface demulsification using multifunctional magnetic hybrid and assembly materials. Journal of Molecular Liquids 312, 113434.

Ali, N., Zaman, H., Bilal, M., Shah, A.-u.-H.A., Nazir, M.S., Iqbal, H.M.N., 2019. Environmental perspectives of interfacially active and magnetically recoverable composite materials – A review. Science of The Total Environment 670, 523-538.

Ali, N., Zhang, B., Zhang, H., Zaman, W., Li, X., Li, W., Zhang, Q., 2015. Interfacially active and magnetically responsive composite nanoparticles with raspberry like structure; synthesis and its applications for heavy crude oil/water separation. Colloids and Surfaces A: Physicochemical and Engineering Aspects 472, 38-49.

Asthana, A., Verma, R., Singh, A.K., Susan, M.A.B.H., 2016. Glycine functionalized magnetic nanoparticle entrapped calcium alginate beads: A promising adsorbent for removal of Cu(II) ions. Journal of Environmental Chemical Engineering 4(2), 1985-1995.

Attallah, O.A., Girgis, E., Abdel-Mottaleb, M.M.S.A., 2016. Tailored super magnetic nanoparticles synthesized via template free hydrothermal technique. Journal of Magnetism and Magnetic Materials 397, 164-175.

Bhavani, P., Rajababu, C.H., Arif, M.D., Reddy, I.V.S., Reddy, N.R., 2017. Synthesis of high saturation magnetic iron oxide nanomaterials via low temperature hydrothermal method. Journal of Magnetism and Magnetic Materials 426, 459-466.

Cabrera, L., Gutierrez, S., Menendez, N., Morales, M.P., Herrasti, P., 2008. Magnetite nanoparticles: Electrochemical synthesis and characterization. Electrochimica Acta 53(8), 3436-3441.

Campos, E.A., Pinto, D.V.B.S., Oliveira, J.I.S.d., Mattos, E.d.C., Dutra, R.d.C.L., 2015. Synthesis, Characterization and Applications of Iron Oxide Nanoparticles - a Short Review. Journal of Aerospace Technology and Management 7, 267-276.

Cao, H., Li, J., Shen, Y., Li, S., Huang, F., Xie, A., 2014. Green synthesis and surface properties of Fe3O4@SA core–shell nanocomposites. Applied Surface Science 301, 244-249.

Chen, H.-J., Hang, T., Yang, C., Liu, G., Lin, D.-a., Wu, J., Pan, S., Yang, B.-r., Tao, J., Xie, X., 2018. Anomalous dispersion of magnetic spiky particles for enhanced oil emulsions/water separation. Nanoscale 10(4), 1978-1986.

Chen, K., He, J., Li, Y., Cai, X., Zhang, K., Liu, T., Hu, Y., Lin, D., Kong, L., Liu, J., 2017. Removal of cadmium and lead ions from water by sulfonated magnetic nanoparticle adsorbents. Journal of Colloid and Interface Science 494, 307-316.

Chen, Y., Tian, G., Liang, H., Liang, Y., 2019. Synthesis of magnetically responsive hyperbranched polyamidoamine based on the graphene oxide: Application as demulsifier for oil-in-water emulsions. International Journal of Energy Research 43(9), 4756-4765.

Deng, D., Prendergast, D.P., MacFarlane, J., Bagatin, R., Stellacci, F., Gschwend, P.M., 2013. Hydrophobic meshes for oil spill recovery devices. ACS Appl Mater Interfaces 5(3), 774-781.

Duan, C., Zhu, T., Guo, J., Wang, Z., Liu, X., Wang, H., Xu, X., Jin, Y., Zhao, N., Xu, J., 2015. Smart Enrichment and Facile Separation of Oil from Emulsions and Mixtures by Superhydrophobic/Superoleophilic Particles. ACS Applied Materials & Interfaces 7(19), 10475-10481.

Eow, J.S., Ghadiri, M., Sharif, A.O., Williams, T.J., 2001. Electrostatic enhancement of coalescence of water droplets in oil: a review of the current understanding. Chemical Engineering Journal 84(3), 173-192.

Feng, X., Xu, Z., Masliyah, J., 2009. Biodegradable Polymer for Demulsification of Water-in-Bitumen Emulsions. Energy & Fuels 23(1), 451-456.

Fortuny, M., Oliveira, C.B.Z., Melo, R.L.F.V., Nele, M., Coutinho, R.C.C., Santos, A.F., 2007. Effect of Salinity, Temperature, Water Content, and pH on the Microwave Demulsification of Crude Oil Emulsions. Energy & Fuels 21(3), 1358-1364.

Fossati, A., Martins Alho, M., Jacobo, S.E., 2019. Covalent functionalized magnetic nanoparticles for crude oil recovery. Materials Chemistry and Physics 238, 121910.

Ge, S., Agbakpe, M., Zhang, W., Kuang, L., 2015. Heteroaggregation between PEI-Coated Magnetic Nanoparticles and Algae: Effect of Particle Size on Algal Harvesting Efficiency. ACS Applied Materials & Interfaces 7(11), 6102-6108.

Goodarzi, F., Zendehboudi, S., 2019. A Comprehensive Review on Emulsions and Emulsion Stability in Chemical and Energy Industries. The Canadian Journal of Chemical Engineering 97(1), 281-309.

Grein-Iankovski, A., Loh, W., 2020. Modulating the interfacial properties of magnetic nanoparticles through surface modification with a binary polymer mixture towards stabilization of double emulsions. Colloids and Surfaces A: Physicochemical and Engineering Aspects 586, 124208.

Griffin, W.C., 1949. Classification of Surface-Active Agents by "HLB". . The Journal of the Society of Cosmetic Chemists 1, 311-326.

Gupta, A.K., Gupta, M., 2005. Synthesis and surface engineering of iron oxide nanoparticles for biomedical applications. Biomaterials 26(18), 3995-4021.

He, M., Wei, Y., Wang, R., Wang, C., Zhang, B., Han, L., 2019. Boronate affinity magnetic nanoparticles with hyperbranched polymer brushes for the adsorption of cis-diol biomolecules. Microchimica Acta 186(10), 683.

He, X., 2020. Interfacially Active Magnetic Nanoparticles for Efficient Oil/Water Separation from Oil-in-Water or Water-in-Oil Emulsions. Alberta, p. 217.

Hong, R.Y., Zhang, S.Z., Di, G.Q., Li, H.Z., Zheng, Y., Ding, J., Wei, D.G., 2008. Preparation, characterization and application of Fe3O4/ZnO core/shell magnetic nanoparticles. Materials Research Bulletin 43(8), 2457-2468.

Hu, Z., Nourafkan, E., Gao, H., Wen, D., 2017. Microemulsions stabilized by in-situ synthesized nanoparticles for enhanced oil recovery. Fuel 210, 272-281.

Ichikawa, T., Itoh, K., Yamamoto, S., Sumita, M., 2004. Rapid demulsification of dense oil-in-water emulsion by low external electric field: I. Experimental evidence. Colloids and Surfaces A: Physicochemical and Engineering Aspects 242(1), 21-26.

Ingham, B., 2015. X-ray scattering characterisation of nanoparticles. Crystallography Reviews 21(4), 229-303.

Issaka, S., Nour, A., Yunus, R.b.M., 2015. Review on the Fundamental Aspects of Petroleum Oil Emulsions and Techniques of Demulsification. Journal of Petroleum & Environmental Biotechnology 6, 1-15.

Khan, I., Saeed, K., Khan, I., 2019. Nanoparticles: Properties, applications and toxicities. Arabian Journal of Chemistry 12(7), 908-931.

Ko, S., Kim, E.S., Park, S., Daigle, H., Milner, T.E., Huh, C., Bennetzen, M.V., Geremia, G.A., 2016. Oil Droplet Removal from Produced Water Using Nanoparticles and Their Magnetic Separation, SPE Annual Technical Conference and Exhibition. Society of Petroleum Engineers, Dubai, UAE, p. 18.

Ko, S., Prigiobbe, V., Huh, C., Bryant, S.L., Bennetzen, M.V., Mogensen, K., 2014. Accelerated Oil Droplet Separation from Produced Water Using Magnetic Nanoparticles, SPE Annual Technical Conference and Exhibition. Society of Petroleum Engineers, Amsterdam, The Netherlands, p. 14.

Kokal, S.L., 2005. Crude Oil Emulsions: A State-Of-The-Art Review. SPE Production & Facilities 20(01), 5-13.

Kwon Kaang, B., Han, N., Jang, W., Young Koo, H., Boo Lee, Y., San Choi, W., 2018. Crossover magnetic amphiprotic catalysts for oil/water separation, the purification of aqueous and non-aqueous pollutants, and organic synthesis. Chemical Engineering Journal 331, 290-299.

Lesiak, B., Rangam, N., Jiricek, P., Gordeev, I., Tóth, J., Kövér, L., Mohai, M., Borowicz, P., 2019. Surface Study of Fe3O4 Nanoparticles Functionalized With Biocompatible Adsorbed Molecules. Frontiers in chemistry 7(642).

Li, W., Zhang, L., Ge, X., Xu, B., Zhang, W., Qu, L., Choi, C.-H., Xu, J., Zhang, A., Lee, H., Weitz, D.A., 2018. Microfluidic fabrication of microparticles for biomedical applications. Chemical Society Reviews 47(15), 5646-5683.

Li, Y., Liu, J., Fu, Y., Xie, Q., Li, Y., 2019. Correction to: Magnetic-core@dual-functional-shell nanocomposites with peroxidase mimicking properties for use in colorimetric and electrochemical sensing of hydrogen peroxide. Microchimica Acta 186.

Li, Y., Liu, Y., Tang, J., Lin, H., Yao, N., Shen, X., Deng, C., Yang, P., Zhang, X., 2007. Fe3O4@Al2O3 magnetic core–shell microspheres for rapid and highly specific capture of phosphopeptides with mass spectrometry analysis. Journal of Chromatography A 1172(1), 57-71.

Liang, C., He, X., Liu, Q., Xu, Z., 2018. Adsorption-Based Synthesis of Magnetically Responsive and Interfacially Active Composite Nanoparticles for Dewatering of Water-in-Diluted Bitumen Emulsions. Energy & Fuels 32(8), 8078-8089.

Liang, J., Du, N., Song, S., Hou, W., 2015. Magnetic demulsification of diluted crude oil-in-water nanoemulsions using oleic acid-coated magnetite nanoparticles. Colloids and Surfaces A: Physicochemical and Engineering Aspects 466, 197-202.

Liang, J., Li, H., Yan, J., Hou, W., 2014. Demulsification of Oleic-Acid-Coated Magnetite Nanoparticles for Cyclohexane-in-Water Nanoemulsions. Energy & Fuels 28(9), 6172-6178.

Lin, K.-Y.A., Yang, H., Petit, C., Lee, W.-d., 2015. Magnetically controllable Pickering emulsion prepared by a reduced graphene oxide-iron oxide composite. Journal of Colloid and Interface Science 438, 296-305.

Lin, Y., Yang, Y., Shan, Y., Gong, L., Chen, J., Li, S., Chen, L., 2017. Magnetic Nanoparticle-Assisted Tunable Optical Patterns from Spherical Cholesteric Liquid Crystal Bragg Reflectors. Nanomaterials (Basel, Switzerland) 7(11), 376.

Liu, Z., Yang, H., Zhang, H., Huang, C., Li, L., 2012. Oil-field wastewater purification by magnetic separation technique using a novel magnetic nanoparticle. Cryogenics 52(12), 699-703.

Low, L.E., Ooi, C.W., Chan, E.S., Ong, B.H., Tey, B.T., 2020. Dual (magnetic and pH) stimuli-reversible Pickering emulsions based on poly(2-(dimethylamino)ethyl methacrylate)-bonded Fe3O4 nanocomposites for oil recovery application. Journal of Environmental Chemical Engineering 8(2), 103715.

Lozano, I., Casillas, N., de León, C.P., Walsh, F.C., Herrasti, P., 2017. New Insights into the Electrochemical Formation of Magnetite Nanoparticles. Journal of The Electrochemical Society 164(4), D184-D191.

Lu, A.-H., Salabas, E.L., Schüth, F., 2007. Magnetic Nanoparticles: Synthesis, Protection, Functionalization, and Application. Angewandte Chemie International Edition 46(8), 1222-1244.

Lü, T., Chen, Y., Qi, D., Cao, Z., Zhang, D., Zhao, H., 2017. Treatment of emulsified oil wastewaters by using chitosan grafted magnetic nanoparticles. Journal of Alloys and Compounds 696, 1205-1212.

Lü, T., Qi, D., Zhang, D., Fu, K., Li, Y., Zhao, H., 2020. Fabrication of recyclable multi-responsive magnetic nanoparticles for emulsified oil-water separation. Journal of Cleaner Production 255, 120293.

Lü, T., Qi, D., Zhang, D., Lin, S., Mao, Y., Zhao, H., 2018a. Facile synthesis of N-(aminoethyl)-aminopropyl functionalized core-shell magnetic nanoparticles for emulsified oil-water separation. Journal of Alloys and Compounds 769, 858-865.

Lü, T., Qi, D., Zhang, D., Lü, Y., Zhao, H., 2018b. A facile method for emulsified oil-water separation by using polyethylenimine-coated magnetic nanoparticles. Journal of Nanoparticle Research 20(4), 88.

Lü, T., Zhang, S., Qi, D., Zhang, D., Zhao, H., 2018c. Enhanced demulsification from aqueous media by using magnetic chitosan-based flocculant. Journal of Colloid and Interface Science 518, 76-83.

Lu, Y., Yin, Y., Mayers, B.T., Xia, Y., 2002. Modifying the Surface Properties of Superparamagnetic Iron Oxide Nanoparticles through A Sol−Gel Approach. Nano Letters 2(3), 183-186.

Mao, X., Gong, L., Xie, L., Qian, H., Wang, X., Zeng, H., 2019. Novel Fe3O4 based superhydrophilic core-shell microspheres for breaking asphaltenes-stabilized water-in-oil emulsion. Chemical Engineering Journal 358, 869-877.

McClements, D., 2007. Critical Review of Techniques and Methodologies for Characterization of Emulsion Stability. Critical reviews in food science and nutrition 47, 611-649.

McClements, D.J., Jafari, S.M., 2018. Improving emulsion formation, stability and performance using mixed emulsifiers: A review. Advances in Colloid and Interface Science 251, 55-79.

Mi, T., Cai, Y., Wang, Q., Habibul, N., Ma, X., Su, Z., Wu, W., 2020. Synthesis of Fe3O4 nanocomposites for efficient separation of ultra-small oil droplets from hexadecane–water emulsions. RSC Advances 10(17), 10309-10314.

Milton, J.R., Joy, T.K., 2012. Characteristic Features of Surfactants. Surfactants and Interfacial Phenomena, 1-38.

Mirshahghassemi, S., Cai, B., Lead, J.R., 2016. Evaluation of polymer-coated magnetic nanoparticles for oil separation under environmentally relevant conditions: effect of ionic strength and natural organic macromolecules. Environmental Science: Nano 3(4), 780-787.

Mohammed, L., Gomaa, H.G., Ragab, D., Zhu, J., 2017. Magnetic nanoparticles for environmental and biomedical applications: A review. Particuology 30, 1-14.

Munjal, S., Khare, N., 2017. Transforming single domain magnetic CoFe2O4 nanoparticles from hydrophobic to hydrophilic by novel mechanochemical ligand exchange. Journal of Nanoparticle Research 19(1), 18.

Murray, C.D., 2014. Durability of Silane Sealer in a Highly Alkaline Environment, Civil Engineering. University of Arkansas, Fayetteville.

Mutyala, S., Fairbridge, C., Pare, J.R.J., Belanger, J., Ng, S., Hawkins, R., 2010. Microwave applications to oil sands and petroleum: A review. Fuel Processing Technology - FUEL PROCESS TECHNOL 91, 127-135.

Nazifa, T.H., Islam, R., Salmiati, Uddin, A.S.M.S., Hadibarata, T., Aris, A., 2018. Fast and Efficient Removal of Oil from Water Surface Through Activated Carbon and Iron Oxide-Magnetic Nanocomposite, 2018 2nd International Conference on Green Energy and Applications (ICGEA). pp. 263-267.

Niculescu, A.-G., Chircov, C., Grumezescu, A.M., 2022. Magnetite nanoparticles: Synthesis methods – A comparative review. Methods 199, 16-27.

Omidinasab, M., Rahbar, N., Ahmadi, M., Kakavandi, B., Ghanbari, F., Kyzas, G., Silva Martínez, S., Jaafarzadeh, N., 2018. Removal of vanadium and palladium ions by adsorption onto magnetic chitosan nanoparticles. Environmental Science and Pollution Research 25.

Peña, A.A., Hirasaki, G.J., Miller, C.A., 2005. Chemically Induced Destabilization of Water-in-Crude Oil Emulsions. Industrial & Engineering Chemistry Research 44(5), 1139-1149.

Petschacher, C., Eitzlmayr, A., Besenhard, M., Wagner, J., Barthelmes, J., Bernkop-Schnürch, A., Khinast, J.G., Zimmer, A., 2013. Thinking continuously: a microreactor for the production and scale-up of biodegradable, self-assembled nanoparticles. Polymer Chemistry 4(7), 2342-2352.

Qiao, K., Tian, W., Bai, J., Wang, L., Zhao, J., Du, Z., Gong, X., 2019. Application of magnetic adsorbents based on iron oxide nanoparticles for oil spill remediation: A review. Journal of the Taiwan Institute of Chemical Engineers 97, 227-236.

Rahimdad, N., Khalaj, A., Azarian, G., Nematollahi, D., 2019. Electrochemical Device for the Synthesis of Fe₃O₄ Magnetic Nanoparticles. Journal of The Electrochemical Society 166(2), E1-E6.

Rahmawati, R., Permana, M.G., Harison, B., Nugraha, Yuliarto, B., Suyatman, Kurniadi, D., 2017. Optimization of Frequency and Stirring Rate for Synthesis of Magnetite (Fe3O4) Nanoparticles by Using Coprecipitation- Ultrasonic Irradiation Methods. Procedia Engineering 170, 55-59.

Rasouli, S., Rezaei, N., Hamedi, H., Zendehboudi, S., Duan, X., 2021a. Design, fabrication, and characterization of a facile superhydrophobic and superoleophilic mesh-based membrane for selective oil-water separation. Chemical Engineering Science 236, 116354.

Rasouli, S., Rezaei, N., Hamedi, H., Zendehboudi, S., Duan, X., 2021b. Superhydrophobic and superoleophilic membranes for oil-water separation application: A comprehensive review. Materials & Design 204, 109599.

Shao, S.L., Y.; Lü, T.; Qi, D.; Zhang, D.; Zhao, H. , 2019. Removal of Emulsified Oil from Aqueous Environment by Using Polyvinylpyrrolidone-Coated Magnetic Nanoparticles. Water 19(10).

Shipunova, V.O., Kotelnikova, P.A., Aghayeva, U.F., Stremovskiy, O.A., Schulga, A.A., Nikitin, M.P., Deyev, S.M., 2018. Data on characterization of magnetic nanoparticles stabilized with fusion protein of Barstar and C-term part of Mms6. Data in Brief 21, 1659-1663.

Silva, V.A.J., Andrade, P.L., Silva, M.P.C., Bustamante D, A., De Los Santos Valladares, L., Albino Aguiar, J., 2013. Synthesis and characterization of Fe3O4 nanoparticles coated with fucan polysaccharides. Journal of Magnetism and Magnetic Materials 343, 138-143.

Simonsen, G., Strand, M., Øye, G., 2018. Potential applications of magnetic nanoparticles within separation in the petroleum industry. Journal of Petroleum Science and Engineering 165, 488-495.

Song, Y., Zhou, J., Fan, J.-B., Zhai, W., Meng, J., Wang, S., 2018. Hydrophilic/Oleophilic Magnetic Janus Particles for the Rapid and Efficient Oil–Water Separation. Advanced Functional Materials 28(32), 1802493.

Stachurski, Michálek, 1996. The Effect of the zeta Potential on the Stability of a Non-Polar Oil-in-Water Emulsion. J. Colloid Interface Sci. 184 2, 433-436.

Su, C., 2017. Environmental implications and applications of engineered nanoscale magnetite and its hybrid nanocomposites: A review of recent literature. Journal of Hazardous Materials 322, 48-84.

Tadros, T.F., 2009. Emulsion Science and Technology: A General Introduction. Emulsion Science and Technology, 1-56.

Tago, T., Hatsuta, T., Miyajima, K., Kishida, M., Tashiro, S., Wakabayashi, K., 2002. Novel Synthesis of Silica-Coated Ferrite Nanoparticles Prepared Using Water-in-Oil Microemulsion. Journal of the American Ceramic Society 85(9), 2188-2194.

Tayefeh, A., Poursalehi, R., Wiesner, M., Mousavi, S.A., 2019. XPS study of size effects of Fe3O4 nanoparticles on crosslinking degree of magnetic TFN membrane. Polymer Testing 73, 232-241.

Turbeville, J., 1973. Ferromagnetic sorbents for oil spill recovery and control. Environmental science & technology 7(5), 433-438.

Waller, G.H., Martin, C.A., Jones, N.J., Paynter, D.M., 2019. Treatment of oil-in-saltwater emulsions by in-situ production of magnetic FeOx nanoparticles. Journal of Water Process Engineering 31, 100851.

Wang, B., Wei, Y., Wang, Q., Di, J., Miao, S., Yu, J., 2020. Superhydrophobic magnetic core–shell mesoporous organosilica nanoparticles with dendritic architecture for oil–water separation. Materials Chemistry Frontiers 4(7), 2184-2191.

Wang, C., Fang, S., Duan, M., Xiong, Y., Ma, Y., Chen, W., 2015. Synthesis and evaluation of demulsifiers with polyethyleneimine as accepter for treating crude oil emulsions. Polymers for Advanced Technologies 26(5), 442-448.

Wang, Q., Puerto, M.C., Warudkar, S., Buehler, J., Biswal, S.L., 2018. Recyclable amine-functionalized magnetic nanoparticles for efficient demulsification of crude oil-in-water emulsions. Environmental Science: Water Research & Technology 4(10), 1553-1563.

Wang, X., Shi, Y., Graff, R.W., Lee, D., Gao, H., 2015. Developing recyclable pH-responsive magnetic nanoparticles for oil–water separation. Polymer 72, 361-367.

Wu, J., Xu, Y., Dabros, T., Hamza, H., 2003. Effect of Demulsifier Properties on Destabilization of Water-in-Oil Emulsion. Energy & Fuels 17(6), 1554-1559.

Xu, H., Wang, J., Ren, S., 2019. Removal of Oil from a Crude Oil-in-Water Emulsion by a Magnetically Recyclable Diatomite Demulsifier. Energy & Fuels 33(11), 11574-11583.

Yang, H., Hou, Q., Wang, S., Guo, D., Hu, G., Xu, Y., Tai, J., Wu, X., Yu, D., Wang, J., 2018. Magnetic-responsive switchable emulsions based on Fe3O4@SiO2–NH2 nanoparticles. Chemical Communications 54(76), 10679-10682.

Yang, Y., Fang, Z., Chen, X., Zhang, W., Xie, Y., Chen, Y., Liu, Z., Yuan, W., 2017. An Overview of Pickering Emulsions: Solid-Particle Materials, Classification, Morphology, and Applications. Frontiers in Pharmacology 8(287).

Zhang, J., Li, L., Wang, J., Sun, H., Xu, J., Sun, D., 2012. Double Inversion of Emulsions Induced by Salt Concentration. Langmuir : the ACS journal of surfaces and colloids 28(17), 6769-6775.

Zhang, J., Li, Y., Bao, M., Yang, X., Wang, Z., 2016. Facile Fabrication of Cyclodextrin-Modified Magnetic Particles for Effective Demulsification from Various Types of Emulsions. Environmental Science & Technology 50(16), 8809-8816.

Zhang, L., Liu, P., Wang, T., 2011. Preparation of superparamagnetic polyaniline hybrid hollow microspheres in oil/water emulsion with magnetic nanoparticles as cosurfactant. Chemical Engineering Journal 171(2), 711-716.

Zhang, S., Lü, T., Qi, D., Cao, Z., Zhang, D., Zhao, H., 2017. Synthesis of quaternized chitosan-coated magnetic nanoparticles for oil-water separation. Materials Letters 191, 128-131.

Zhang, W., Liang, J., Lu, X., Ren, W., Liu, C., 2020. Nanoparticle Tracking Analysis-Based In Vitro Detection of Critical Biomarkers. ACS Applied Nano Materials 3(3), 2881-2888.

Zhang, W., Shi, Z., Zhang, F., Liu, X., Jin, J., Jiang, L., 2013. Superhydrophobic and Superoleophilic PVDF Membranes for Effective Separation of Water-in-Oil Emulsions with High Flux. Advanced Materials 25(14), 2071-2076.

Zhao, H., Zhang, C., Qi, D., Lü, T., Zhang, D., 2019. One-Step Synthesis of Polyethylenimine-Coated Magnetic Nanoparticles and its Demulsification Performance in Surfactant-Stabilized Oil-in-Water Emulsion. Journal of Dispersion Science and Technology 40(2), 231-238.

Zhou, K., Zhou, X., Liu, J., Huang, Z., 2020. Application of magnetic nanoparticles in petroleum industry: A review. Journal of Petroleum Science and Engineering 188, 106943.

Zhu, Y., Jiang, D., Sun, D., Yan, Y., Li, C., 2016. Fabrication of magnetic imprinted sorbents prepared by Pickering emulsion polymerization for adsorption of erythromycin from aqueous solution. Journal of Environmental Chemical Engineering 4(3), 3570-3579.

Zolfaghari, R., Fakhru'l-Razi, A., Luqman Chuah, A., Pendashteh, A., 2016. Demulsification techniques of water-in-oil and oil-in-water emulsions in petroleum industry. Separation and Purification Technology 170, 377-407.

3. CHAPTER THREE

Application of Functionalized Fe_3O_4 Magnetic Nanoparticles Using CTAB and SDS for Oil Separation from Oil-in-Water Nanoemulsion

Preface

A version of this chapter has been published in the Langmuir Journal, 39, 23 (2023) 7995–8007. As the primary author of this paper, I developed methodology and conducted all the experimental studies based on the inputs and plan from the supervisors (Sohrab Zendehboudi and Nima Rezaei). I prepared the first version of the manuscript and then made revisions based on the feedback and comments provided by my co-authors and the reviewers from the journal. The co-authors Ali Azizi and Fereshteh Shahhoseini assisted me in developing methodology and investigation. The co-authors Sohrab Zendehboudi and Nima Rezaei contributed to create a proper manuscript structure and thoroughly correcting the technical and editorial aspects of text.

3.1. Introduction

Large volumes of oily wastewater are generated from different sectors such as industries (e.g., textile, food, leather, oil and gas, metal processing, and mining industries), and frequent oil spill disaster, which can be occurred in oil extraction/production, refining, and transportation [1]. The discharge of oily wastewater into water resources can cause severe environmental impacts. For example, the oil floatation on aqueous surfaces leads to oxygen-poor condition by isolating the water phase from the atmosphere, resulting in aquatic life impairment. Moreover, the evaporation of the lighter hydrocarbons from the water surface can cause air pollution related to the volatile organic compounds [2]. The discharge of oily wastewater to environment not only affects the ecosystem but is also a waste of material and energy that could be used upon properly treated [3]. Therefore, due to the adverse impacts of oily wastewater and oil spills on the entire ecosystem, efficient oil-water separation is indispensable.

Oil contamination can occur in different forms, including free, dispersed, and emulsified oil. Separating the emulsified oil contaminations from waste- or produced water (PW) is of interest to many researchers as a challenging process because of the high stability of emulsion [4-5].

Conventional demulsification techniques (e.g., settling, centrifugation, thermal, and electrical) cannot effectively remove the emulsified oil droplets, and sometimes chemical demulsifiers are required to improve the demulsification performance [6]. However, these demulsifiers are less efficient in separating oil-in-water (O/W) nano-emulsion with small oil droplets (≤ 2 μm) [7]. Innovative membranes with tailored wettability are emerged to treat oily wastewater more effectively [8-9]. They, however, have limitations for efficient removal of emulsified oil droplets. Moreover, the membrane fouling phenomenon has always been considered an unavoidable challenge of these filtration systems [10]. Therefore, researchers have made considerable efforts in

developing efficient and cost-effective demulsifiers, featuring a high separation efficiency (SE) and short separation time [11-12].

Recently, magnetic nanoparticle (MNP) application (iron oxide in particular) has drawn great attention of researchers to capture oil effectively based on magnetic removal mechanism [13-14]. The MNPs features such as high surface area, low toxicity, easy separation from continuous phase, and recyclability have led to their widespread application as a promising option for demulsification [15-16].

Pristine iron oxide MNPs show intrinsic instability because of their high chemical activity, which result in agglomeration, precipitation, and oxidation by air, causing reduced magnetism and dispersibility [17-18]. Therefore, forming a protecting layer on the MNP surface using organic and inorganic components has been of great interest to researchers and engineers for improving their chemical stability, and dispersibility, resulting in a higher oil removal efficiency [19-21]. Organic functional materials such as polymers can prevent the MNP agglomeration through steric effects and increased repulsion force. Moreover, hydrophobic and oleophilic functional groups on MNPs can enhance the oil adsorption capacity by creating a nanoscale network with a high affinity for oil and a larger surface area for oil attachment [19]. For instance, Wang et al. [22] developed core-shell MNPs using a pH-responsive polymer shell made of poly 2-dimethylaminoethyle methacrylate. The fabricated core-shell particles revealed a rapid oil adsorption with tunable interfacial activity to form or break a Pickering emulsion reversibly by adjusting the pH value. However, MNPs coated with organic compounds exhibit a relatively low stability at higher temperature levels; also, they can react in an acidic solution to lose their magnetizations [19].

Coating MNPs with inorganic materials such as carbon and silica results in high stability against oxidation and acid leaching and high chemical and thermal stability [23]. Elmobarak and Almomeni

[24] grafted Fe_3O_4 MNPs with a silica layer to enhance their stability and investigated different silica layer thicknesses. The higher oil adsorption efficiency of >95% was achieved by employing grafted particles with a thinner coating, which was slightly decreased by increasing the coating thickness. The prepared particles indicated a high reusability (nine cycles with 80% oil SE). However, MNP coating using inorganic compounds is much less developed due to some limitations. For instance, MNPs with silica-based coatings result in a dense and nonporous shell that is also unstable under basic conditions [20]. Some researchers have employed hybrid MNP coatings [25-26]. For instance, Wang et al. [27] used core-shell Fe_3O_4 MNPs stabilized using oleic acid and coated with cetyltrimethylammonium bromide (CTAB) and natrium salicylicum. The dispersivity of the synthesized particles was increased by adding octadecyl trimethoxysilane to tetraethylorthosilicate at a ratio of 1:8. The dendritic structure of the synthesized particles with a mesoporous silica shell resulted in more than 98.1% SE.

In our previous comprehensive review [28] on the applications of MNPs in oil-water separation, a wide range of MNPs with different coatings were reviewed. Although O/W contaminations are important in various industries, some of these synthesized MNPs in the literature are only dispersible in organic solvents and not in water, which can result in inefficient demulsification by the MNPs and by applying an external magnetic field [29-30]. Therefore, we use surfactants as amphiphilic coatings to improve the dispersivity in the continuous phase and attraction to the dispersed phase. We compare the demulsification performances of CTAB as a cationic surfactant and also sodium dodecyl sulfate (SDS) as an anionic surfactant to further understand the contribution of electrostatic interactions in demulsification by MNPs, which has not been discussed in the literature to the best of our knowledge [28]. In this study, we aim to demulsify O/W using functionalized MNPs for oil droplets of nanometer size that are finer (and more stable) than

those studied in the literature. Additionally, the effect of MNPs size on demulsification is controversial in the literature [28] which is studied in this work by considering two different sizes of Fe_3O_4 nanoparticles and different mass ratios of surfactant-to-MNPs. The optimum MNP features, such as the size, coating chemistry, and coating ratio, are achievable by comparing the results of oil adsorption capacities for various scenarios via gas chromatography equipped with flame ionization detector (FID).

3.2. Materials and Methods

Iron oxide powder (Fe_3O_4, 99% with a size of 50–100 nm), and iron oxide nano particles (Fe_3O_4, >99.5% with a size of 15–20 nm) were purchased from US Research Nanomaterials, Inc., Houston, TX 77084, USA. Ethanol absolute was purchased locally; CTAB was bought from Millipore Sigma Corporation, Burligton MA, USA; SDS ~99% was purchased from MP Biomedical, LLC, Canada; chloroform (HPLC grade, >99.5%) was obtained from Thermo Scientific; *n*-dodecane ≥ 99% was bought from Thermo Scientific Alfa Aesar, Canada; and On/Off square welding magnet was provided from Master Magnetics, Inc. Deionized water (18.2 MΩ) was provided using a SYBRON/Barnstead water purification system, Boston, MA, USA. The composition and physical properties of oil, coating materials, and MNPs are provided in Table 3. 1. All materials are used as purchased and without further purification.

Table 3. 1. Physical Properties of Oil, MNPs, and Surfactants [31].

Materials	Molecular Formula	Molecular Weight (g/mol)	Boiling Point (°C)	Melting Point (°C)	Viscosity (mPa.s)	Density (g/cm^3)
Dodecane	$C_{12}H_{26}$	170.3	215–217	−10	1.34	0.74

CTAB	$C_{19}H_{42}BrN$	364.5	–	237–243	–	0.5
SDS	$C_{12}H_{25}NaSO_4$	288.4	–	206	–	1.01
Iron oxide	Fe_3O_4	231.53	2623	1597	–	5

3.2.1. Functionalization of Magnetic Nanoparticles

A summary of all the experiments conducted in this study is illustrated in Figure 3. 1. As the first step of the experiments, we develop our functionalized magnetic particles by employing different sizes of iron oxide nanoparticles. Two types of surfactants, including SDS and CTAB, are employed as various types of coatings to change the functionality/wettability of the magnetic particles.

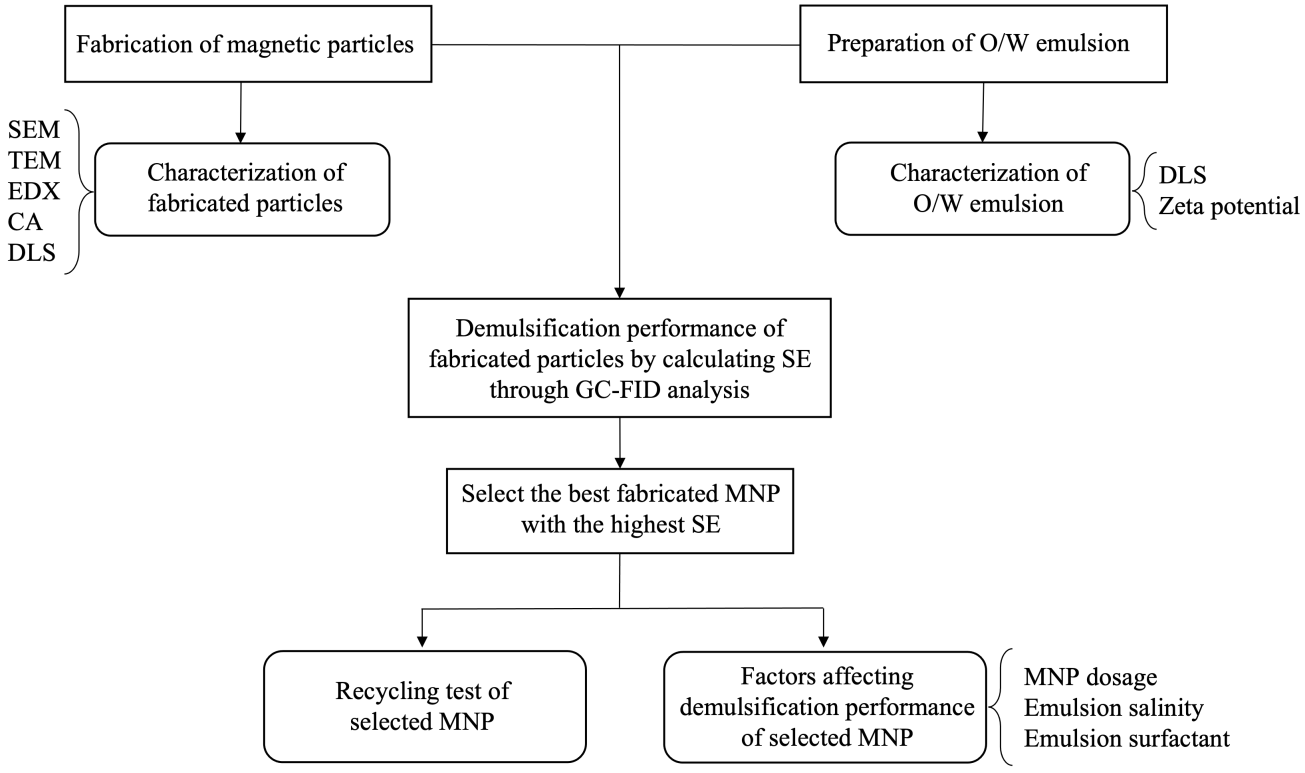

Figure 3. 1. Flowchart of the main steps of the experimental work.

The synthesis process of functionalized particles is shown in Figure 3. 2. First, Fe_3O_4 nanoparticles (500 mg) are dispersed in a 25 mL ethanol solution (4:1 ethanol/DI water) at 25 °C and ultrasonically mixed for 15 min. The ethanol/DI water solution has a much lower interfacial tension (IFT), which results in better wetting, and therefore better dispersivity of the MNPs in the solution and cause a more uniform coating [32]. Then, different dosages of the coating materials (200 and 400 mg) are dissolved in ethanol (25 mL) ultrasonically at 25 °C for 15 min to make different mass ratios between the surfactant and MNPs ($M_{surfactant}/M_{MNP}$) of 0.4, and 0.8, respectively (Figure 3. 2. a). The surfactant dosage for both SDS and CTAB surfactants is below their critical micelle concentration (CMC) level [33-34]. The prepared coating solution is added to the MNP solution in a round flask and heated at 80 °C under N_2 gas for 2 h in an oil bath (Figure 3. 2. b). The coated MNPs are separated by applying an external magnetic field and are washed with DI water and ethanol several times (Figure 3. 2. c), then dried in a vacuum oven at 60 °C for 24 h (Figure 3. 2. d).

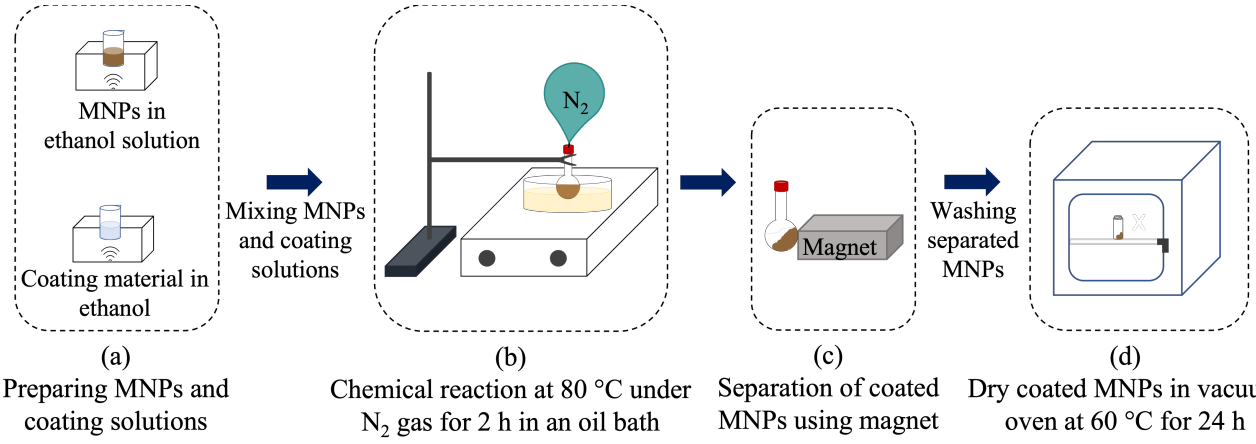

Figure 3. 2. Synthetic procedure of functionalized MNPs: (a) MNPs and coating preparation, (b) chemical reaction, (c) MNPs separation, and (d) MNPs drying.

3.2.2. Characterization of Functionalized Particles

The chemical structure and morphology of the MNPs are assessed using energy dispersive X-ray (EDX), transmission electron microscopy (TEM), and scanning electron microscopy (SEM). Dynamic light scattering (DLS) analysis is conducted to quantify the hydrodynamic diameter (D_H) and oil droplets' zeta potential. We also perform static contact angle (CA) measurements to analyze the CA of water and oil droplets on the functionalized MNP surfaces. Except for TEM and SEM analyses, other characteristics tests are conducted for the smaller size of bare and coated MNPs. All experiments are conducted at the room temperature.

The elemental and morphology analyses are specified using SEM (FEI MLA 650F, Hillsboro, USA) equipped with Bruker EDX (Ringoes, NJ, USA). For the SEM and EDX experiments, we place the particles on the alumina stub with double-sided carbon sticky tape. Then, the particles are sputter coated with gold under vacuum and using argon and plasma to prepare for SEM and EDX analyses. The TEM images are taken by employing Tecnai Spirit TEM (FEI, OR, USA), using a field emission electron of 80 kV, equipped with a 4 Mega pixel AMG digital camera. The TEM samples are prepared by dispersing the MNPs in ethanol ultrasonically for 5 min. Then, a small drop of dispersion is added onto the copper grid. After sputter coating the particles with gold, they are placed in the SEM equipment to check their morphology.

DLS analysis is performed using the Zetasizer Nano ZS90 instrument (Malvern Instruments Ltd., UK) at room temperature and pH 6–8. For measuring D_H, the particles are sonicated in ethanol (1 mg/mL) for 2 min to enhance the dispersivity of the particles (with no agglomeration) which is essential for accurate size measurement. Then, the dispersed particles are injected into a glass cuvette and put in the DLS sample holder for measurements. The calculated hydrodynamic diameters are averaged based on three independent runs. The surface charge measurements are

conducted by dispersing the particles in DI water and sonicating for 2 min. Then, the suspension is directly injected to the zeta cells for zeta potential measurements.

The static CA of water droplets on the particles is measured using a sessile water drop method through KRUSS Drop Shape Analyzer DSA25S (see Figure 3. 3). For measuring the water CA (WCA), the MNPs are dispersed in ethanol, spread onto the surface of the glass slide, and dried at room temperature. This step is repeated several times to achieve a thin film of particles on the glass surface. For each sample, three water droplets of 3 μL are dispensed on different parts of the thin film of a particle, and the average WCA for each sample is reported.

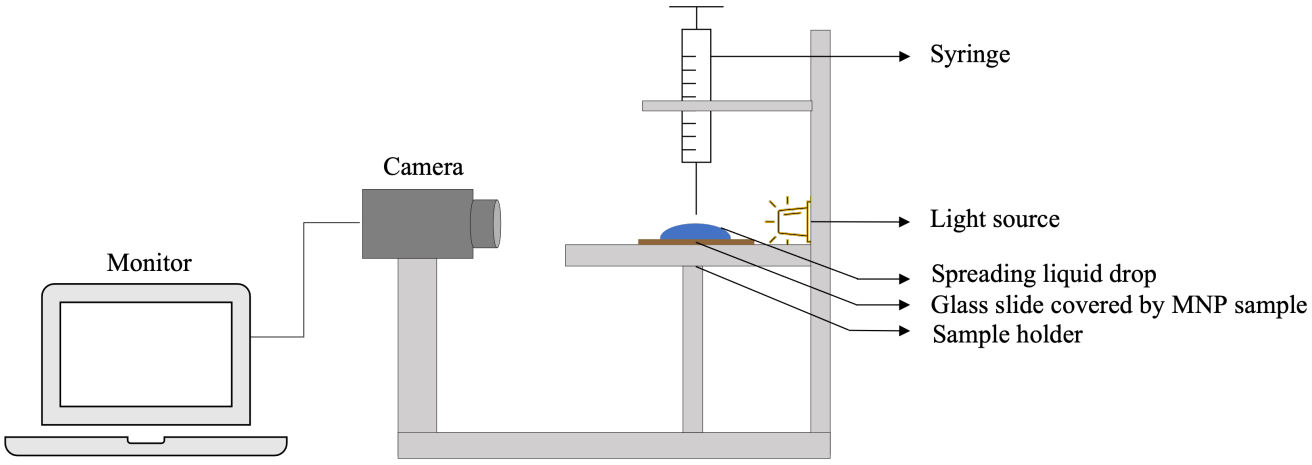

Figure 3. 3. Experimental setup to measure contact angle (CA).

3.2.3. Preparation of O/W Nanoemulsion

The O/W nanoemulsion is prepared by mixing dodecane with DI water using a probe sonicator for 5 min, through applying a pulsed sequence (work 10 s, break 5 s) in a water bath to control the temperature. The concentration of oil in the prepared emulsion is 1000 ppm. The emulsion droplet size is measured using a DLS analysis.

3.2.4. Oil-Water Separation (Demulsification)

The demulsification performances of both bare and coated MNPs are examined by mixing a given quantity of the particles (0.5 mg/mL) in a freshly prepared nanoemulsion (Figure 3. 4. a) and under vigorous vibrations at 2000 rpm for 20 min to allow reaching equilibrium oil adsorption capacity. The MNPs containing the adsorbed oil are collected using a magnet (Figure 3. 4. b) and washed using a solvent (Figure 3. 4. c). Finally, the cleaned MNPs are recovered by applying an external magnet so they can be reused in the next cycle (Figure 3. 4. d). The reusability test will be discussed in the next section.

The Design-Expert® v.11 is used to design our experiments by using a two-level full factorial design, in which each variable is studied at two levels with the upper and lower bounds coded as +1 and –1. Table 3. 2 reports the experiment design with the upper and lower levels of our variables to find the best fabricated MNPs with the highest oil SE. We selected CTAB and SDS to investigate the electrostatic interaction between adsorbate and adsorbent; two sizes of MNPs to study the effect of size on demulsification performance; and two mass ratios of surfactant to MNPs to evaluate the effect of coating dosage on the particles' performance.

Table 3. 2. Design of Experiment of Oil Separation Process Using Different MNPs.

Variables		Levels	
		Low (–1)	High (+1)
Input	Coating type	CTAB	SDS
	MNP size (nm)	MNP-S (15–20 nm)	MNP-L (50–100 nm)
	Mass ratio of surfactant to MNPs dosage	0.4	0.8
Output	Separation efficiency (SE%)	–	

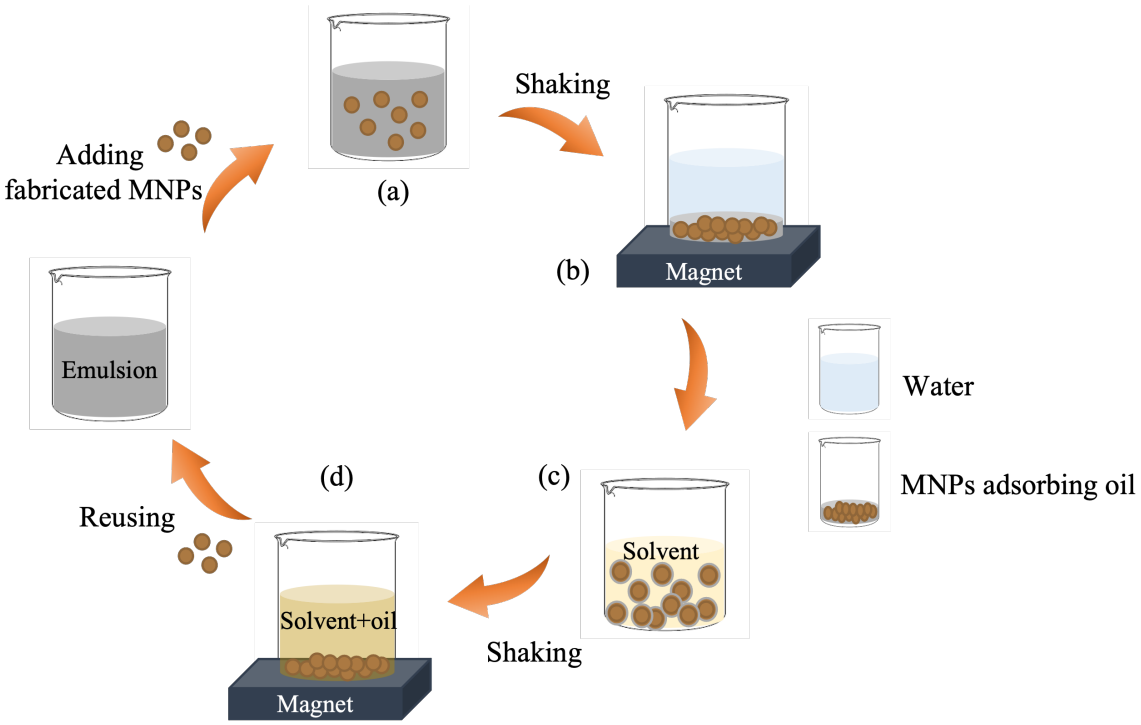

Figure 3. 4. Schematic illustration of demulsification and reusing process using functionalized MNPs: (a) MNPs preparation, (b) MNPs collection, (c) MNPs cleaning with solvent, and (d) MNPs recovery.

The residual oil content of the liquid phase after demulsification for both bare and coated MNPs cases are examined via an Agilent 7890B gas chromatography equipped with an FID to compare the separation efficiencies of the coated MNPs. Chromatographic separation is conducted using an HP-5MS UI column (30 m × 0.250 mm × 0.25 µm) (Agilent Technologies, USA). The applied carrier gas is N_2 with 5.0 ultra-high purity (UHP) at a flow rate of 1.0 mL/min (Praxair, Canada). The oven temperature setting is as follows: an initial temperature of 50 °C hold for 2 min; then ramp at 25 °C min^{-1} to 270 °C. A post-run program at 280 °C is maintained for 2 min, ensuring there is no injection's residual in the column. The total run time is 15 min for the gas chromatography (GC). The FID temperature is held at 320 °C, with flow rates of 400 mL/min of Ultra Zero Air, 30 mL/min of H_2 (5.0 UHP), and 25 mL/min of N_2 (Praxair, Canada). The samples

are kept in the autosampler injected (1 µL) using a sample manager flow-through needle (SM-FTN).

The GC calibration curve is required for evaluation steps of the developing method and the calculation of the extracted mass. Multi-standard solutions (0.5 to 500 mg/L) are prepared from the stock solution of dodecane in chloroform (1000 mg/L) by diluting in pure chloroform to achieve the required concentration. Each concentration is measured three times. All the standard solutions are kept in a refrigerator at 4 °C before utilization.

The percentage of oil removal by MNPs (SE %) and the amount of adsorbed oil onto MNPs (adsorption capacity, q_e) are calculated by the following equations:

$$SE\% = \left(\frac{C_0 - C_e}{C_0}\right) 100 \tag{3-1}$$

$$q_e = \left(\frac{C_0 - C_e}{w}\right) V \tag{3-2}$$

where C_0 stands for the initial oil concentration in the emulsion (ppm); C_e is the residual oil concentration after separation (ppm); q_e represents the amount of adsorbed oil per unit mass of the adsorbent (mg/g adsorbent); V refers to the total volume of the emulsion (L); and w denotes the weight of the adsorbent (g).

The experiments are conducted three times for each run to examine the reproducibility of the tests. In this research study, the potential sources of errors can be human error, material impurities, lack of instrumental sensitivity, and measurement errors.

3.2.5. Reusability Test

A unique characteristic of MNP demulsifiers is their ability to be reused after demulsification, leading to environmental impact reduction of the conventional chemical demulsifiers. The reusability of the MNPs is investigated for the emulsion with an oil concentration of 1000 ppm using around 0.5 g/L dosage of MNPs. After conducting the oil-water separation experiments, the MNPs are recovered and collected using a magnet. Since the recovered particles adsorb the oil droplets, these MNPs cannot be reused immediately and need to be washed using ethanol (ultrasonically) for 1 min. Finally, the cleaned MNPs are dried in a vacuum oven at 60 ºC for 1 h. The MNPs (after measuring their mass) are subsequently reused in the next cycle of the oil-water separation test. The reusability evaluation is conducted by considering the adsorption capacity (the quantity of adsorbed oil per unit mass of MNPs) in each cycle due to losing some fraction of MNPs during washing process in every cycle.

3.3. Results and Discussion

In this section, we report the results of functionalized MNPs' application for demulsification of dodecane-in-water (O/W) nanoemulsion and MNP characterization using SEM, TEM, EDX, CA, and DLS.

3.3.1. Magnetic Particles Characterization

SEM and TEM images of both sizes of bare and functionalized MNPs are displayed in Figure 3. 5 and Figure 3. 6, respectively. Notably, both bare MNP-S (Figure 3. 5. a) and MNP-L (Figure 3. 5. d) appear in large agglomeration forms. This observation is due to the magnetic nature of the MNPs [35]. As can be seen, bare MNP-S exhibits a denser aggregation in comparison with MNP-L, which is attributed to the higher surface energy of the smaller particles due to their higher surface area. Compared to the bare MNPs (Figure 3. 5. a, d), the functionalized particles aggregate less because

of their surface modification with cationic and anionic surfactants. MNPs coated with CTAB in both images of SEM (Figure 3. 5. c, f) and TEM (Figure 3. 6 c, f) show less aggregation than the ones coated with SDS according to SEM images (Figure 3. 5. b, e) and TEM images (Figure 3. 6 b, e). We observe that the surface modification using surfactant does not significantly affect the morphology of the functionalized MNPs, while it results in less aggregation and a better dispersivity.

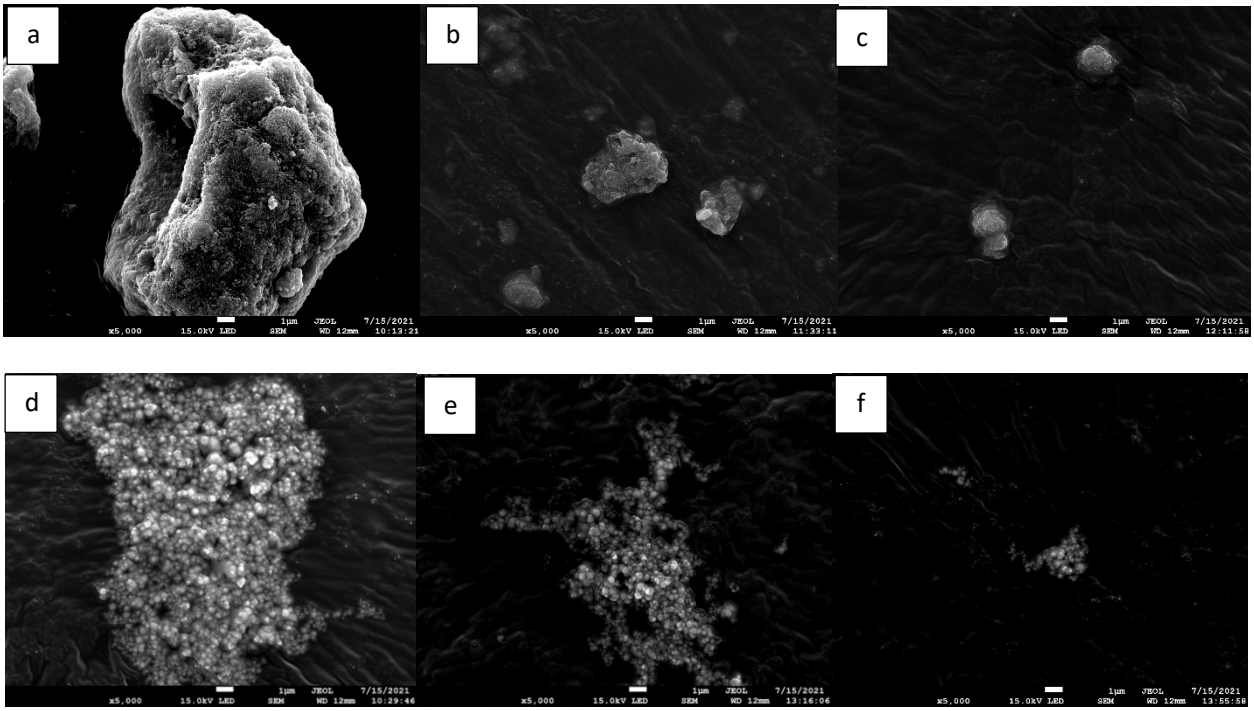

Figure 3. 5. SEM images of (a) bare MNP-S, (b) MNP-S@SDS, (c) MNP-S@CTAB, (d) bare MNP-L, (e) MNP-L@SDS, and (f) MNP-L@CTAB.

According to the TEM images (Figure 3. 6), the particles feature spherical agglomerated structures which is considered as an advantage compared to the other shapes such as nano-disk or nano-cube shapes because it provides a superior internalization rate and cellular take-up [24]. Moreover, the particle size measurements using TEM show that the sizes of bare MNP-S and bare MNP-L are equal to 15–20 nm and 50–100 nm, respectively.

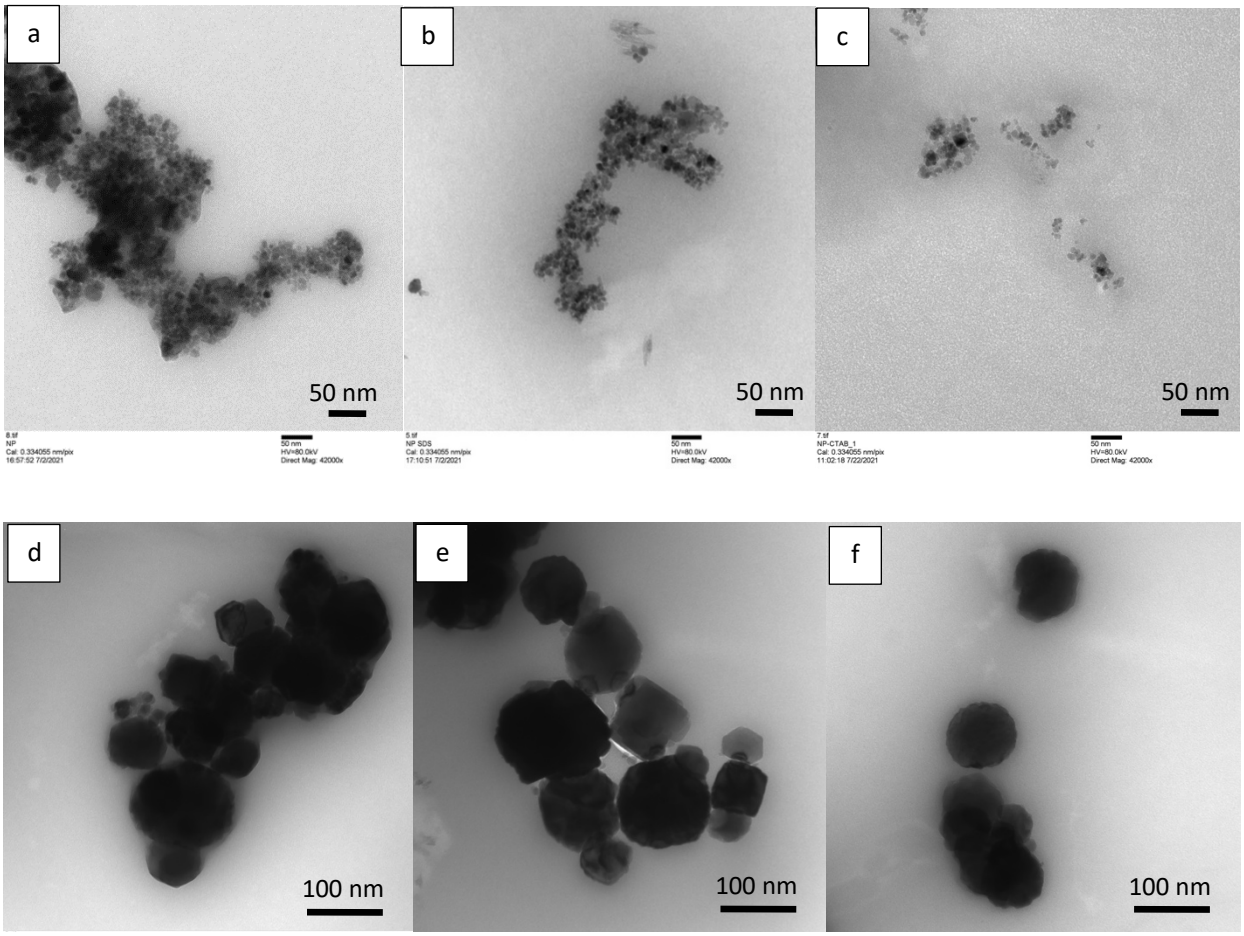

Figure 3. 6. TEM images of (a) bare MNP-S, (b) MNP-S@SDS, (c) MNP-S@CTAB, (d) bare MNP-L, (e) MNP-L@SDS, and (f) MNP-L@CTAB.

The EDX analysis is performed to demonstrate how the functional groups appear on the surface of the iron oxide MNPs. We only examine MNP-S because the chemical compositions of both sizes are the same. During the EDX measurements, different areas in the images are analyzed, for which the corresponding peaks are illustrated in Figure 3. 7. The elements' weight percentages and standard deviation (sigma) are also presented on Figure 3. 7. The EDX results show that the highest detected element counts, and X-ray energy belong to Fe with 78.01, 79.84, and 51.42% for MNP-S, MNP-S@SDS, and MNP-S@CTAB, respectively. The biggest change upon MNP functionalization is the high wt% of nitrogen in the MNP-S@CTAB (Figure 3. 7. c), which can

provide stronger electrostatic attraction with the oil droplets due to having more positive charge on the particles' surfaces and also a longer carbon chain compared to SDS-coated particles.

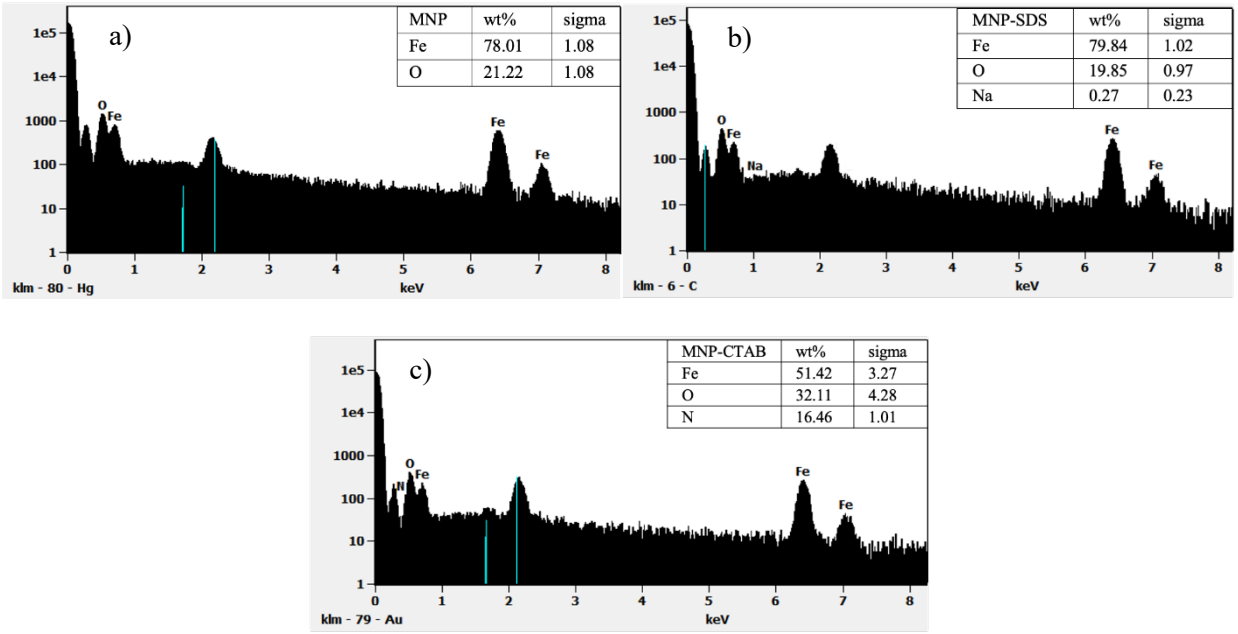

Figure 3. 7. EDX images of MNP-S with different coatings: (a) bare, (b) SDS, and (c) CTAB.

The hydrodynamic properties of nanoparticles are characterized using DLS analysis (Figure 3. 8), indicating that the hydrodynamic diameter (D_H) of bare MNP-S and MNP-L increases after being coated using SDS and CTAB, respectively. While the D_H of MNP-S reduces from 1008.2 nm to 718.9 nm after modification using CTAB. The results confirm less agglomeration of MNP-S@CTAB, implying that the dispersion of MNP-S increases upon being modified by CTAB, which is consistent with the SEM and TEM results (Figure 3. 5 and Figure 3. 6, respectively). Moreover, measuring D_H after 30 min shows that the larger particles are less stable, especially for the bare MNP-L without functionalization.

The differences in the particle size measurements of the DLS and TEM analyses is commonly reported in the literature [36-37] because the scattering intensity is proportional to the sixth power of particles radius for a fixed wavelength. Moreover, the higher scattering for larger particles in the

DLS measurements can be attributed to several factors such as the hydration shell of the particles, the slight shape of anisotropy of particles due to coating (which is not symmetrical in all three dimensions), and possible formation of small clusters [38].

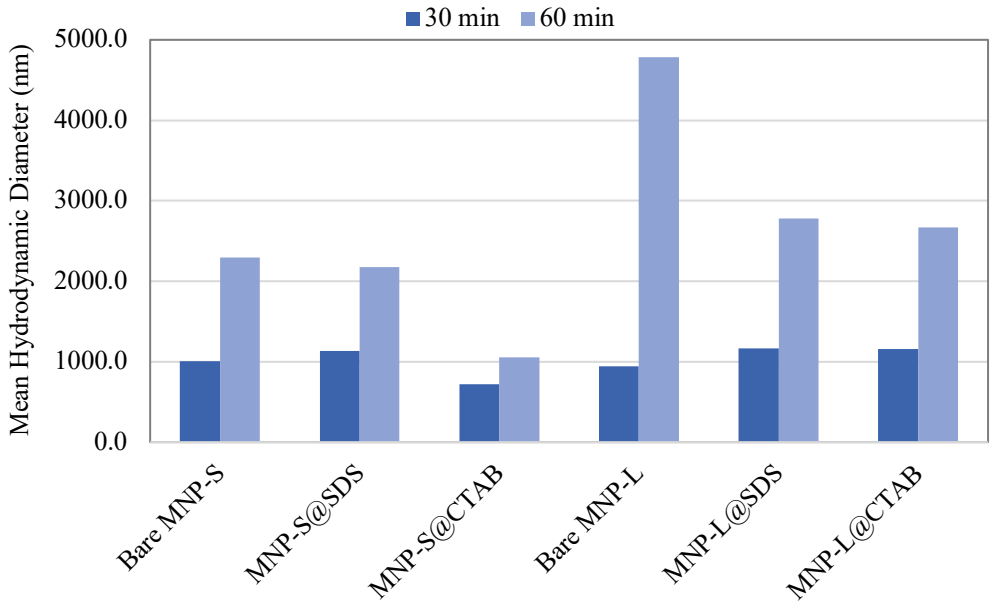

Figure 3. 8. DLS analysis of particles for mean DH.

The zeta potential measurements indicate that the bare MNP-S is positively charged with a zeta potential value of +4.24 mV at pH 5.0. At a higher pH, the particles are hydrated in DI water with their surface being covered by Fe-OH, which are deprotonated. Therefore, the Fe-O^- groups are formed, leading to the negative surface charge for the bare MNPs [39]. However, at a lower pH, the hydroxyl group (Fe-OH) on the MNP's surface is protonated and Fe-OH_2^+ are formed, resulting in a positive surface charge [40]. This phenomenon is commonly observed in aqueous solutions of iron oxide particles. After coating the MNPs with CTAB, the zeta potential changes to +35.8 (±0.34) mV, confirming the positive charges of the particles coated with cationic surfactant, as expected. The particles coated with SDS (as an anionic surfactant) also indicate that the particles are

positively charged with a zeta potential of +23.6 (±0.15) mV. This result can be explained by the electrostatic attraction of the negative head on the SDS surfactant to the positive charges of MNPs. The SDS molecules enable the adsorbent to form hydrophobic interaction with the adsorbate (oil droplets) through the SDS tails. Ranjbari et al. [41] concluded that higher SDS concentration results in the formation of a secondary layer of SDS adsorbing onto the particles by hydrophobic interaction through which the zeta potential could change sign (to values) because of the negative charge of SDS [41].

The wettability of MNPs is investigated through CA measurements of the liquid/air/solid three-phase system. As illustrated in Figure 3. 9, the WCA measurements indicate that the apparent CA of water droplets on the surface of MNP-S@CTAB is 0° (Figure 3. 9. a), which increases to 25° on MNP-S@SDS (Figure 3. 9. b). The lower WCA for MNP-S@CTAB reflects higher hydrophilicity of CTAB compared to SDS, despite the presence of a longer alkyl chains on the CTAB. This observation is consistent with the studies in the literature, indicating cationic surfactants (e.g., CTAB) being more effective compared to anionic surfactants (e.g., SDS) in changing the wettability toward water wet [42-43]. The water droplets spread immediately on the surface of MNP@CTAB and reach a CA of 0° within 2 s. In addition, the dodecane droplets spread rapidly on the MNP-S@CTAB surfaces and give a CA of 0°. The results verify the hydrophilic and oleophilic properties of MNP-S@CTAB. Recent studies also show that nanostructures containing oleophilic and hydrophilic behaviors exhibit amphiphilicity [44-46].

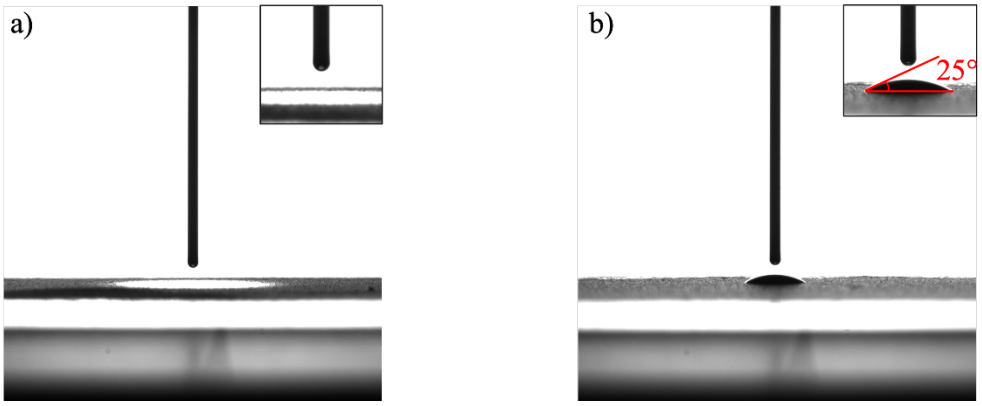

Figure 3. 9. Water contact angle (WCA) measurements of (a) MNP-S@CTAB, and (b) MNP-S@SDS.

3.3.2. Emulsion Properties

The emulsion stability is quantified by emulsion droplet size measurements using DLS. According to Figure 3. 10, the initial measurement shows that the mean oil droplet size is around 320 nm, and no significant change in the size of oil droplets is observed within 6 h of the DLS analysis. The zeta potential of the emulsion is around –55.9 (±2.44) mV at low pH (pH=5). The negative charge of the oil droplets can be neutralized by adding MNPs in the demulsification process.

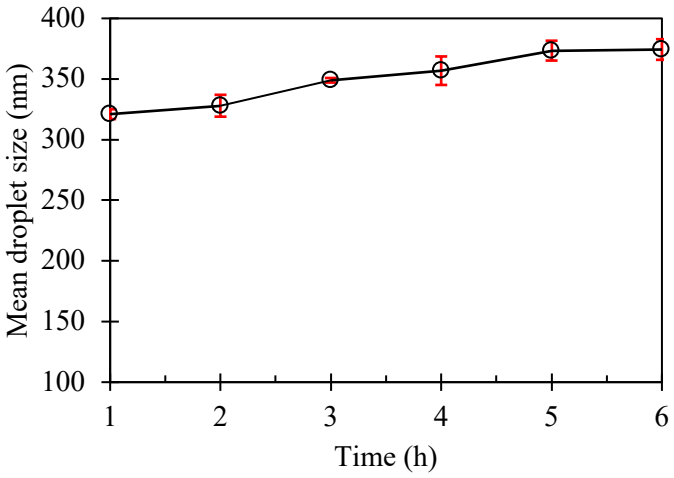

Figure 3. 10. Analyzing emulsion stability by dynamic measurements of mean droplet diameter for 1000 ppm O/W emulsion.

3.3.3. Demulsification Results

To find the best functionalized MNP in terms of demulsification efficiency, we investigate oil SE using GC-FID analysis, considering three input variables, including MNP size, coating type, and mass ratio of surfactant to MNPs dosage (Table 3. 2). Demulsification tests are conducted by adding 0.5 g/L bare and functionalized particles to separate 1000 ppm dodecane-in-water fresh nanoemulsion with a D_H of around 320 nm. After adding the particles into the emulsion, they are dispersed at 2000 rpm mixing rate for 20 min. In this study, we perform analysis of variance (ANOVA) to assess the statistical significance of each input variable. As illustrated in Table 3. 3, the ANOVA analysis shows that all the input variables and their interactions are significant at the significance level of 0.05 based on the p–values.

Table 3. 3. ANOVA Table to Assess Design Parameters [*d.f* stands for the degree of freedom].

Variables	Sum of Squares	*d.f*	F–value	P–value
A: Coating type	1479.57	1	12894.83	<0.0001
B: MNP size (nm)	250.13	1	2179.96	<0.0001
C: Mass ratio of surfactant to MNPs dosage	183.49	1	1599.12	<0.0001
AB	38.35	1	334.27	<0.0001
AC	109.48	1	954.17	<0.0001
BC	5.32	1	46.37	<0.0001
Error	1.53	16		
Total	2068.29	23		

The results of SE analysis using GC-FID in Table 3. 4 indicate that MNP-S with a smaller size features a higher SE due to a larger surface area compared to MNP-L having a larger size. At the same surface charge, the smaller particles have a higher charge density and feature a stronger

electrostatic attraction force, if other particle properties are fixed. Similarly, several studies reveal that smaller MNPs cause a higher oil recovery by considerably increasing the disjoining pressure [47-49]. The disjoining pressure is influenced by the MNPs size, charge density, and dosage, temperature, and salinity [50]. Therefore, a higher concentration of smaller particles with a higher charge density will lead to increasing the disjoining pressure [51].

The bare MNP-S shows a lower performance SE = 57.5%, because of more agglomeration compared to the bare MNP-L with SE = 86.3%, which can be seen in the SEM and TEM images (panels a and d of Figure 3. 5 and Figure 3. 6, respectively).

Moreover, among the coating types, CTAB as a cationic surfactant, results in a better performance, with SE > 99% for MNP-S and > 90% for MNP-L. This observation is justified by the positive charge of CTAB (with a zeta potential of +35.8 mV) that provides a stronger electrostatic attraction with the negatively charged oil droplets.

The application of MNPs with different coating mass ratios in the demulsification process indicate that an increase in coating ratio leads to the reduction of SE. Because adding more coating materials to a given MNPs can increase the steric hindrance and reduce the accessibility of the active surface sites, thereby decrease the binding capacity of the MNPs [52]. This finding is consistent with previous studies in the literature, which suggest that smaller particles with a lower coating ratio have a better dispersibility in the O/W, resulting in the higher SE [53-55].

Table 3. 4. The Effect of Size of Particles, Coating Type, and Coating Ratio on Oil-Water SE.

Particle Size	Coating Type	Coating Ratio	Peak Area Mean	RSD (%), *n*=3	Residual Oil (ppm)	SE (%)
MNP-S (15–20 nm)	Bare	-	6807.0	8.8	425.4	57.5
	SDS	0.4	2224.0	3.3	139.0	86.1

		0.8	3684.2	1.6	230.3	77.0
	CTAB	0.4	32.2	7.1	2.0	99.8
		0.8	41.2	1.6	2.6	99.7
MNP-L (50–100 nm)	Bare	-	2190.6	3.0	136.9	86.3
	SDS	0.4	2744.4	2.1	171.5	82.9
		0.8	4421.1	1.7	276.3	72.4
	CTAB	0.4	1277.5	3.3	79.9	92.0
		0.8	1671.1	1.1	104.4	89.6

Generally, the highest efficiency of oil separation (99.8%) is obtained using MNP-S@CTAB at a coating ratio of 0.4. As it can be seen in Figure 3. 11, the *x*-axis shows the amount of time taken for the dodecane to pass through the column and reach the detector, which is around 6.8 min. The retention time is generally affected by the type of column used during the analysis and the GC parameters, such as flow rate, injection temperature, and oven temperature. The *y*-axis indicates the area of the peak, reflecting the amount of the dodecane, which decreases from 1000 ppm (peak area ~10,000) to around 2 ppm (peak area ~30) after adding MNP-S@CTAB. The positive charge of the cationic surfactant provides a stronger electrostatic attraction to the oil droplets dispersed in water. Moreover, the higher SE% for MNP-S@CTAB is attributed to the amphiphilicity of MNP-S@CTAB that is evident from the CA measurements, showing simultaneous hydrophilic and oleophilic properties.

Our fabricated amphiphilic MNPs with cationic surfactant (MNP@CTAB) provide a great potential in oil-water separation, which is compatible with the research results by Lu et al. [56], where a great performance of amphipathic MNPs with cationic functional groups was attained for demulsification of both oil-in-water and water-in-oil emulsions. Also, Zhou et al. [57] achieved up

to 95.5% demulsification efficiency using amphiphilic MNPs. It was concluded that the hydrophilic segments of the functionalized particles could form hydrogen bonds with water, facilitating the interfacial adsorption of as-prepared particles [57].

The following experimental analyses are conducted by using MNP-S@CTAB that feature the highest SE. For instance, we use MNP-S@CTAB for PW treatment. According to Figure 3. 12, after addition of functionalized particles to PW, a significant quantity of hydrocarbon contaminations is removed through adsorption onto the particles.

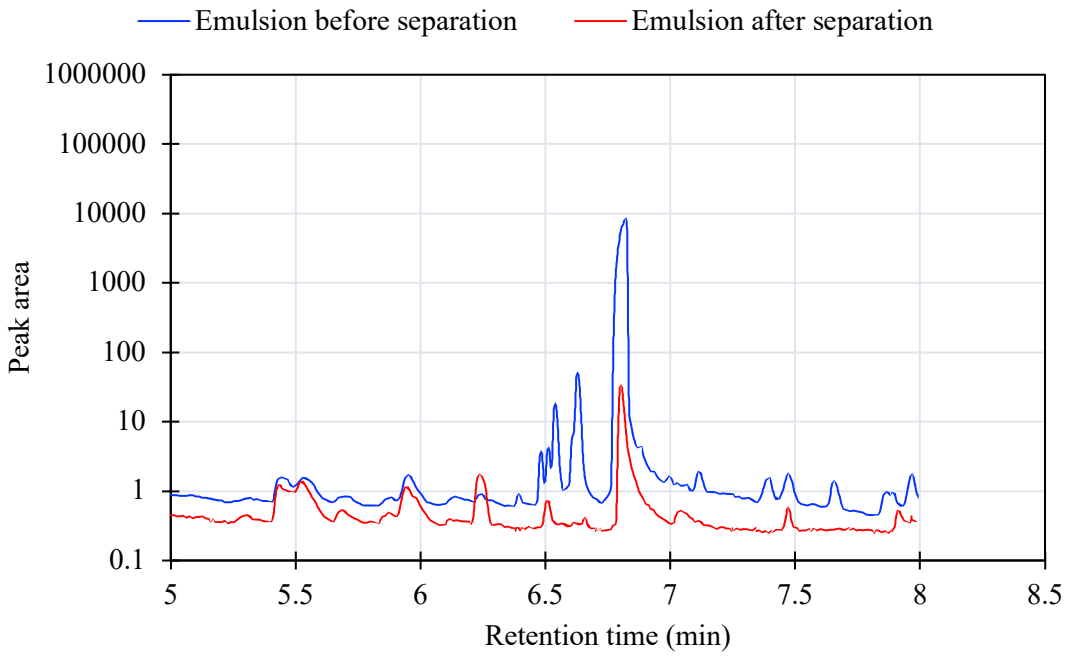

Figure 3. 11. GC-FID analysis of oil adsorption results from 1000 ppm O/W emulsion before and after utilizing 0.5 g/L MNP-S@CTAB within 20 min mixing time at 2000 rpm.

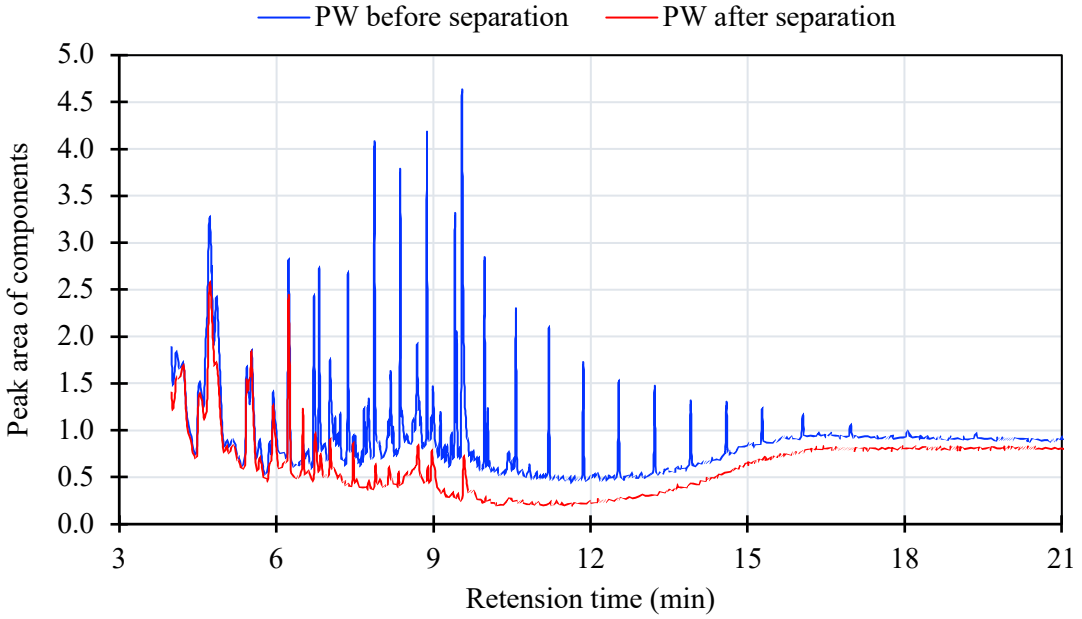

Figure 3. 12. GC-FID analysis of produced water (PW) treatment analysis using 0.5 g/L MNP-S@CTAB within 20 min mixing time at 2000 rpm.

3.3.4. Demulsification Performance of MNP-S@CTAB

Effect of MNP Dosage on Demulsification Performance

The MNP concentration is an important measure for the demulsification performance. It is obvious that demulsification efficiency increases with MNP concentration before reaching a plateau [58-59]. It implies that there is an optimal MNP dosage at which the most effective separation performance can be achieved, and adding MNP beyond the optimum concentration does not further enhance the demulsification efficiency [60]. Increasing MNP dosage although enhances the repulsion forces, it will decrease the IFT between the oil and MNPs beyond the optimal MNP concentration [49].

Figure 3. 13 presents the influence of MNP-S@CTAB dosage in the range of 0.025–1.5 g/L on the SE and q_e of 1000 ppm dodecane-in-water nanoemulsion. With increasing the MNP concentration from 0.025 to 0.05 g/L, the SE improves from 45.3 to 73.5% and q_e decreases from 181.3 to 147.0 mg/g. For MNP dosage ≥ 0.1 g/L, the oil SE is stabilized at 98%. By increasing MNPs concentration, the adsorption capacity is continuously reduced due to either unsaturation of adsorption sites or aggregation of the particles. The latter can lead to a reduced surface area of MNPs [61-62].

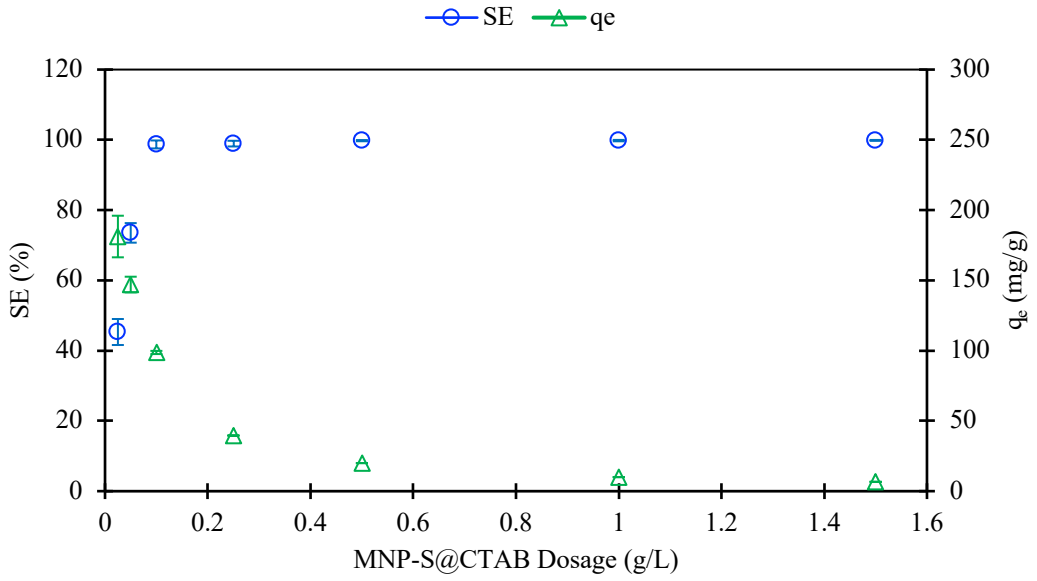

Figure 3. 13. The effect of MNP-S@CTAB dosage on the oil adsorption efficiency for 1000 ppm O/W emulsion within 20 min mixing time at 2000 rpm.

Demulsification Performance at Different Salinity Levels

The emulsion salinity/ionic strength impact on the SE% is evaluated by adding 0.5 g/L MNP-S@CTAB to 10,000 ppm dodecane-in-water emulsions containing different concentrations of NaCl in the range of 0 to 2 g/L. Figure 3. 14 depicts that the addition of salt increases the ionic strength of the emulsion, resulting in a electrostatic screening effect which reduces the electrostatic repulsion between the oil droplets and MNPs [63]. Therefore, the zeta potential of the particles decreases, which can affect their stability and facilitate their agglomeration [47, 64]. Moreover, increasing the IFT between oil droplets and MNPs due to the electrostatic screening effect leads to an enhancement of imbibition, thereby increases SE%. The addition of salt in the emulsion may also affect the SE% by reducing the hydrophilicity of MNPs because of the salt's hydration [65]. Paixao and Balaban [66] highlighted the "salting-out" effect, which leads to decreasing the surfactants' hydrophilicity and thereby reducing the IFT of the emulsion.

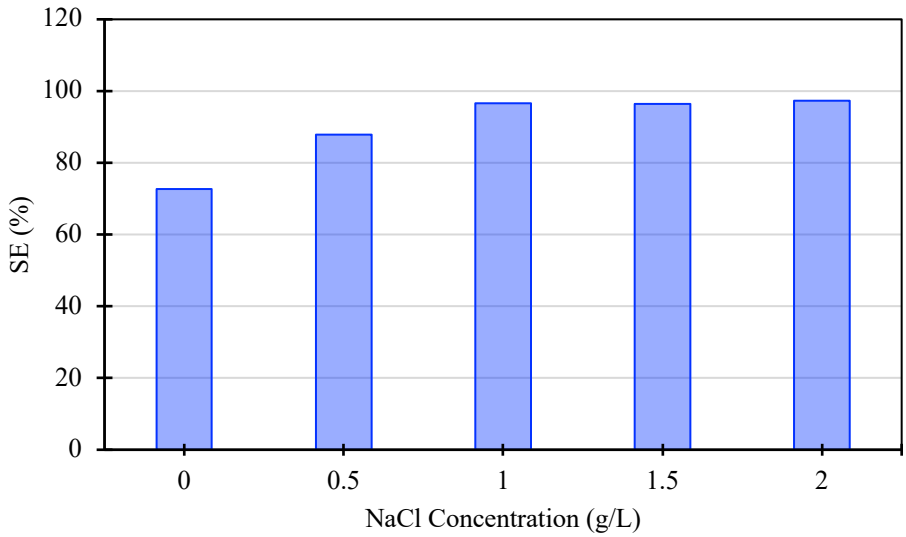

Figure 3. 14. Oil adsorption efficiency from 10000 ppm O/W emulsion containing different amounts of NaCl using 0.5 g/L MNP-S@CTAB within 20 min mixing time at 2000 rpm.

Demulsification Performance at Different Surfactant Concentrations

Given that the O/W emulsions commonly contain surfactants as surface active substances [67-68], it is essential to investigate their effects on the SE%. Various experimental levels of SDS (as a surfactant) in the range of 0 - 2.5 g/L are added to DI water to make a 1000 ppm dodecane-in-water nanoemulsion. The demulsification tests are conducted using 0.5 g/L MNP-S@CTAB and mixing at 2000 rpm for 20 min. As illustrated in Figure 3. 15, the SE% analysis using the GC-FID indicates that increasing the surfactant concentration leads to slight SE% reduction. When SDS is added to an emulsion, can adsorb onto both oil droplets and MNPs, reducing the IFT between them by forming a stabilizing monolayer that reduces the attraction between two phases, which can in turn decline SE% [65, 69-70]. A higher surfactant concentration results in the emulsion's stability by improving the oil droplets stability inside the emulsion, while reducing the surface tension forces, resulting in oil adsorption reduction over MNP particles [24]. Conversely, by increasing the SDS concentration >2 g/L, the SE% begins to increase. According to the literature, the CMC of SDS in

water is around 0.2 wt%, which is equivalent to a molarity of 0.008 mol/L (equal to 2.45 g/L) [71]. Increasing the SDS concentration beyond the CMC results in micelle formation. Micelles are dispersed aggregates in a liquid that form colloidal suspension having spherical shapes in which the hydrophilic heads are in contact with water and the hydrophobic tails are in the micelle center. The addition of more SDS beyond the CMC concentration can form a stable and rigid interfacial film at the oil-water interface. Therefore, SDS micelles can help to increase the number of exposed MNP active sites by reducing the steric hindrance and increasing the accessibility of the active surface sites, resulting in enhancing SE%.

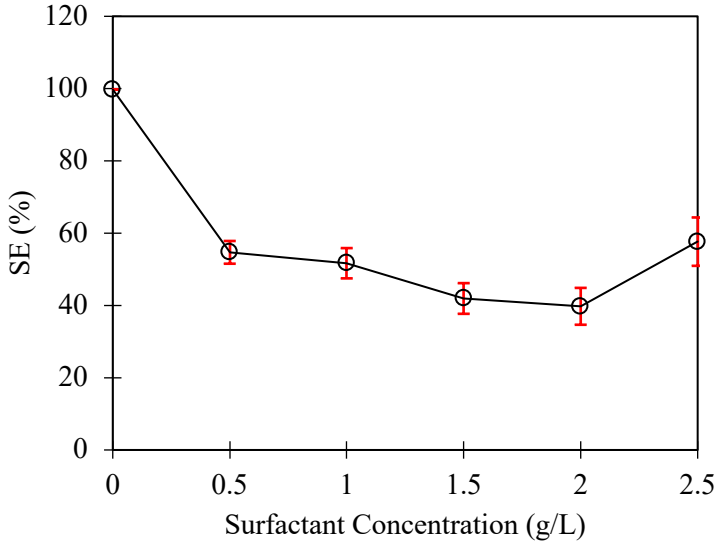

Figure 3. 15. The effect of surfactant concentration on the oil-water separation efficiency of 1000 ppm O/W emulsion using 0.5 g/L MNP-S@CTAB within 20 min mixing time at 2000 rpm.

3.3.5. Demulsification Mechanism

The main demulsification mechanism in our study is found to be electrostatic attraction forces for the opposite surface charges of functionalized particles and oil droplets, which is verified by the zeta potential measurements. MNPs are first dispersed into the emulsion phase, and then negatively charged oil droplets are adsorbed onto positively charged MNPs through electrostatic attraction [72].

Finally, by applying an external magnetic field, the MNPs containing the adsorbed oil can be separated from the medium. Moreover, the anti-ionic action of positive charge of the particles and the negative charge of the oil droplets leads to destruction of the interface film of oil droplets [7]. Therefore, the oil droplets aggregate with each other, allowing the oil and water to be separated. Because the interface activity has a significant impact on demulsification efficiency, demulsifying impact occurs by adding the interfacially active MNPs into the emulsion [24, 73]. In our study, MNP@CTAB exhibits a higher demulsification efficiency due to its more positive charge that is evident from a higher zeta potential and an improved interface activity that is attributed to the abundance of the alkyl chains of CTAB compared to SDS. Elmobarak and Almomani [24] show that changing the interfacial features (e.g., interfacial film thickness, IFT, mechanical strength, and elasticity) leads to the oil droplets coalescence and flocculation.

The other important mechanism, which significantly impacts the demulsification, is wettability alteration by functional groups in the coating materials. Based on the WCA measurements, MNP@CTAB exhibits more hydrophilicity compared to the MNP@SDS, which results in more dispersity of the particles in the emulsion. Better MNP dispersity can be considered as the important step of the demulsification process, leading to a higher demulsification efficiency.

3.3.6. Reusability Tests

In addition to the high performance of the MNP-S@CTAB during the demulsification process, they are also able to be reused several times. Due to losing some fraction of particles during the washing process in each cycle, we consider adsorption capacity (the amount of oil adsorbed per unit mass of the MNPs) for each cycle, instead of SE%. Figure 3. 16 demonstrates the reusability of MNP-S@CTAB over 10 cycles. After reusing MNPs for four times, the oil adsorption capacity decreases from 20 (for 100% adsorption) to 19.39 mg/g in cycle five. However, in the subsequent

cycles (till cycle nine), the adsorption capacity is kept at around 19.3 mg/g without further change, indicating the good reusing stability of the MNPs. After the 10th cycle, the adsorption capacity is reduced to around 19 mg/g, implying that the MNP-S@CTAB remains effective for the next cycles [74]. The gradually decline in the oil adsorption efficiency through the reusability tests is likely owing to the retainment of small oil droplets on the MNPs surfaces which cannot be washed by ethanol [7]. This is also explained in the literature with the loss of some of the coating materials from the MNPs surfaces upon the sequential cleaning process [24].

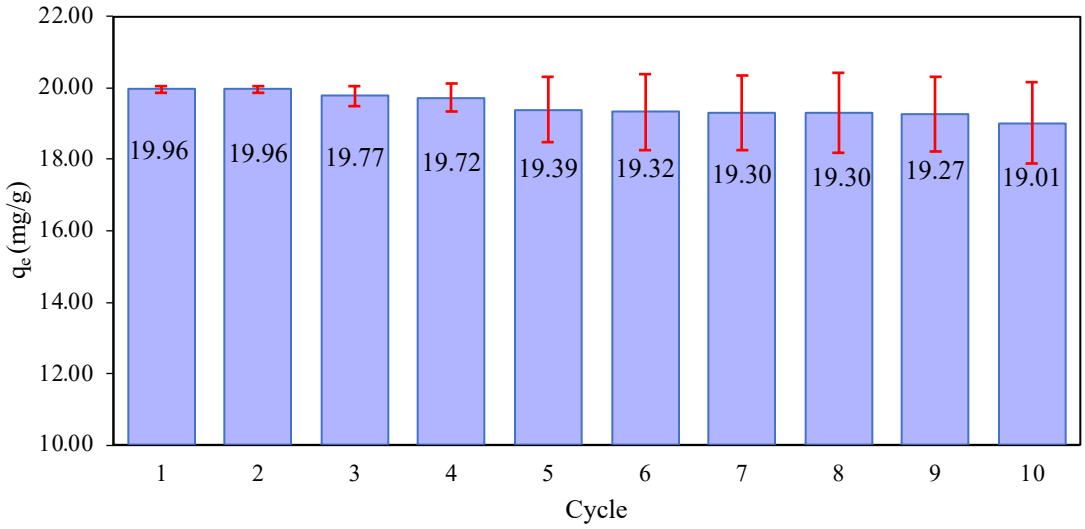

Figure 3. 16. Reusing demulsification experiment of MNP-S@CTAB for 1000 ppm O/W emulsion within 20 min mixing time at 2000 rpm.

3.4. Summary

Two different sizes of functionalized Fe_3O_4 MNPs using SDS and CTAB and two different mass ratios of surfactant to MNPs (e.g., 0.4 and 0.8) are employed to assess their demulsification performances for dodecane-in-water nanoemulsion. Oil-water separation analysis is conducted using GC-FID to evaluate the effect of size of nanoparticles, coating material, and coating mass ratio on the separation efficiency (SE). The following conclusions are drawn:

- The oil-water separation results reveal that the smaller MNPs coated with CTAB (MNP-S@CTAB) using the lower surfactant to MNP ratio of 0.4 lead to the highest oil SE (around 99.8%). This high SE is attributed to the more positive surface charge density on CTAB (compared to SDS) which is confirmed by the zeta potential measurements; better hydrophilicity of the CTAB-coated MNPs (compared to SDS-coated MNPs) is noticed as indicated from WCA analysis, and less aggregation of MNP@CTAB in the aqueous phase is obtained as illustrated in the SEM and TEM images.
- For the bare MNPs, the smaller particles (MNP-S with size 15-20 nm) are less stable than the larger particles (MNP-L with size 50-100 nm) tested, indicating denser aggregation that is evident from the TEM and SEM images and their less dispersibility in the O/W emulsion. While smaller functionalized particles exhibit higher stability and SE compared to the larger functionalized particles due to their higher surface energy and charge density.
- The fabricated MNP-S@CTAB indicates a good reusability feature with high performance after 10 cycles. Adsorption capacity is reduced gradually during the 10^{th} cycle but is still significant, revealing that the particles can be applied in the following cycles efficiently.
- By increasing MNPs concentration, SE increases and it reach the optimal dosage, while the adsorption capacity constantly decreases, which is attributed to the unsaturation the adsorption sites or aggregation of the particles, leading to reduction of the available surface area of the MNPs.
- Increasing the concentration of salt (NaCl) in the emulsion results in increasing the IFT between oil droplets and MNPs and decreasing zeta potential of each particle due to the electrostatic screening effect. Therefore, reducing the electrostatic repulsion between the MNPs and oil leads to a higher SE%. In contrast, adding surfactant (e.g., SDS) into the

emulsion decreases the IFT between the MNPs and oil droplets; therefore, oil adsorption is reduced. It follows that increasing surfactant dosage at, and above CMC leads to increase SE% due to increasing the number of exposed MNP active sites by reducing the steric hindrance and increasing the accessibility of the active surface sites through forming SDS micelles.

- The effects of pH and temperature alteration on the demulsification performance of the functionalized particles need to be considered for future investigations to further comprehend the governing mechanisms of the demulsification process.
- Modelling and optimization of the adsorption process can help to find optimal operating conditions for attaining a higher oil adsorption capacity. An effective modelling/optimization strategy can be useful in minimizing the number of tests in future experimental studies.

Declaration of competing interest

The authors declare that they have no known competing financial interest or personal relationships that could have appeared to influence the work reported in this paper.

Acknowledgments

The authors would like to acknowledge the financial support offered by Memorial University (NL. Canada), Natural Sciences and Engineering Research Council of Canada (NSERC), and Suncor Energy Inc. /Terra Nova Young Innovator Award.

Nomenclatures

Acronyms

ANOVA	-	Analysis of variance
CA	-	Contact angle
CMC	-	Critical micelle concentration
CTAB	-	Cetyltrimethylammonium bromide
DI	-	Deionized
DLS	-	Dynamic light scattering
EDX	-	Energy Dispersive X-ray
GC-FID	-	Gas Chromatography equipped with Flame Ionization Detector
IFT	-	Interfacial tension
MNPs	-	Magnetic nanoparticles
O/W	-	Oil-in-water
ODTMS	-	Organic tethers, trimethoxy(octadecyl)silane
PW	-	Produced water
SDS	-	Sodium dodecyl sulfate
SE	-	Separation efficiency
SEM	-	Scanning Electron Microscopy
TEM	-	Transmission Electron Microscopy
WCA	-	Water contact angle

Variables and Parameters

C_0	-	Initial oil concentration in emulsion

C_e	-	Residual oil concentration after separation
q_e	-	Oil adsorption capacity
$C_{12}H_{25}NaSO_4$	-	Sodium dodecyl sulfate
$C_{12}H_{26}$	-	Dodecane
$C_{19}H_{42}BrN$	-	Critical micelle concentration
D_H	-	Hydrodynamic diameter
Fe_3O_4	-	Iron oxide
V	-	Total volume of emulsion
w	-	Weight vector

References

1. Ali, N.; Zaman, H.; Bilal, M.; Shah, A.-u.-H. A.; Nazir, M. S.; Iqbal, H. M. N., Environmental perspectives of interfacially active and magnetically recoverable composite materials – A review. *Sci. Total Environ.* **2019,** *670*, 523-538.

2. Dubansky, B.; Whitehead, A.; Miller, J. T.; Rice, C. D.; Galvez, F., Multitissue Molecular, Genomic, and Developmental Effects of the Deepwater Horizon Oil Spill on Resident Gulf Killifish (Fundulus grandis). *Environ. Sci. Technol.* **2013,** *47* (10), 5074-5082.

3. Joye, S. B., Deepwater Horizon, 5 years on. *Science* **2015,** *349* (6248), 592-593.

4. Faisal, W.; Almomani, F., A critical review of the development and demulsification processes applied for oil recovery from oil in water emulsions. *Chemosphere* **2022,** *291*, 133099.

5. Goodarzi, F.; Zendehboudi, S., A Comprehensive Review on Emulsions and Emulsion Stability in Chemical and Energy Industries. *The Canadian Journal of Chemical Engineering* **2019,** *97* (1), 281-309.

6. Issaka, S.; Nour, A.; Yunus, R. b. M., Review on the Fundamental Aspects of Petroleum Oil Emulsions and Techniques of Demulsification. *Journal of Petroleum & Environmental Biotechnology* **2015,** *6*, 1-15.

7. Chen, Y.; Tian, G.; Liang, H.; Liang, Y., Synthesis of magnetically responsive hyperbranched polyamidoamine based on the graphene oxide: Application as demulsifier for oil-in-water emulsions. *International Journal of Energy Research* **2019,** *43* (9), 4756-4765.

8. Rasouli, S.; Rezaei, N.; Hamedi, H.; Zendehboudi, S.; Duan, X., Design, fabrication, and characterization of a facile superhydrophobic and superoleophilic mesh-based membrane for selective oil-water separation. *Chem. Eng. Sci.* **2021,** *236*, 116354.

9. Rasouli, S.; Rezaei, N.; Hamedi, H.; Zendehboudi, S.; Duan, X., Superhydrophobic and superoleophilic membranes for oil-water separation application: A comprehensive review. *Materials & Design* **2021,** *204*, 109599.

10. Hamedi, H.; Ehteshami, M.; Mirbagheri, S. A.; Rasouli, S. A.; Zendehboudi, S., Current Status and Future Prospects of Membrane Bioreactors (MBRs) and Fouling Phenomena: A Systematic Review. *The Canadian Journal of Chemical Engineering* **2019,** *97* (1), 32-58.

11. Mohammed, L.; Gomaa, H. G.; Ragab, D.; Zhu, J., Magnetic nanoparticles for environmental and biomedical applications: A review. *Particuology* **2017,** *30*, 1-14.

12. Niculescu, A.-G.; Chircov, C.; Mihai Grumezescu, A., Magnetite nanoparticles: synthesis methods - a comparative review. *Methods* **2021**.

13. Zhou, K.; Zhou, X.; Liu, J.; Huang, Z., Application of magnetic nanoparticles in petroleum industry: A review. *Journal of Petroleum Science and Engineering* **2020,** *188*, 106943.

14. Su, C., Environmental implications and applications of engineered nanoscale magnetite and its hybrid nanocomposites: A review of recent literature. *J. Hazard. Mater.* **2017,** *322*, 48-84.

15. Tang, X.; Si, Y.; Ge, J.; Ding, B.; Liu, L.; Zheng, G.; Luo, W.; Yu, J., In situ polymerized superhydrophobic and superoleophilic nanofibrous membranes for gravity driven oil–water separation. *Nanoscale* **2013,** *5* (23), 11657-11664.

16. Kokal, S., Crude Oil Emulsions: A State-Of-The-Art Review. In *SPE Annual Technical Conference and Exhibition*, 2002; pp SPE-77497-MS.

17. Simonsen, G.; Strand, M.; Øye, G., Potential applications of magnetic nanoparticles within separation in the petroleum industry. *Journal of Petroleum Science and Engineering* **2018,** *165*, 488-495.

18. Qiao, K.; Tian, W.; Bai, J.; Wang, L.; Zhao, J.; Du, Z.; Gong, X., Application of magnetic adsorbents based on iron oxide nanoparticles for oil spill remediation: A review. *Journal of the Taiwan Institute of Chemical Engineers* **2019,** *97*, 227-236.

19. Kharissova, O. V.; Dias, H. V. R.; Kharisov, B. I., Magnetic adsorbents based on micro- and nano-structured materials. *RSC Advances* **2015,** *5* (9), 6695-6719.

20. Yang, Y.; Fang, Z.; Chen, X.; Zhang, W.; Xie, Y.; Chen, Y.; Liu, Z.; Yuan, W., An Overview of Pickering Emulsions: Solid-Particle Materials, Classification, Morphology, and Applications. *Frontiers in Pharmacology* **2017,** *8* (287).

21. Abdullah, M. M. S.; Al-Lohedan, H. A., Fabrication of Environmental-Friendly Magnetite Nanoparticle Surface Coatings for the Efficient Collection of Oil Spill. *Nanomaterials (Basel, Switzerland)* **2021,** *11* (11).

22. Wang, X.; Shi, Y.; Graff, R. W.; Lee, D.; Gao, H., Developing recyclable pH-responsive magnetic nanoparticles for oil–water separation. *Polymer* **2015,** *72*, 361-367.

23. Nazifa, T. H.; Islam, R.; Salmiati; Uddin, A. S. M. S.; Hadibarata, T.; Aris, A. In *Fast and Efficient Removal of Oil from Water Surface Through Activated Carbon and Iron Oxide-Magnetic*

Nanocomposite, 2018 2nd International Conference on Green Energy and Applications (ICGEA), 24-26 March 2018; 2018; pp 263-267.

24. Elmobarak, W. F.; Almomani, F., Functionalization of silica-coated magnetic nanoparticles as powerful demulsifier to recover oil from oil-in-water emulsion. *Chemosphere* **2021,** *279*, 130360.

25. Lü, T.; Chen, Y.; Qi, D.; Cao, Z.; Zhang, D.; Zhao, H., Treatment of emulsified oil wastewaters by using chitosan grafted magnetic nanoparticles. *J. Alloys Compd.* **2017,** *696*, 1205-1212.

26. Zhang, S.; Lü, T.; Qi, D.; Cao, Z.; Zhang, D.; Zhao, H., Synthesis of quaternized chitosan-coated magnetic nanoparticles for oil-water separation. *Mater. Lett.* **2017,** *191*, 128-131.

27. Wang, B.; Wei, Y.; Wang, Q.; Di, J.; Miao, S.; Yu, J., Superhydrophobic magnetic core–shell mesoporous organosilica nanoparticles with dendritic architecture for oil–water separation. *Materials Chemistry Frontiers* **2020,** *4* (7), 2184-2191.

28. Hamedi, H.; Rezaei, N.; Zendehboudi, S., A comprehensive review on demulsification using functionalized magnetic nanoparticles. *Journal of Cleaner Production* **2022,** *380*, 134868.

29. Lü, T.; Zhang, S.; Qi, D.; Zhang, D.; Zhao, H., Enhanced demulsification from aqueous media by using magnetic chitosan-based flocculant. *J. Colloid Interface Sci.* **2018,** *518*, 76-83.

30. Lü, T.; Qi, D.; Zhang, D.; Fu, K.; Li, Y.; Zhao, H., Fabrication of recyclable multi-responsive magnetic nanoparticles for emulsified oil-water separation. *Journal of Cleaner Production* **2020,** *255*, 120293.

31. Kim, S., Chen, J., Cheng, T., Gindulyte, A., He, J., He, S., Li, Q., Shoemaker, B. A., Thiessen, P. A., Yu, B., Zaslavsky, L., Zhang, J., & Bolton, E. E., PubChem in 2021: new data content and improved web interfaces. **2019,** *49(D1),* .

32. Li, Z.; Lu, B. C. Y., Surface tension of aqueous electrolyte solutions at high concentrations — representation and prediction. *Chem. Eng. Sci.* **2001,** *56* (8), 2879-2888.

33. Li, W.; Zhang, M.; Zhang, J.; Han, Y., Self-assembly of cetyl trimethylammonium bromide in ethanol-water mixtures. *Frontiers of Chemistry in China* **2006,** *1* (4), 438-442.

34. Plastinin, I. V.; Burikov, S.; Gofurov, S. P.; Ismailova, O. B.; Mirgorod, Y. A.; Dolenko, T. A., Features of self-organization of sodium dodecyl sulfate in water-ethanol solutions: Theory and vibrational spectroscopy. *J. Mol. Liq.* **2020,** *298*, 112053.

35. Schweiger, C.; Pietzonka, C.; Heverhagen, J.; Kissel, T., Novel magnetic iron oxide nanoparticles coated with poly(ethylene imine)-g-poly(ethylene glycol) for potential biomedical application: synthesis, stability, cytotoxicity and MR imaging. *International journal of pharmaceutics* **2011,** *408* (1-2), 130-7.

36. Grein-Iankovski, A.; Loh, W., Modulating the interfacial properties of magnetic nanoparticles through surface modification with a binary polymer mixture towards stabilization of double emulsions. *Colloids Surf. Physicochem. Eng. Aspects* **2020,** *586*, 124208.

37. Neha, R.; Jaiswal, A.; Bellare, J.; Sahu, N. K., Synthesis of Surface Grafted Mesoporous Magnetic Nanoparticles for Cancer Therapy. *Journal of Nanoscience and Nanotechnology* **2017,** *17* (8), 5181-5188.

38. Berret, J. F.; Sandre, O.; Mauger, A., Size distribution of superparamagnetic particles determined by magnetic sedimentation. *Langmuir : the ACS journal of surfaces and colloids* **2007,** *23* (6), 2993-9.

39. Zhu, A.; Yuan, L.; Liao, T., Suspension of Fe3O4 nanoparticles stabilized by chitosan and o-carboxymethylchitosan. *International journal of pharmaceutics* **2008,** *350*, 361-8.

40. Illés, E.; Tombácz, E., The effect of humic acid adsorption on pH-dependent surface charging and aggregation of magnetite nanoparticles. *Journal of Colloid and Interface Science* **2006,** *295* (1), 115-123.

41. Ranjbari, E.; Hadjmohammadi, M. R.; Kiekens, F.; De Wael, K., Mixed Hemi/Ad-Micelle Sodium Dodecyl Sulfate-Coated Magnetic Iron Oxide Nanoparticles for the Efficient Removal and Trace Determination of Rhodamine-B and Rhodamine-6G. *Analytical chemistry* **2015,** *87* (15), 7894-901.

42. Hosseini, E.; Hajivand, F.; Tahmasebi, R., The effect of alkaline–surfactant on the wettability, relative permeability and oil recovery of carbonate reservoir rock: experimental investigation. *Journal of Petroleum Exploration and Production Technology* **2019,** *9* (4), 2877-2891.

43. Jarrahian, K.; Seiedi, O.; Sheykhan, M.; Sefti, M. V.; Ayatollahi, S., Wettability alteration of carbonate rocks by surfactants: A mechanistic study. *Colloids and Surfaces A: Physicochemical and Engineering Aspects* **2012,** *410*, 1-10.

44. Song, Y.; Zhou, J.; Fan, J.-B.; Zhai, W.; Meng, J.; Wang, S., Hydrophilic/Oleophilic Magnetic Janus Particles for the Rapid and Efficient Oil–Water Separation. *Adv. Funct. Mater.* **2018,** *28* (32), 1802493.

45. Hammouda, S. b.; Chen, Z.; An, C.; Lee, K.; Zaker, A., Buoyant oleophilic magnetic activated carbon nanoparticles for oil spill cleanup. *Cleaner Chemical Engineering* **2022,** *2*, 100028.

46. Song, X.; Chen, Y.; Rong, M.; Xie, Z.; Zhao, T.; Wang, Y.; Chen, X.; Wolfbeis, O. S., A Phytic Acid Induced Super-Amphiphilic Multifunctional 3D Graphene-Based Foam. *Angewandte Chemie International Edition* **2016,** *55* (12), 3936-3941.

47. El-Diasty, A. I.; Aly, A. M., Understanding the Mechanism of Nanoparticles Applications in Enhanced Oil Recovery. In *SPE North Africa Technical Conference and Exhibition*, 2015; p D021S009R004.

48. Sun, X.; Zhang, Y.; Chen, G.; Gai, Z., Application of Nanoparticles in Enhanced Oil Recovery: A Critical Review of Recent Progress. *Energies* **2017,** *10* (3).

49. Hendraningrat, L.; Li, S.; Torsæter, O., Effect of Some Parameters Influencing Enhanced Oil Recovery Process using Silica Nanoparticles: An Experimental Investigation. In *SPE Reservoir Characterization and Simulation Conference and Exhibition*, 2013; pp SPE-165955-MS.

50. Agista, M. N.; Guo, K.; Yu, Z., A State-of-the-Art Review of Nanoparticles Application in Petroleum with a Focus on Enhanced Oil Recovery. *Applied Sciences* **2018,** *8*, 871.

51. Kondiparty, K.; Nikolov, A.; Wu, S.; Wasan, D., Wetting and Spreading of Nanofluids on Solid Surfaces Driven by the Structural Disjoining Pressure: Statics Analysis and Experiments. *Langmuir : the ACS journal of surfaces and colloids* **2011,** *27* (7), 3324-3335.

52. Gupta, A. K.; Gupta, M., Synthesis and surface engineering of iron oxide nanoparticles for biomedical applications. *Biomaterials* **2005,** *26* (18), 3995-4021.

53. Sonmez, M.; Georgescu, M.; Alexandrescu, L.; Gurau, D.; Ficai, A.; Ficai, D.; Andronescu, E., Synthesis and Applications of Fe3O4/SiO2 Core-Shell Materials. *Current pharmaceutical design* **2015,** *21*.

54. Yang, H.; Hou, Q.; Wang, S.; Guo, D.; Hu, G.; Xu, Y.; Tai, J.; Wu, X.; Yu, D.; Wang, J., Magnetic-responsive switchable emulsions based on Fe3O4@SiO2–NH2 nanoparticles. *Chem. Commun.* **2018,** *54* (76), 10679-10682.

55. Yu, L.; Hao, G.; Gu, J.; Zhou, S.; Zhang, N.; Jiang, W., Fe3O4/PS magnetic nanoparticles: Synthesis, characterization and their application as sorbents of oil from waste water. *Journal of Magnetism and Magnetic Materials* **2015,** *394*, 14-21.

56. Lü, T.; Wu, Y.; Qi, D.; Sun, Y.; Zhang, D.; Zhao, H., Fabrication of alkyl/amino siloxane-modified magnetic nanoparticles for simultaneous demulsification of O/W and W/O emulsions. *Colloids Surf. Physicochem. Eng. Aspects* **2022,** *648*, 129295.

57. Zhou, J.; Sui, H.; Ma, J.; Li, X.; Al-shiaani, N. H. A.; He, L., Fast demulsification of oil-water emulsions at room temperature by functionalized magnetic nanoparticles. *Separation and Purification Technology* **2021,** *274*, 118967.

58. Ko, S.; Prigiobbe, V.; Huh, C.; Bryant, S. L.; Bennetzen, M. V.; Mogensen, K., Accelerated Oil Droplet Separation from Produced Water Using Magnetic Nanoparticles. In *SPE Annual Technical Conference and Exhibition*, Society of Petroleum Engineers: Amsterdam, The Netherlands, 2014; p 14.

59. Wang, Q.; Puerto, M. C.; Warudkar, S.; Buehler, J.; Biswal, S. L., Recyclable amine-functionalized magnetic nanoparticles for efficient demulsification of crude oil-in-water emulsions. *Environmental Science: Water Research & Technology* **2018,** *4* (10), 1553-1563.

60. Xu, H.; Wang, J.; Ren, S., Removal of Oil from a Crude Oil-in-Water Emulsion by a Magnetically Recyclable Diatomite Demulsifier. *Energy & Fuels* **2019,** *33* (11), 11574-11583.

61. Singh, R.; Bhateria, R., Experimental and Modeling Process Optimization of Lead Adsorption on Magnetite Nanoparticles via Isothermal, Kinetics, and Thermodynamic Studies. *ACS Omega* **2020,** *5* (19), 10826-10837.

62. Nanta, P.; Kasemwong, K.; Skolpap, W., Isotherm and kinetic modeling on superparamagnetic nanoparticles adsorption of polysaccharide. *Journal of Environmental Chemical Engineering* **2018,** *6* (1), 794-802.

63. Lü, T.; Qi, D.; Zhang, D.; Lü, Y.; Zhao, H., A facile method for emulsified oil-water separation by using polyethylenimine-coated magnetic nanoparticles. *J. Nanopart. Res.* **2018,** *20* (4), 88.

64. McElfresh, P.; Holcomb, D.; Ector, D., Application of Nanofluid Technology to Improve Recovery in Oil and Gas Wells. **2012**.

65. Zhao, H.; Zhang, C.; Qi, D.; Lü, T.; Zhang, D., One-Step Synthesis of Polyethylenimine-Coated Magnetic Nanoparticles and its Demulsification Performance in Surfactant-Stabilized Oil-in-Water Emulsion. *J. Dispersion Sci. Technol.* **2019,** *40* (2), 231-238.

66. Paixão, M. V. G.; Balaban, R. d. C., Application of guar gum in brine clarification and oily water treatment. *International journal of biological macromolecules* **2018,** *108*, 119-126.

67. Kakati, A.; Kumar, G.; Sangwai, J. S., Oil Recovery Efficiency and Mechanism of Low Salinity-Enhanced Oil Recovery for Light Crude Oil with a Low Acid Number. *ACS omega* **2020,** *5* (3), 1506-1518.

68. Liang, J.; Du, N.; Song, S.; Hou, W., Magnetic demulsification of diluted crude oil-in-water nanoemulsions using oleic acid-coated magnetite nanoparticles. *Colloids Surf. Physicochem. Eng. Aspects* **2015,** *466*, 197-202.

69. Shao, S. L., Y.; Lü, T.; Qi, D.; Zhang, D.; Zhao, H. , Removal of Emulsified Oil from Aqueous Environment by Using Polyvinylpyrrolidone-Coated Magnetic Nanoparticles. *Water* **2019,** *19* (10).

70. Zhang, J.; Li, L.; Wang, J.; Sun, H.; Xu, J.; Sun, D., Double Inversion of Emulsions Induced by Salt Concentration. *Langmuir* **2012,** *28* (17), 6769-6775.

71. Hammouda, B., Temperature Effect on the Nanostructure of SDS Micelles in Water. *Journal of research of the National Institute of Standards and Technology* **2013,** *118*, 151-67.

72. Yau, X. H.; Khe, C. S.; Mohamed Saheed, M. S.; Lai, C. W.; You, K. Y.; Tan, W. K., Magnetically recoverable magnetite-reduced graphene oxide as a demulsifier for surfactant stabilized crude oil-in-water emulsion. *PloS one* **2020,** *15* (4), e0232490.

73. Mi, T.; Cai, Y.; Wang, Q.; Habibul, N.; Ma, X.; Su, Z.; Wu, W., Synthesis of Fe3O4 nanocomposites for efficient separation of ultra-small oil droplets from hexadecane–water emulsions. *RSC Advances* **2020,** *10* (17), 10309-10314.

74. Li, S.; Li, N.; Yang, S.; Liu, F.; Zhou, J., The synthesis of a novel magnetic demulsifier and its application for the demulsification of oil-charged industrial wastewaters. *Journal of Materials Chemistry A* **2014,** *2* (1), 94-99.

4. CHAPTER FOUR

Investigation of Emulsified Oil Adsorption onto Functionalized Magnetic Nanoparticles – Kinetic and Isotherm Models

Preface

A version of this chapter has been published in the Energies Journal. Both experimental and modelling phases of this research are conducted by the primary author of this manuscript (Hamideh Hamedi). I provided my co-authors, Nima Rezaei and Sohrab Zendehboudi, with the first version of the manuscript to receive their feedback. The co-author, Nima Rezaei, helped me in results interpretation, and statistical analysis. The co-author, Sohrab Zendehboudi, contributed through providing the outline of manuscript, and technical points on previous works in the related area.

4.1. Introduction

Conventional oil–water separation techniques have limitations, especially for separating dispersed and emulsified oily wastewater [1–4]. The emulsion stability is affected by the oil droplet size and challenges the treatment of emulsified oily wastewater; the high emulsion stability for oil-in-water (O/W) nanoemulsions decreases the efficiency of adsorbents for removing the oil contamination [5,6]. Using magnetic nanoparticle (MNP) as a nanoadsorbent is proven to be successful for demulsifying such nanoemulsions with small oil droplet sizes [7]. Iron oxide (Fe_3O_4) is a common MNP with promising application in oil adsorption due to its superparamagnetic properties, biocompatibility, high adsorption capacity, and recyclability [6]. However, large-scale application of MNPs is limited by the intrinsic instability and agglomeration of Fe_3O_4, resulting from high chemical activity [8].

The surface modification of MNPs using organic and inorganic materials is proposed as an effective process to improve the MNP stability, dispersivity in the emulsion, and oil removal effectiveness [9]. Functionalizing MNPs using amphiphilic compounds has attracted great interest for demulsification because of featuring simultaneously hydrophilic and hydrophobic properties. Therefore, these amphiphilic particles can be easily dispersed in the aqueous phase (as the continuous emulsion phase for O/W) to adsorb onto the emulsified oil droplets effectively [10]. For instance, Hammouda et al. [11] developed oleophilic magnetic activated carbon nanoparticles decorated by soybean oil and stearic acid for oil spill removal. The water and oil contact angle measurements indicated super-amphiphilicity, causing rapid and effective oil droplet adsorption following their coalescence in a magnetic field. Amphipathic magnetically diatomite demulsifier was developed by Xu et al. [12] to remove oil from an O/W emulsion. Their grafted Fe_3O_4 particles showed a great demulsification performance. Song et al. [13] fabricated hydrophilic/oleophilic

Janus magnetic particles for oil adsorption. They confirmed the effectiveness of these amphiphilic Janus particles for oil removal (from O/W) due to their high interfacial activity, which enabled them to adsorb onto the oil–water interfaces quickly.

To obtain a better understanding of the adsorption mechanisms, equilibrium adsorbate adsorption information is crucial to study the adsorption isotherm and kinetics [14–16]. The adsorption isotherm behavior can effectively describe the interactions between the adsorbent (MNPs) and adsorbate (oil droplets), using empirical mathematical equations. Different isotherm models have been developed. Some of the important models include Langmuir, Freundlich, Temkin, Sips, Dubinin–Radushkevich, and Brunauer–Emmett–Teller [17,18]. In all isotherm models, the oil adsorption capacity is estimated using batch studies conducted at a fixed temperature, using different initial oil concentration levels and under equilibrium. Adsorption kinetics can help to identify the adsorption mechanisms, such as diffusion and chemical reactions; it quantifies the adsorption dynamics for an adsorbate-adsorbent system [19,20]. The rate of adsorption depends on the physical and chemical properties of the adsorbent [21,22] and the operating conditions [23,24]. There are several kinetic models in the literature, such as pseudo-first-order (PFO), pseudo-second-order (PSO), intra-particle diffusion (IPD), and Elovich kinetic models, which quantify the dynamics of adsorption. In the literature, linear regression analysis has been widely applied to investigate the adsorption kinetics and isotherms to assess the equilibrium adsorption behavior [19,25]. However, due to errors resulting from linearization, the non-linear regression analysis is proposed as a more rigorous mathematical method to calculate the adsorption kinetics and isotherms [15]. For instance, Nanta et al. [26] investigated isotherm and kinetic modeling of superparamagnetic nanoparticles for polysaccharide adsorption using Langmuir, Freundlich, and Sips isotherm models, and non-linear PFO and PSO kinetic models. Based on their findings, the

non-linear analysis was more accurate than the linear method to predict the optimum adsorption isotherm. Their results revealed that the Freundlich and PFO models are more accurate in estimating the adsorption isotherm and kinetic behavior, respectively, compared to the other tested models. Mirzaee and Sartaj [27] developed an activated carbon-based magnetic composite for polycyclic aromatic hydrocarbons (PAH) adsorption. They then studied the isotherm and kinetic models using a non-linear regression method. It was found that PAH adsorption from aqueous solution fitted well to the Langmuir isotherm and PSO kinetic models. Jaafari et al. [20] studied the equilibrium data for removing dye using magnetic chitosan and observed a better fit to the Freundlich isotherm and PFO kinetic models.

Based on the literature, several materials have been employed to functionalize MNPs, while most of them are only dispersible in organic solvents. However, excellent dispersivity of MNPs is crucial in attaining an effective demulsification. In this regard, we use surfactant as amphiphilic compound with both hydrophilic and oleophilic properties to provide a greater dispersivity of MNPs in the emulsion to prevent their aggregation and achieve higher oil adsorption capacity. Moreover, previous research studies have focused on the separation of micrometer oil contaminations; meanwhile, in this research, we aim to separate nanometer oil droplets from the emulsion, which is more challenging. To this end, we apply cetyltrimethylammonium bromide (CTAB) as a cationic surfactant to synthesize amphiphilic MNPs for oil removal from dodecane oil-in-water (O/W) nanoemulsion. The prepared MNP@CTAB particles are characterized using transmission electron microscopy (TEM), water and oil contact angle (CA) measurements, and zeta potential analysis. The adsorption isotherm and kinetic models are investigated to interpret the adsorption mechanisms for improving the demulsification process. Furthermore, this research provides valuable insight into the adsorption behavior in terms of electrostatic interaction between

adsorbate and adsorbents, which has not been thoroughly investigated in previous studies to the best of our knowledge. We employ three adsorption isotherms, including Langmuir, Freundlich, Temkin, and three kinetic models: PFO, PSO, and IPD. The oil adsorption equilibrium data is calculated by oil adsorption capacity measurements using gas chromatography with flame ionization detector (GC-FID).

4.2. Material and Methods

4.2.1. Materials

Iron oxide nano powder (Fe3O4, >99.5% with size of 15–20 nm) was supplied by US Research Nanomaterials, Houston, TX, USA. Cetyltrimethylammonium bromide (CTAB) was purchased from MilliporeSigma, Burlington, NV, USA; chloroform (HPLC grade, >99.5%) and n-dodecane ≥ 99% were obtained from Thermo Scientific, Mississauga, ON, Canada; On/Off magnetic welding square was provided by Master Magnetics, Inc., Castle Rock, CO, USA. Ethanol absolute was purchased locally; deionized water (18.2 MΩ) was obtained using a water purification system (SYBRON/Barnstead, East Lyme, CT, USA).

4.2.2. Preparation of functionalized magnetic nanoparticles

Figure 4. 1 presents a summary of the main steps conducted throughout this research. As the first step of the experimental phase of our research, 500 mg Fe3O4 nanoparticles (magnetite) are dissolved in 25 mL ethanol–water (4:1) solution for 15 min in a sonication bath at 25 °C. Then, 200 mg CTAB is dispersed into ethanol solution (25 mL) for 15 min in a sonication bath at 25 °C to make a 2.5:1 mass ratio of CTAB/magnetite. The prepared CTAB solution is added to the MNP solution in a round volumetric flask, which is sealed and purged with N2 to avoid MNP oxidation. Then, the mixture is heated to 80 °C for 2 h in an oil bath. A magnet is placed next to the round flask to separate the coated MNPs from the liquid. The coated nanoparticles are washed with

deionized (DI) water and ethanol several times and placed in a vacuum oven at 60 °C to be dried for 24 h. More details of the experimental procedure for synthesizing the MNPs particles can be found in our previous study [7].

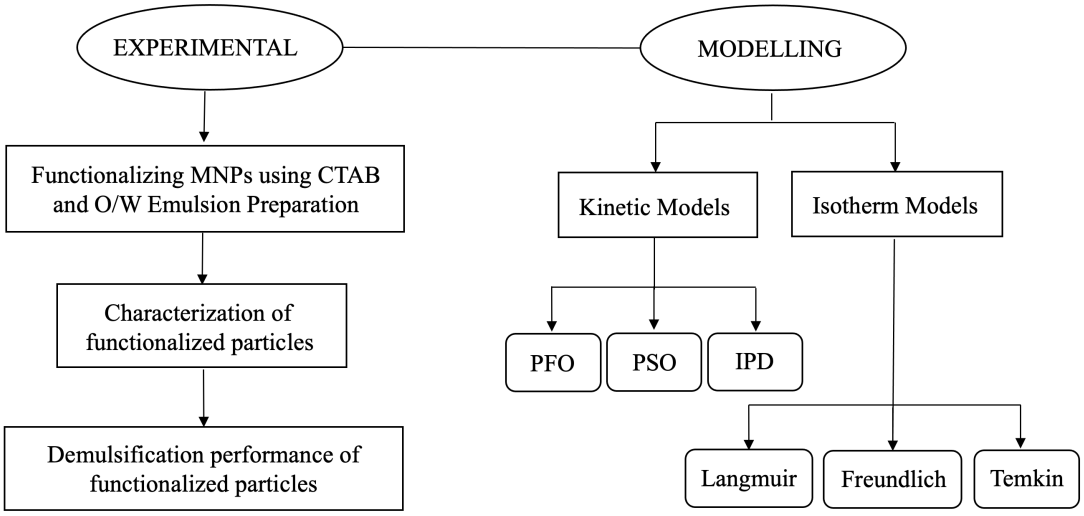

Figure 4. 1. Flowchart of the main steps of the research

4.2.3. Characterization of functionalized magnetic nanoparticles

MNP morphology and surface charge are important factors affecting the effectiveness of demulsification process [28]. In this study, the morphology of the MNPs is assessed using SecnaiTM Spirit TEM (FEI, Hillsboro, OR, USA) with 4 Megapixel AMG digital camera and 80 kV field emission electron gun. We also measure zeta potential to estimate the effective charge on functionalized MNPs using the Zetasizer Nano ZS90 instrument (Malvern Instruments Ltd., UK). CA measurements for water and oil cased are conducted to assess the wettability of the prepared particles through sessile drop method using DSA25S drop shape analyzer (KRÜSS, Germany). Details of the TEM, zeta potential, and CA measurements and sample preparation can be seen in our previous research study [7].

4.2.4. Adsorption experiment

The n-dodecane-in-water nanoemulsion is prepared via a probe sonicator, running at a power of 70 watts (10% amplitude) for 5 min. The adsorption isotherm study for the synthesized MNPs is conducted by adding the same amount of functionalized MNP@CTAB (0.5 g/L) to a freshly prepared nanoemulsion under violent vibration at 2000 rpm [7]. The adsorption isotherm analysis is carried out at constant room temperature of 25 °C using different initial oil concentration levels 2500–20,000 mg/L in the emulsion.

The equilibrium oil concentration after demulsification is determined using Agilent 7890B gas chromatography equipped with a flame ionization detector (GC-FID). The GC characterization is described with details in our previous study [7]. The equilibrium oil adsorption capacity (q_e) is the oil concentration adsorbed per unit weight of the adsorbent (MNP@CTAB) under equilibrium (mg/g), which is estimated by the following equation:

$$q_e = \left(\frac{C_0 - C_e}{w}\right) V \tag{4-1}$$

where C_0 and C_e refer to the initial and residual oil concentration after separation (mg/L), respectively; V introduces the total volume of emulsion (L); and w stands for the weight of the adsorbent (g).

The oil adsorption capacity at time *t*, q_t (mg/g), is calculated from the following expression:

$$q_t = \left(\frac{C_0 - C_t}{w}\right) V \tag{4-2}$$

where C_t represents aqueous-phase oil concentration at time *t* (mg/L). Moreover, the percentage of oil removal by MNP@CTAB (separation efficiency, SE%) is calculated as follows:

$$\text{SE\%} = \left(\frac{C_0 - C_e}{C_0}\right) 100 \tag{4-3}$$

All the experiments are repeated three times, and their mean values are used to evaluate the data.

The goodness of fitting of non-linear isotherm and kinetic models with the experimental data is evaluated using coefficient of determination (R^2) as defined below:

$$R^2 = 1 - \frac{\sum_{i=1}^{n}[y_i - \hat{y}_i]^2}{\sum_{i=1}^{n}[\hat{y}_i - \bar{y}_i]^2} \tag{4-4}$$

in which, y_i and $\hat{y}_i$ are the experimental and estimated values for the oil adsorption capacity (mg/g) at time t, respectively; and n represents the number of observations. A higher value of R^2 close to one is favored.

4.2.5. Adsorption isotherms

The adsorption isotherm analysis for the emulsified oil droplets adsorbing onto the MNPs is conducted at a constant room temperature of 25 °C using three isotherm models: Langmuir, Freundlich, and Temkin. These isotherm models were developed based on different assumptions and limitations [29].

Langmuir isotherm. This isotherm is based on the assumption that a fixed number of adsorption sites are homogenously distributed on the adsorbent surface. These adsorption sites have the same affinity for the adsorbate molecules (with the same energies) and are independent of the site occupancy, resulting in a single monolayer adsorption, in which there is no interaction between the adsorbed molecules [17,20]. Moreover, the Langmuir isotherm considers the surface coverage by maintaining a balance between the rates of adsorption and desorption, representing a dynamic

equilibrium. Adsorption is related to the proportion of the adsorbent surface that is available, while desorption is related to the proportion of the adsorbent surface that is already covered. The following equation describes the Langmuir model [15]:

$$q_e = \frac{q_{max}\, K_L C_e}{1 + K_L C_e} \tag{4-5}$$

where K_L introduces the Langmuir equilibrium constant (L/g adsorbent) and q_{max} is the maximum adsorption quantity, corresponding to the formation of monolayer (mg/g adsorbent).

The Langmuir constants can be determined from linearized equation, upon mathematical manipulation/rearrangement:

$$\frac{C_e}{q_e} = \frac{1}{K_L\, q_{max}} + \frac{C_e}{q_{max}} \tag{4-6}$$

The following equation represents the separation factor (R_L), as a dimensionless constant, which can be calculated using the Langmuir model parameters [16]:

$$R_L = \frac{1}{1 + C_0 K_L} \tag{4-7}$$

where C_0 stands for the maximum initial oil concentration (mg/L). The separation factor value is in the range of 0–1, indicating the favorability of the adsorption process. When $R_L = 1$, it means the adsorption isotherm is linear, which occurs when $K_L = 0$; when $R_L = 0$, it signifies the adsorption isotherm is irreversible, and the reason being is that K_L should be infinite, showing that the adsorption is very strong; $R_L > 1$ and $0 < R_L < 1$ indicate unfavorable and favorable adsorption processes, respectively [17,30].

Freundlich isotherm. This isotherm model is applicable for heterogeneous adsorption surfaces having various potential adsorption capacities at the active sites, for which the stronger binding sites are occupied first. The potential adsorption (strength binding) of active sites decreases by increasing the adsorption site occupation. These exponential reductions in binding energy of adsorption sites support multilayer adsorption. Freundlich equation is given by the following expression [17,19]:

$$q_e = K_F \, {C_e}^{1/n} \tag{4-8}$$

where K_F is the Freundlich constant, showing the adsorbent capacity (mg/g adsorbent), and $1/n$ is the surface heterogeneity parameter related to the adsorption intensity. The non-linear form of the Freundlich model can be linearized as follows:

$$\ln q_e = \ln K_F + \frac{1}{n} \ln C_e \tag{4-9}$$

Temkin isotherm. This isotherm describes indirect interactions between the adsorbate and adsorbent by considering the adsorption heat to quantify the interaction strength. This isotherm assumes that the adsorption heat for all adsorbate molecules linearly decreases with increasing the surface coverage, leading to a uniform distribution of the binding energies. The following equilibrium equation explains the Temkin isotherm [15,31]:

$$q_e = \frac{RT}{b} ln K_T C_e \tag{4-10}$$

where $\frac{RT}{b}$ is an indicator of the adsorption heat (J/mol); R is the universal gas constant (8.314 J/mol.K); T refers to the absolute temperature (K); b is the Temkin isotherm constant and relates

to the heat of adsorption; and K_T introduces the equilibrium binding constant (L/g). The linear Temkin isotherm is given as follows:

$$q_e = \frac{RT}{b} \ln K_T + \frac{RT}{b} \ln C_e \tag{4-11}$$

4.2.6. Adsorption kinetics

The adsorption kinetic studies for the emulsified oil droplets adsorbing onto the functionalized MNPs is performed using PFO, PSO, and IPD kinetic models. We only apply the non-linear regression technique to describe the adsorption kinetics with a need for linearization.

Pseudo-first-order model. This adsorption kinetic model is commonly used to describe adsorption in solid–liquid systems using Lagergren's equation [27]. Based on the PFO model, the adsorption process is considered as physisorption without electron transfer occurring. Physisorption is commonly a reversible process involving van der Waals and physical bonding between the adsorbate molecules and the adsorptive sites. The PFO equation of Lagergren is given as follows [32]:

$$\frac{\mathrm{d}q_t}{\mathrm{d}t} = k_1(q_e - q_t) \tag{4-12}$$

where q_t and q_e stand for the amounts of oil adsorbed at time t and equilibrium (mg/g), respectively; and k_1 is the PSO rate constant for the adsorption process (min^{-1}).

Pseudo-second-order model. This adsorption kinetic model assumes that the adsorption process involves chemisorption, forming a chemical bond between the adsorbate molecules and the adsorptive sites through sharing or exchanging electrons to form π–π and H–π interactions. The following equation describes the PSO model [17,27]:

$$\frac{\mathrm{d}q_t}{\mathrm{d}t} = k_2(q_e - q_t)^2 \quad (4\text{-}13)$$

where k_2 is the equilibrium rate constant for the PSO equation.

Intra-particle diffusion model. This adsorption kinetic model describes the transport and diffusion of the adsorbate (oil droplets) from the aqueous phase to the surface of adsorbents (MNPs) during the adsorption process [17]. The IPD model provides information about the rate-controlling step, controlling the adsorption kinetics in the adsorption process [19]. The IPD model is affected by different factors, such as the adsorbents' physical properties, adsorbate concentration, temperature, and mixing/rotation speed [22]. The following equation is suggested by Weber and Morris [33] and explains the IPD model:

$$q_t = k_i t^{0.5} + C \quad (4\text{-}14)$$

where k_i is the IPD rate constant; and C represents the boundary layer thickness. Higher values of C imply more significant impact of the boundary layer on the adsorption process [34].

4.3. Limitations of the Research

When interpreting the results of the study and applying them to practical applications or future research, it is important to consider the identified limitations of the study. These limitations highlight the importance of caution in extrapolating the findings beyond the specific experimental conditions and material used. Understanding the potential variability in other types of MNPs, different coatings, various types of oil, and real-world conditions is crucial. Factors such as temperature, pH, and the presence of other substances in the oil–water system could impact the adsorption process differently than in the controlled laboratory environment. The feasibility and challenges of scaling up the process for practical implementations need to be evaluated considering

effective variables such as the cost, availability, and scalability of the materials and methods. Additionally, alternative kinetic and isotherm models could potentially provide a better fit to the experimental data, and the suitability of all the available models cannot be carefully assessed.

4.4. Results and Discussion

This section discusses the characterization of the functionalized particles with TEM, zeta potential, and CA measurements, and oil adsorption capacity of the functionalized particles using GC-FID analysis. Then, the performance of fabricated particles for oil capturing from dodecane-in-water nanoemulsion as well as the results of adsorption isotherm and kinetic model investigations are given.

4.4.1. Functionalized MNP characterization

TEM images of bare and functionalized MNPs are illustrated in panels a and b of Figure 4. 2, respectively. As depicted in Figure 4. 2, the bare MNP appears as a denser aggregate compared to the functionalized MNP@CTAB. The lower aggregation of the functionalized MNPs is attributed to the surface modification using a cationic surfactant that results in steric repulsion for the solid phase while improving their dispersivity in the aqueous phase. The spherical structure of the particles is an advantage because it provides a higher external surface area, leading to a higher adsorption capacity.

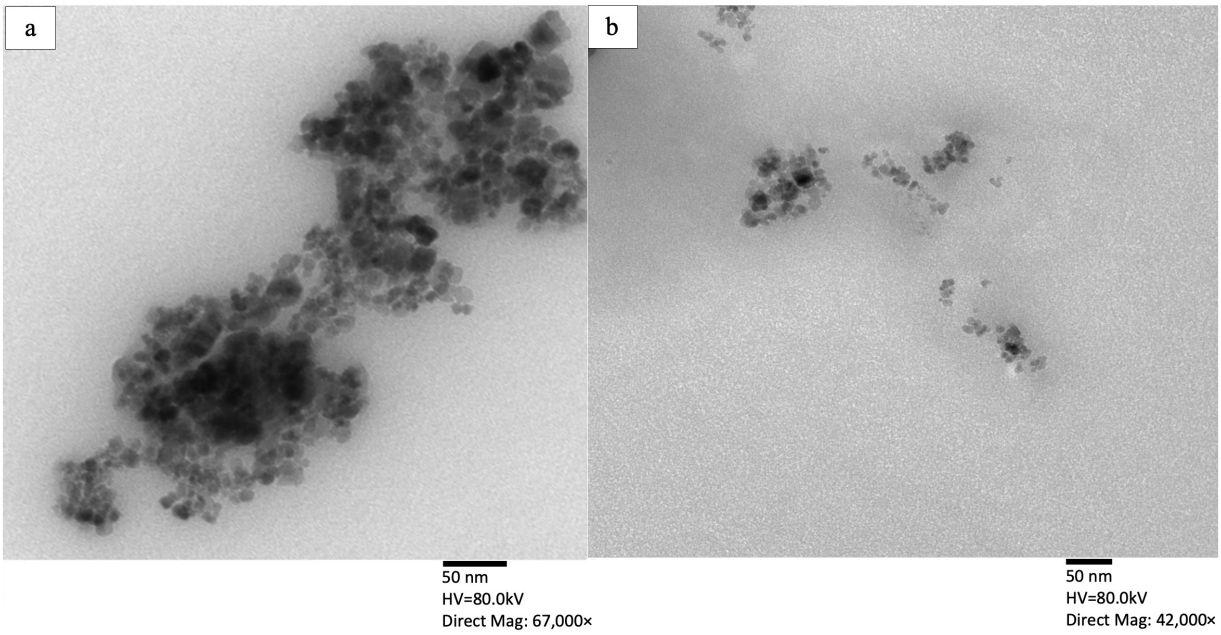

Figure 4. 2. TEM images of (a) bare MNP, and (b) MNP@CTAB

The effective surface charge of the functionalized particles is analyzed using zeta potential measurements. The results indicate a zeta potential of +4.24 mV for the bare MNPs at pH 5.0, which verifies a positive charge on bare MNPs. The magnitude of 4.24 mV shows a low stability for the bare particles and predicts their tendency to agglomerate, which is also verified by the TEM images (see Figure 4. 2. a). The measured zeta potential values for the functionalized MNPs increases significantly to +35.8 (±0.34) mV. We also measure a negative zeta potential for the prepared nanoemulsion (−55.9 ± 2.44 mV), indicating that the negatively charged droplets are able to bind to the positively charged functionalized MNP@CTAB.

The wettability of prepared particles is examined using CA measurements, as shown in Figure 4. 3. Both water and oil droplets spread immediately on the MNP@CTAB surfaces, giving a water contact angle (WCA) of 0° (Figure 4. 3. a) and oil contact angle (OCA) of 0° (Figure 4. 3. b). These results confirm the amphiphilicity of the particles, which provide better demulsification performance.

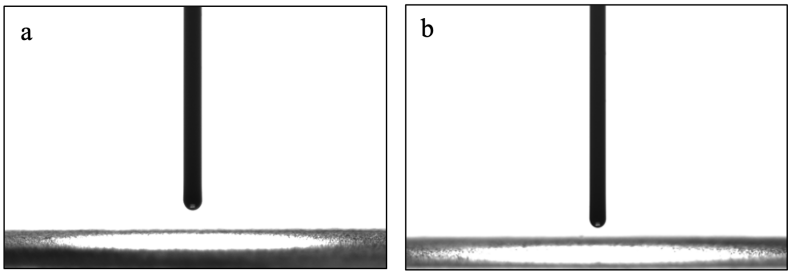

Figure 4. 3. (a) WCA and (b) dodecane OCA measurements of MNP@CTAB

4.4.2. Oil adsorption results

The oil adsorption performance for the functionalized particles is examined by estimating the oil separation efficiency (SE) from nanoemulsion (O/W) using GC-FID analysis. The SE is determined by adding 0.5 g/L MNP@CTAB to the freshly prepared 1000 ppm dodecane-in-water nanoemulsion. Particles are mixed at 2000 rpm for 20 min to ensure their dispersivity in the emulsion. The SE analysis indicates that the prepared MNP@CTAB provides a better performance with SE = 99.80%, compared to the bare MNP with SE = 57.46%. As indicated in Figure 4. 4, such improvement in the oil separation efficiency is mainly due to the more positive surface charge on MNP@CTAB that leads to a stronger electrostatic attraction to negatively charged oil droplets, as verified by the zeta potential analysis. Generally, in the oil adsorption process, the behavior of the surfactant with the particles and the water is crucial for the effectiveness of demulsification. After introducing surfactant into the emulsion, they adsorbed onto the surface of MNPs with their hydrophobic tails, while extending their hydrophilic heads into the surrounding water phase, forming a monolayer around the MNPs (Figure 4. 4,). This stable coating on the MNPs makes the particles hydrophilic and prevents their aggregation. Therefore, surfactant coating on the MNPs helps to stabilize the nanoparticles in the emulsion, which is essential for ensuring their effective contact with the oil phase. Moreover, oil adsorption occurs through hydrophobic tails of CTAB

and the amphiphilicity of MNP@CTAB, confirmed by CA measurements, provides a better dispersivity of the functionalized MNPs, resulting in a higher oil separation efficiency.

Surfactants, in general, can be effective for emulsifying the oil and water phases as their hydrophilic heads are soluble in the water, while the hydrophobic tails are oriented towards the oil phase. They can help to prevent demulsification or phase separation by forming a stable interfacial layer between the oil and water, thereby reducing the interfacial tension between them. However, the behavior of surfactants with water phase of emulsion depends on the type of surfactant. In this research, CTAB as cationic surfactant with positively charged head groups tends to interact primarily with the negatively charged oil droplets. Emphasize that the surfactant's positive charge cannot be effective in creating a stable interfacial layer as it cannot interact with water molecules directly. Moreover, CTAB surfactant with a high value of hydrophilic–lipophilic balance (HLB) of around 15.8, cannot effectively reduce the interfacial tension between oil and water, which is a key factor in preventing demulsification.

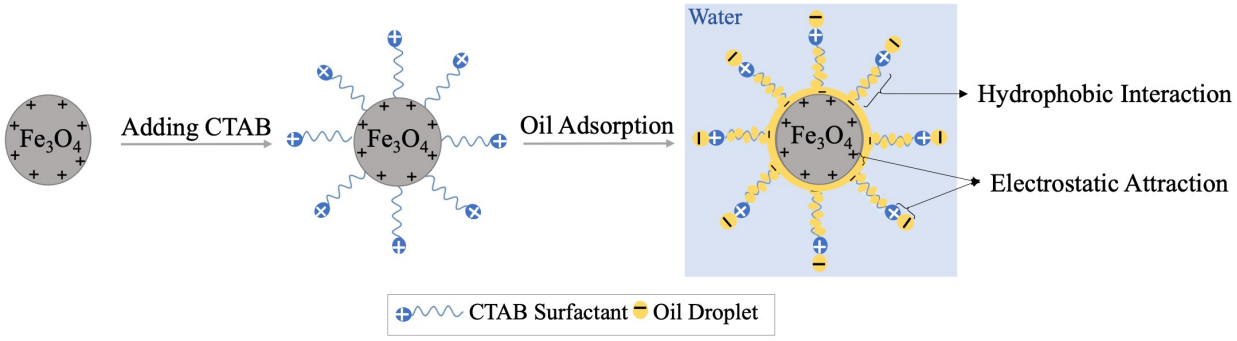

Figure 4. 4. oil adsorption mechanism using MNP@CTAB

4.4.3. Adsorption isotherms results

As displayed in Figure 4. 5, the Langmuir constants of q_{max} and K_L are estimated, respectively, from the slope and intercept of the linear plot of $\frac{C_e}{q_e}$ versus C_e.

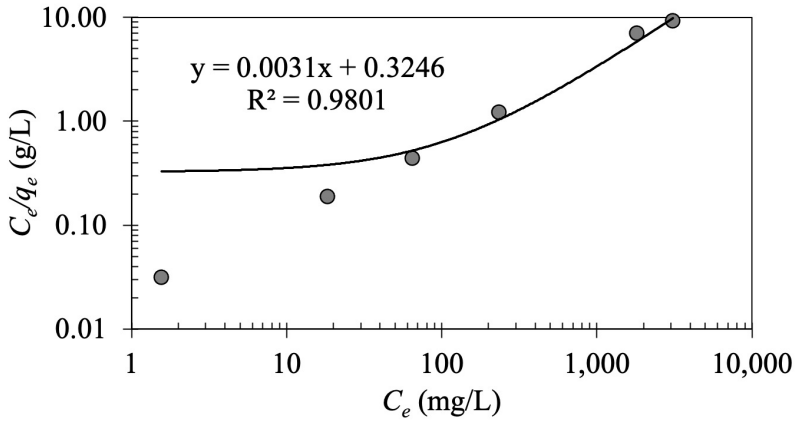

Figure 4. 5. Linear Langmuir plot of oil adsorption on MNP@CTAB

The linear regression indicates R^2 = 0.902 for the Langmuir model with estimated values of q_{max} and K_L at 327.647 mg/g and 0.009 L/g, respectively (Table 4. 1). Based on the Langmuir model, R_L value is in the range of 0.005–0.04, implying that the oil adsorption process using MNP@CTAB is favorable ($0 < R_L < 1$). As illustrated in Figure 4. 6, increasing the initial oil concentration results in less favorable oil adsorption.

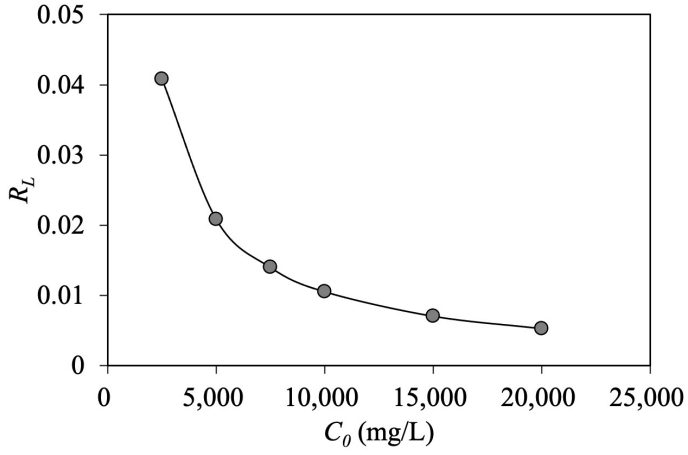

Figure 4. 6. Separation factor of Langmuir isotherm model

As shown in Figure 4. 7, the intercept and slope of ln q_e versus ln C_e give the values of Freundlich constants of K_F and $1/n$, respectively. The value of $1/n$ in the literature is in the range of 0.1–1; $n > 1$ implies a favorable adsorption process with a stronger interaction between the adsorbate and adsorbent [35]. Moreover, this value indicates the shape of C_e vs. q_e plot as follows: when $n = 1$, the plot is linear, while $n \neq 1$ yields a non-linear plot; and $n > 1$ and $n < 1$ correspond to physisorption and chemisorption, respectively [31]. As listed in Table 4. 1, the estimated value of $1/n$ in our research is 0.24 ($n = 4.156$), which refers to the favorable physical adsorption with a strong interaction between the emulsified oil droplets and MNP@CTAB particles. Moreover, the obtained oil adsorption capacity in the linearized regression analysis of the Freundlich model is 48.716 mg/g (Table 4. 1).

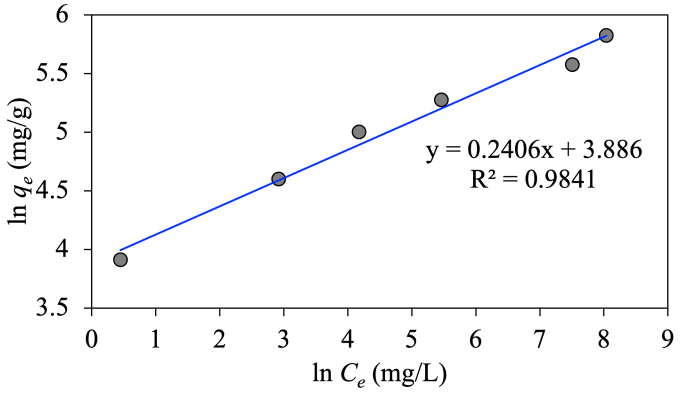

Figure 4. 7. Linear Freundlich plot of oil adsorption on MNP@CTAB

To investigate the Temkin isotherm, the constant values of b and K_T are determined, respectively, from the slope and intercept, based on the linear plot of q_e versus ln C_e, as shown in Figure 4. 8.

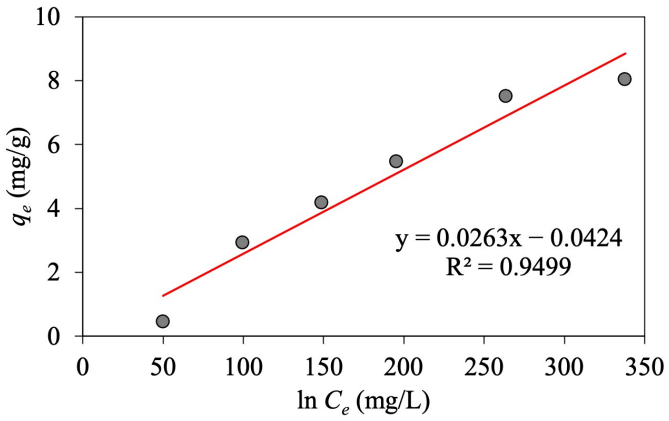

Figure 4. 8. Linear Temkin plot of oil adsorption on MNP@CTAB

As seen in Table 4. 1, linearized regression analyses show a relatively greater R^2 value for the Freundlich isotherm (0.975) compared to the two other models. Hence, this model is selected as the best fit for the equilibrium data in the oil adsorption process.

To estimate the non-linear isotherm parameters, the obtained isotherm constant values from linear analytical methods are used as an initial guess. Using a trial-and-error procedure, we apply the solver add-in with Microsoft Excel to minimize the calculated regression coefficient (R^2) between experimental data and isotherm models. Figure 4. 9 depicts the non-linear plots of different isotherm models versus experimental data for emulsified oil adsorption onto produced MNP@CTAB.

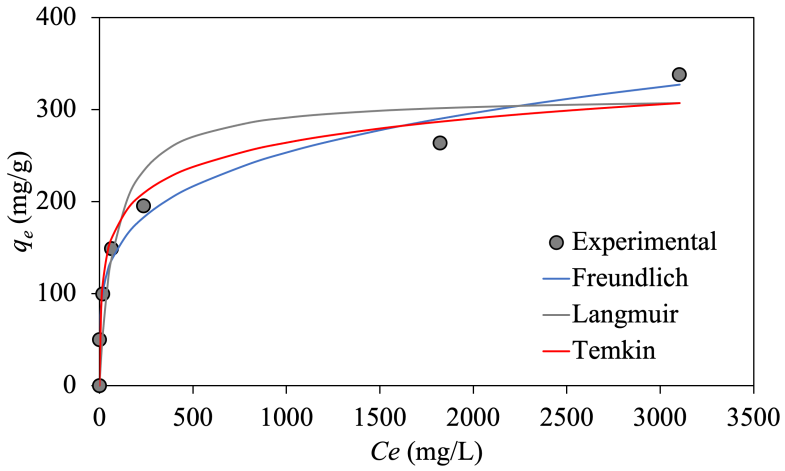

Figure 4. 9. Non-linear adsorption isotherm models for emulsified oil adsorption onto MNP@CTAB

The isotherm parameters are optimized using non-linear regression analysis for Langmuir, Freundlich, and Temkin models based on the experimental data, as summarized in Table 4. 1. As it can be seen, the linear and non-linear regression analyses give similar results, based on the estimated R^2. Therefore, the adsorption equilibrium data fit well to the isotherm models with the order of Freundlich > Temkin > Langmuir. The greater R^2 value in the Freundlich isotherm model (~ 0.98) in comparison with the other two models confirms reversible physical adsorption of emulsified oil droplets onto the functionalized MNP@CTABs.

Table 4. 1. Linearized and non-linearized adsorption isotherm parameters of emulsified oil droplets onto MNP@CTAB.

Analysis	Langmuir			Freundlich			Temkin		
	R^2	K_L (L/g)	q_{max} (mg/g)	R^2	K_F (mg/g)	n	R^2	K_T (L/g)	b
Linear	0.902	0.009	327.647	0.975	48.716	4.156	0.947	1.344	68.652
Non-linear	0.905	0.012	315.195	0.979	53.259	4.428	0.950	1.043	65.213

4.4.4. Adsorption kinetic results

The estimated adsorption kinetic parameters and the corresponding R^2 values are provided in Table 4. 2. According to the non-linear regression analysis, the PFO kinetic model with a higher R^2 value (0.99), is the best model to describe the oil adsorption process using functionalized MNPs, verifying the physical adsorption of emulsified oil droplets onto the prepared MNP@CTABs. Moreover, the estimated value of q_e from the PFO model is 99.99 mg/g, which is close to the experimental value of 99.90 mg/g, reflecting an excellent fit to experimental data.

The lower R^2 value of the IPD kinetic model (0.67) indicates that this model is not applicable for predicting the oil adsorption capacity. This means that the adsorption rate is not limited by the mass transfer of oil droplets from emulsion to the external surfaces of MNPs.

Table 4. 2. Non-linearized adsorption kinetic parameters for the sorption of emulsified oil droplets onto MNP@CTAB.

PFO			PSO			IPD		
R^2	k_1 (L/g)	q_e (mg/g)	R^2	k_2 (g/mg.min)	q_e (mg/g)	R^2	k_i (L/g)	C
0.99	0.187	99.99	0.94	0.0025	109.87	0.67	8.71	46.41

Figure 4. 10 demonstrates the amount of oil adsorption capacity (q_t) as a function of time. The higher initial slope in the adsorption kinetic plots shows a higher rate of oil adsorption at initial contact times until the system reaches equilibrium (quantified by plateau) after 30 min. Most of the adsorption occurs within 20 min, indicating a high oil adsorption rate using functionalized MNP@CTABs. As depicted in Figure 4. 10, the PFO model kinetic model describes the adsorption kinetic the best as there is a better agreement between the experimental and calculated oil adsorption capacities from this model.

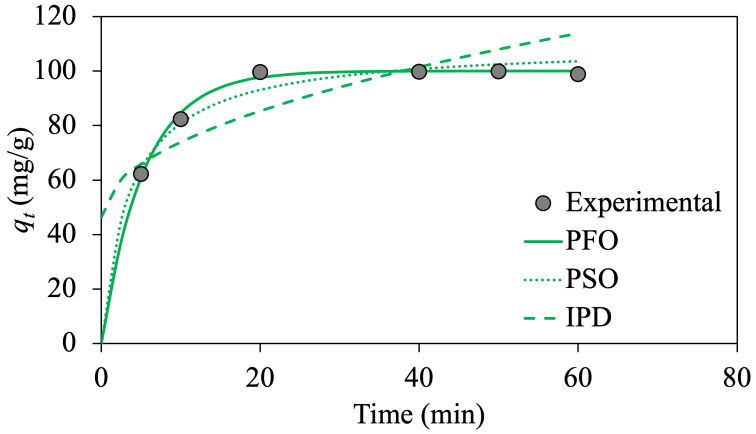

Figure 4. 10. Non-linear kinetic models plot of emulsified oil adsorption onto MNP@CTAB

Similar observations are reported in the literature for polysaccharide adsorption using superparamagnetic nanoparticles [26] and dye removal using magnetic chitosan nanoparticles [20]. Therefore, the PFO and Freundlich models are successful in describing the kinetic and isotherm adsorption process in our study, respectively. As mentioned, kinetic and isotherm adsorption models are essential to understand adsorption behaviors and provide valuable insights for scale-up and optimization purposes. A kinetic investigation focuses on the rate and mechanism of adsorption, while an isotherm study determines the maximum amount of adsorption capacity. This information is valuable for designing efficient adsorption systems through optimizing the adsorption process, selecting the most suitable adsorbents, and predicting adsorption behavior under different conditions. In summary, the indication of physical adsorption in your studies suggests that the adsorbent material is well-suited for oil adsorption applications. It's important to consider the specific characteristics of the adsorbent and the nature of the oil being adsorbed to optimize the process for practical applications.

4.5. Summary

The CTAB functionalized MNPs are employed for oil capturing from dodecane-in-water nanoemulsion. The adsorption behavior and the capacity of MNP@CTAB to adsorb emulsified oil droplets from nanoemulsion are investigated using the adsorption isotherm and kinetic models. We measure the equilibrium oil adsorption capacity using GC-FID analysis. The main conclusions drawn from this research are summarized as follows:

- Based on the SE estimations using GC-FID analysis, the SE of MNP@CTAB increases from 57.46% for bare MNP to 99.80% for the functionalized MNP due to more positive surface charge on the functionalized particles, which provides stronger interactions with negatively charged oil droplets.
- Characterization results, including one order of magnitude larger zeta potential value, less aggregation confirmed by TEM images, and amphiphilicity property verified through CA measurements reveal that our surface modification improves the functionalized particles' performance by providing higher stability and more dispersibility of MNP@CTAB particles in the emulsion.
- Both linear and non-linear regression analyses convey the message that the behavior of adsorption process is properly described in the order of Freundlich > Temkin > Langmuir isotherm models, indicating greater adaptability of Freundlich isotherm to the experimental equilibrium data.
- The favorable physical adsorption of emulsified oil droplets onto MNP@CTAB is suggested by the obtained Freundlich model's constant value of $1/n$ equal to 0.24 ($n = 4.156$), referring to the strong interactions between the adsorbents and adsorbate.

- The maximum oil adsorption capacity achieved from the Langmuir model is 327.647 mg/g. Moreover, based on the Langmuir model, the estimated R_L value is in the range of 0.005–0.04, implying favorable oil adsorption onto MNP@CTAB.
- The non-linear regression analysis of kinetic models state that the PFO model (with a higher R^2 value of 0.99) is the best model to describe the oil adsorption process compared to the PSO and IPD models, implying physical adsorption through van der Waals and physical bonding, which is also confirmed by the zeta potential measurements.
- The predicted adsorption capacity (q_e) by the PFO model is approximately 99.99 mg/g, verifying an excellent fitness with the experimental equilibrium value of q_e (99.90 mg/g).
- Simulating the adsorption process using molecular simulation techniques is recommended to better understand the adsorbent behavior for oil capturing in a molecular scale to design and optimize the adsorption process.
- Additionally, it is recommended to investigate the adsorption of various types of oil using different surfactants and coating materials to broaden the understanding of adsorption phenomena and extend the practical applicability of the research findings.

Declaration of competing interest

The authors declare that they have no known competing financial interest or personal relationships that could have appeared to influence the work reported in this paper.

Acknowledgments

The authors would like to greatly appreciate the financial support offered by Memorial University (NL. Canada), Equinor Canada, Natural Science and Engineering Research Council of Canada (NSERC), Suncor Energy Inc. /Terra Nova Young Innovator.

Nomenclatures

Acronyms

CA	-	Contact angle
CTAB	-	Cetyltrimethylammonium bromide
DI	-	Deionized
GC-FID	-	Gas Chromatography equipped with Flame Ionization Detector
IPD	-	Intra-particle diffusion
MNP	-	Magnetic nanoparticle
O/W	-	Oil-in-water
PAH	-	polycyclic aromatic hydrocarbons
PFO	-	Pseudo-first-order
PSO	-	Pseudo-second-order
SE	-	Separation efficiency
TEM	-	Transmission Electron Microscopy

Variables and Parameters

$\hat{y}_i$	-	Predicted value
C_0	-	Initial oil concentration in emulsion
C_e	-	Residual oil concentration after separation
K_F	-	Freundlich equilibrium constant
K_L	-	Langmuir equilibrium constant
K_T	-	Temkin equilibrium binding constant
q_e	-	Oil adsorption capacity

q_{max}	-	Maximum adsorption capacity
R^2	-	Coefficient of determination
R_L	-	Langmuir separation factor
y_i	-	Experimental value
b	-	Temkin isotherm constant
Fe_3O_4	-	Iron oxide
R	-	Universal gas constant
T	-	Absolute temperature
V	-	Total volume of emulsion
w	-	Weight vector

References

1. Faisal, W.; Almomani, F., A critical review of the development and demulsification processes applied for oil recovery from oil in water emulsions. *Chemosphere* **2022,** *291*, 133099.

2. Rasouli, S.; Rezaei, N.; Hamedi, H.; Zendehboudi, S.; Duan, X., Superhydrophobic and superoleophilic membranes for oil-water separation application: A comprehensive review. *Materials & Design* **2021,** *204*, 109599.

3. Rasouli, S.; Rezaei, N.; Hamedi, H.; Zendehboudi, S.; Duan, X., Design, fabrication, and characterization of a facile superhydrophobic and superoleophilic mesh-based membrane for selective oil-water separation. *Chem. Eng. Sci.* **2021,** *236*, 116354.

4. Rasouli, S.; Rezaei, N.; Zendehboudi, S.; Duan, X.; Legge, R. L.; Chatzis, I., Selective and Continuous Oil Removal from Oil–Water Mixtures Using a Superhydrophobic and Superoleophilic Stainless Steel Mesh Tube. *Langmuir* **2023,** *39* (11), 4100-4112.

5. Goodarzi, F.; Zendehboudi, S., A Comprehensive Review on Emulsions and Emulsion Stability in Chemical and Energy Industries. *The Canadian Journal of Chemical Engineering* **2019,** *97* (1), 281-309.

6. Hamedi, H.; Rezaei, N.; Zendehboudi, S., A comprehensive review on demulsification using functionalized magnetic nanoparticles. *Journal of Cleaner Production* **2022,** *380*, 134868.

7. Hamedi, H.; Zendehboudi, S.; Rezaei, N.; Azizi, A.; Shahhoseini, F., Application of Functionalized Fe3O4 Magnetic Nanoparticles Using CTAB and SDS for Oil Separation from Oil-in-Water Nanoemulsions. *Langmuir* **2023,** *39* (23), 7995-8007.

8. Low, L. E.; Ooi, C. W.; Chan, E. S.; Ong, B. H.; Tey, B. T., Dual (magnetic and pH) stimuli-reversible Pickering emulsions based on poly(2-(dimethylamino)ethyl methacrylate)-bonded Fe3O4 nanocomposites for oil recovery application. *Journal of Environmental Chemical Engineering* **2020,** *8* (2), 103715.

9. Zhou, K.; Zhou, X.; Liu, J.; Huang, Z., Application of magnetic nanoparticles in petroleum industry: A review. *Journal of Petroleum Science and Engineering* **2020,** *188*, 106943.

10. Lü, T.; Zhang, S.; Qi, D.; Zhang, D.; Zhao, H., Enhanced demulsification from aqueous media by using magnetic chitosan-based flocculant. *J. Colloid Interface Sci.* **2018,** *518*, 76-83.

11. Hammouda, S. b.; Chen, Z.; An, C.; Lee, K.; Zaker, A., Buoyant oleophilic magnetic activated carbon nanoparticles for oil spill cleanup. *Cleaner Chemical Engineering* **2022**.

12. Xu, H.; Wang, J.; Ren, S., Removal of Oil from a Crude Oil-in-Water Emulsion by a Magnetically Recyclable Diatomite Demulsifier. *Energy & Fuels* **2019,** *33* (11), 11574-11583.

13. Song, Y.; Zhou, J.; Fan, J.-B.; Zhai, W.; Meng, J.; Wang, S., Hydrophilic/Oleophilic Magnetic Janus Particles for the Rapid and Efficient Oil–Water Separation. *Adv. Funct. Mater.* **2018,** *28* (32), 1802493.

14. Zendehboudi, S.; Ahmadi, M. A.; Rajabzadeh, A. R.; Mahinpey, N.; Chatzis, I., Experimental study on adsorption of a new surfactant onto carbonate reservoir samples—application to EOR. *Can. J. Chem. Eng.* **2013,** *91*, 1439-1449.

15. Ayawei, N.; Ebelegi, A. N.; Wankasi, D., Modelling and Interpretation of Adsorption Isotherms. *Journal of Chemistry* **2017,** *2017*, 3039817.

16. Nouri, N.; Tasviri, M.; Zendehboudi, S., Effect of Poly(vinyl alcohol) on Catalytic Performance of Al-Pillared Clay in Alkylation of Aromatic Hydrocarbons with Olefins. *Industrial & Engineering Chemistry Research* **2023**.

17. Bameri, I.; Saffari, J.; Baniyaghoob, S.; Ekrami-Kakhki, M.-S., Synthesis of magnetic nano-NiFe2O4 with the assistance of ultrasound and its application for photocatalytic degradation of Titan Yellow: Kinetic and isotherm studies. *Colloid and Interface Science Communications* **2022,** *48*, 100610.

18. Unuabonah, E. I.; Omorogie, M. O.; Oladoja, N. A., 5 - Modeling in Adsorption: Fundamentals and Applications. In *Composite Nanoadsorbents*, Kyzas, G. Z.; Mitropoulos, A. C., Eds. Elsevier: 2019; pp 85-118.

19. Kumbhar, P.; Narale, D.; Bhosale, R.; Jambhale, C.; Kim, J.-H.; Kolekar, S., Synthesis of tea waste/Fe3O4 magnetic composite (TWMC) for efficient adsorption of crystal violet dye: Isotherm, kinetic and thermodynamic studies. *Journal of Environmental Chemical Engineering* **2022,** *10* (3), 107893.

20. Jaafari, J.; Barzanouni, H.; Mazloomi, S.; Amir Abadi Farahani, N.; Sharafi, K.; Soleimani, P.; Haghighat, G. A., Effective adsorptive removal of reactive dyes by magnetic chitosan nanoparticles: Kinetic, isothermal studies and response surface methodology. *Int. J. Biol. Macromol.* **2020,** *164*, 344-355.

21. Costa, J. A. S.; de Jesus, R. A.; Santos, D. O.; Neris, J. B.; Figueiredo, R. T.; Paranhos, C. M., Synthesis, functionalization, and environmental application of silica-based mesoporous materials of the M41S and SBA-n families: A review. *Journal of Environmental Chemical Engineering* **2021,** *9* (3), 105259.

22. El-Naas, M.; Alhaija, M. A., Modelling of adsorption processes. *Mathematical Modelling* **2013**, 579-600.

23. Mazloom, M. S.; Hemmati-Sarapardeh, A.; Husein, M. M.; Behbahani, H. S.-z.; Zendehboudi, S., Application of nanoparticles for asphaltenes adsorption and oxidation: A critical review of challenges and recent progress. *Fuel* **2020,** *279*, 117763.

24. Mazloom, M. S.; Rezaei, F.; Hemmati-Sarapardeh, A.; Husein, M. M.; Zendehboudi, S.; Bemani, A., Artificial Intelligence Based Methods for Asphaltenes Adsorption by Nanocomposites: Application of Group Method of Data Handling, Least Squares Support Vector Machine, and Artificial Neural Networks. *Nanomaterials (Basel, Switzerland)* **2020,** *10* (5).

25. Ranjbari, E.; Hadjmohammadi, M. R.; Kiekens, F.; De Wael, K., Mixed Hemi/Ad-Micelle Sodium Dodecyl Sulfate-Coated Magnetic Iron Oxide Nanoparticles for the Efficient Removal and Trace Determination of Rhodamine-B and Rhodamine-6G. *Anal. Chem.* **2015,** *87* (15), 7894-7901.

26. Nanta, P.; Kasemwong, K.; Skolpap, W., Isotherm and kinetic modeling on superparamagnetic nanoparticles adsorption of polysaccharide. *Journal of environmental chemical engineering* **2018,** *6*, 794-802.

27. Mirzaee, E.; Sartaj, M., Activated Carbon-Based Magnetic Composite as an Adsorbent for Removal of Polycyclic Aromatic Hydrocarbons from Aqueous Phase: Characterization, Adsorption Kinetics and Isotherm Studies. *Journal of Hazardous Materials Advances* **2022**.

28. Torlopov, M. A.; Vaseneva, I. N.; Mikhaylov, V. I.; Martakov, I. S.; Moskalev, A. A.; Koval, L. A.; Zemskaya, N. V.; Paderin, N. M.; Sitnikov, P. A., Pickering emulsions stabilized by partially acetylated cellulose nanocrystals for oral administration: oils effect and in vivo toxicity. *Cellulose* **2021,** *28* (4), 2365-2385.

29. Ahmadi, M. A.; Zendehboudi, S.; Shafiei, A.; James, L., Nonionic Surfactant for Enhanced Oil Recovery from Carbonates: Adsorption Kinetics and Equilibrium. *Industrial & Engineering Chemistry Research* **2012,** *51* (29), 9894-9905.

30. Mirahsani, A.; Giorgi, J.; Sartaj, M., Ammonia removal from aqueous solution by sodium functionalized graphene oxide: isotherm, kinetics, and thermodynamics. *DESALINATION AND WATER TREATMENT* **2020,** *178*, 143-154.

31. Nezhadali, A.; Koushali, S. E.; Divsar, F., Synthesis of polypyrrole – chitosan magnetic nanocomposite for the removal of carbamazepine from wastewater: Adsorption isotherm and kinetic study. *Journal of Environmental Chemical Engineering* **2021,** *9* (4), 105648.

32. López-Luna, J.; Ramírez-Montes, L. E.; Martinez-Vargas, S.; Martínez, A. I.; Mijangos-Ricardez, O. F.; González-Chávez, M. d. C. A.; Carrillo-González, R.; Solís-Domínguez, F. A.; Cuevas-Díaz, M. d. C.; Vázquez-Hipólito, V., Linear and nonlinear kinetic and isotherm adsorption models for arsenic removal by manganese ferrite nanoparticles. *SN Applied Sciences* **2019,** *1* (8), 950.

33. Weber, W. J.; Morris, J. C., Kinetics of Adsorption on Carbon from Solution. *Journal of the Sanitary Engineering Division* **1963,** *89*, 31-59.

34. Jain, M.; Yadav, M.; Kohout, T.; Lahtinen, M.; Garg, V. K.; Sillanpää, M., Development of iron oxide/activated carbon nanoparticle composite for the removal of Cr(VI), Cu(II) and Cd(II) ions from aqueous solution. *Water Resources and Industry* **2018,** *20*, 54-74.

35. Eeshwarasinghe, D.; Loganathan, P.; Kalaruban, M.; Sounthararajah, D. P.; Kandasamy, J.; Vigneswaran, S., Removing polycyclic aromatic hydrocarbons from water using granular activated carbon: kinetic and equilibrium adsorption studies. *Environmental science and pollution research international* **2018,** *25* (14), 13511-13524.

5. CHAPTER FIVE

Modelling and optimization of oil adsorption capacity on functionalized magnetic nanoparticles using machine learning approach

Preface

A version of this manuscript has been published in the Journal of Molecular Liquids, 392, 123378. I am the primary author of this manuscript. I carried out the majority of the literature review, data collection, model development, and investigation based on the inputs and plan provided by the supervisors. Sohrab Zendehboudi and Nima Rezaei have a considerable contribution in revising the manuscript in terms of editorial and technical aspects. Moreover, Saady Noori and Helen Zhang, provide feedback on artificial intelligence parts and discission section.

5.1. Introduction

Oil capturing of the emulsified oily wastewater is challenging due to the inherent high stability of emulsion [1]. The limitations of conventional demulsification techniques, such as gravity separation, floatation, electrochemical and membrane filtration, illustrate the need to develop efficient and cost-effective demulsification techniques [2]. Industries most commonly use flocculation by adding flocculating agents, including acids, alkalis, salts, and chemical demulsifiers. However, using large quantities of these irrecoverable demulsifiers cause secondary pollution [3]. More efforts have been devoted to finding novel materials to remove oil from emulsified oily wastewater efficiently.

Recently, nanotechnology has emerged as an ideal solution for oil capturing from an aqueous phase. Magnetic nanoparticles (MNPs), iron oxide (Fe_3O_4) nanoparticles (NP), have attracted tremendous attention due to their high oil adsorption capacity, low toxicity, recoverability, and reusability [4, 5]. However, their inherent instability due to their high chemical activity leads to agglomeration, precipitation, and oxidation by air, thereby losing their magnetism and dispersibility. MNPs must be stabilized by developing a protective layer such as organic and inorganic materials on their surfaces to change their functionality towards more hydrophilicity to provide better dispersivity [6]. During the last few years, many studies focused on applying MNPs for oil-water separation [7-10]. To the best of our knowledge, no study investigated the optimization of emulsified oil adsorption process using MNPs. Mathematical modeling can provide a better understanding of the process and all the effective parameters. However, conventional mathematical models (mechanistic models) experience some limitations; thus, they cannot fully model and simulate adsorption mechanisms due to the complexity of the adsorption process, which is affected by various factors and their non-linear interactions [11, 12].

To this end, smart tools such as artificial intelligence (AI) have been of great interest in many investigations because they can provide high computational speed and performance with no need to the knowledge of targeted systems [13]. For instance, artificial neural network (ANN) is a powerful AI technique inspired by biological neurons that can model complex non-linear systems [14].

Fuzzy neural network models are becoming more popular because they offer the benefit of the learning capability in the ANNs and the knowledge demonstration capability of the fuzzy logic [15]. An adaptive network-based fuzzy inference system (ANFIS) is an adaptive multi-layer feed-forward network without the ANN's defects (e.g., lack of interpretation and the weaknesses of the learning stage of fuzzy logic) [16]. ANFIS has been extensively used to estimate target variables in complex non-linear systems. However, the high dimensionality of the ANFIS model and its training complexity for large datasets are limitations of this model. In addition, finding the number and type of membership functions, clustering input values, and initial fuzzy inference system (FIS) for the training process is relatively difficult [17, 18].

Support vector machine (SVM) is a non-parametric and non-linear powerful technique to estimate output parameters in complex and high-dimensional processes [19]. SVM is a supervised machine learning with more stability, robustness, and generality, leading to more popularity of this tool compared to ANN [20, 21]. Least square SVM (LSSVM) is a modified version of SVM with less complexity and computational effort, thereby less running time when implemented for a large dataset with high accuracy [22]. Moreover, the LSSVM approach has more flexibility, generalization, and predictive accuracy with no need a large datasets [23].

Gene expression programming (GEP) is a robust AI-based optimization technique inspired by natural phenomena to obtain a relation between input and target variables which has been widely

applied to various engineering cases [24-26]. However, its performance for modeling and optimizing the oil adsorption capacity has not been investigated yet. The predicted target using the developed GEP model is an analytical function without complexity compared to ANN models [27, 28].

To the best of our knowledge, despite the importance of AI models, there is no research in the literature that focuses on optimizing emulsified oil capturing using MNPs. However, numerous studies have investigated the predictive capability of smart models for either modeling crude oil adsorption using various adsorbents or modeling MNPs application for removing other contaminants. For instance, Asadu et al. [29] applied ANN, ANFIS, and response surface methodology (RSM) to model and optimize crude oil adsorption using organic acid-functionalized biomass. Analysis of these three smart models indicated great oil removal prediction with quite a similar correlation coefficient of 0.999, but statistically, the RSM performance was marginally better than ANN and ANFIS. Ike et al. [30] investigated the removal of crude oil modeling using organic acid-grafted banana pseudo stem fiber by employing ANN-GA, ANFIS-GA, and RSM. The results showed that all three models adequately predicted the oil removal with a correlation coefficient of more than 0.97; however, statistical analysis suggested ANN-GA was the best model, followed by ANFIS-GA and RSM. Foroutan et al. [31] employed ANFIS model to assess the influence of MNPs and chitosan on chromium adsorption capacity of natural clay. The statistical analysis indicated good agreement between the ANFIS model and experimental outcomes. Fan et al. [11] investigated copper removal from an aqueous area using MNPs by applying ANN-GA, RSM, and ANN-PSO models. They found that the ANN-GA model offers more accurate predictions than RSM, and the ANN-PSO model is the most effective tool for optimizing/predicting the Cu(II) removal. Moreover, Debs et al. [32] verified the robustness of the

statistical analysis for oil spill cleanup using MNPs and yeast-based magnetic bio-nanocomposite by employing the ANN approach. The results revealed a good match between the ANN model predictions and measurements with $R^2 = 0.94$ for new motor oil, $R^2 = 0.86$ for mixed used motor oil, and $R^2 = 0.90$ for Petroleum 28° API, with considerably low relative errors of 0.8, 0.4, and 4%, respectively.

In this work, we first prepare functionalized MNPs to use as adsorbents to adsorb oil from oil-in-water nanoemulsion. After conducting experiments and gathering our data, three advanced machine learning approaches, including ANFIS, LSSVM, and GEP are used to optimize the emulsified oil adsorption using functionalized MNPs. The performance of these models is evaluated and compared based on statistical criteria such as the coefficient of determination (R^2), mean percentage error (MPE), and mean absolute percentage error (MAPE) to introduce the most reliable and accurate model. A sensitivity analysis is conducted to estimate the relative importance of input variables affecting the target (the oil adsorption capacity) using the best-developed model. Developing comprehensive smart models that consider complex factors influencing oil adsorption, lead to optimized design for efficient oil removal. This would enhance environmental protection efforts, improve cost-effectiveness by making the process more sustainable, and promote resource optimization. Furthermore, our research would contribute to the advancement of knowledge in the field, driving more innovation and applications of MNPs in oil spill cleanup and wastewater treatment. Overall, our work would have a positive impact on industries, communities, and ecosystems affected by oil pollution.

After the introduction part, the paper gives a brief theory and background on smart models (ANFIS, LSSVM, and GEP) is given in Section 2. Section 3 presents the research methodology to achieve the dataset used in this research, data pre-processing, model development, and evaluation

strategy. Modeling results, comparison of the accuracy of the developed models based on statistical criteria, and relative importance analysis are provided in Section 4. The final section highlights the main conclusion remarks of this research study.

5.2. Theoretical aspects of smart models

5.2.1. ANFIS Model

Jang first developed the adaptive network-based fuzzy inference system (ANFIS) by integrating artificial neural network (ANN) and fuzzy inference system (FIS) to eliminate the drawbacks of these standalone models [17, 33]. ANNs have some limitations, such as low convergence speed, lack of interpretation, and low prediction accuracy for small datasets [34]. FIS have some drawbacks, such as the need for experience and knowledge of the issue [17, 35]. ANFIS incorporates the learning ability and computational power of ANNs into FIS to develop a fast and accurate model [36].

The ANFIS model is a universal estimator based on the Takagi-Sugeno inference system in the form of if-then fuzzy rules. The structure consists of input nodes and five hidden layers, including fuzzification, multiplication, normalization, defuzzification, and output layers [30, 37, 38]. In the hidden layers, several fixed and adjustable nodes are designed using their membership function. The O_i^j represents the output of the node i in the layer j and A_j^i is the linguistic label for each node. Figure 5. 1 illustrates the ANFIS structure with two inputs (x_1, x_2), one output (O^5), and layers defined as follows:

Layer one (fuzzification layer). This layer serves as membership function for the input. In this layer every node i is an adaptive node with a node function as shown in Eq. 5-1 [30, 37]:

$$O_i^1 = \mu_{A_j}^{\ i}(x_j) \quad i = 1, 2 \tag{5-1}$$

where O_i^1 represents the output of layer one and $\mu_{A_j}^{\ i}$ is the membership function of A_j^i.

Layer two (multiplication or rule layer). This layer acts as the fuzzy rules indicating the requirements and consequences of the rules. In this layer each node is a fixed node labelled as Π and the output is the product of all the incoming signals (i.e. the outputs of layer one) and introduces the firing strength (w_i) as shown in Eq. 5-2 [30, 37]:

$$O_i^2 = \prod_{j=1}^{n} \mu_{A_j}^{\ i}(x_j) = w_i(x) \tag{5-2}$$

where O_i^2 is the output of layer two.

Layer three (normalization layer). In this layer the nodes are the normalized values of the firing strength in Eq. 5-3 [36]:

$$O_i^3 = \overline{w}_i(x) = \frac{w_i(x)}{\sum_{i=1}^{n} w_i(x)} \tag{5-3}$$

where O_i^3 represents the output of layer three and $\overline{w}_i$ is the normalized firing strength of the i^{th} rule.

Layer four (defuzzification layer). Every node in his layer is an adaptive node with a node function, indicating the contribution of the i^{th} rule towards the overall output defined as in Eq. 5-4 [30, 37]:

$$O_i^4 = \overline{w}_i(x) f_i(x) = \overline{w}_i \, (p_i x + q_i y + r_i) \tag{5-4}$$

where O_i^4 is the output of layer four; $\overline{w}_i$ represents the normalized firing strength (the output of layer three); p_i, q_i, and r_i refer to the consequent variables.

Layer five (output layer). This layer is the addition of all incoming signals resulting in s overall output as in Eq. 5-5:

$$O_i^5 = \sum_{i=1}^{n} \overline{w}_i(x) f_i(x) = \frac{\sum_{i=1}^{n} w_i(x) f_i(x)}{\sum_{i=1}^{n} w_i\,(x)} \tag{5-5}$$

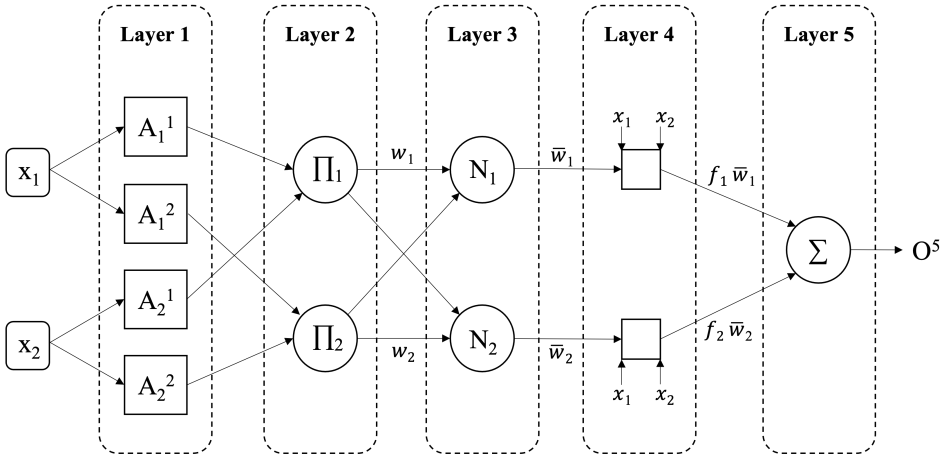

Figure 5. 1. ANFIS model structure for two inputs (x_1, x_2) and one output

5.2.2. LSSVM Model

The support vector machine (SVM) is a powerful mathematical technique to solve complicated and non-linear systems; it was first introduced by Vapnik [39]. SVM is a robust supervised learning algorithm for various scenarios, including predicting, classification, and regression analysis. More details of the SVM approach are available in the literature [34, 37]. Suykens and Vandewalle developed a modified version of SVM, called least square SVM (LSSVM), to reduce the computational complexity and run time [22]. Instead of using a quadratic programming approach in the corresponding SVM, the LSSVM model finds the solution by solving a set of linear equations. The regression error of the LSSVM is defined as the difference between the predicted

and the experimental values, while in the SVM, regression error is optimized during the calculations. It means that the LSSVM model involves equality constraint with a least-squares of cost function instead of the inequality constraints of SVM [40]. Therefore, the LSSVM algorithm can be applied to a large dataset with high accuracy. For a specific set of experimental data $\{(x_1, y_1), (x_2, y_2), \ldots, (x_N, y_N)\}$ where x_i and y_i defer to the input and output data, respectively; Eq. 5-6 can be applied for regression modeling:

$$y_i = w^T \phi(x_i) + b \tag{5-6}$$

where w refers to the weight vector, $\phi(x_i)$ is a non-linear mapping function, T represents the matrix transpose operation, and b is the bias term. The data (x_i) are mapped into the n-dimensional feature space. In the LSSVM model, the regression error is considered an addition to the constraint of the optimization problem. The cost function of the LSSVM needs to be minimized to perform regression (Eq. 5-7) [34, 41]:

$$Q_{LSSVM} = \frac{1}{2} w^T w + \frac{1}{2} \gamma \sum_{i=1}^{N} e_i^2 \tag{5-7}$$

Subject to the following equality constraint (Eq. 5-8):

$$y_i = w^T \phi(x_i) + b + e_i \quad \text{and} \quad i = 1, 2, 3, \ldots, N \tag{5-8}$$

where w represents the regression weight, γ is the regularization constant, the subscript i symbolizes each training data point, and e_i refers to the regression error. Eq. 5-9 can be used to estimate the Lagrange function:

$$L_{LSSVM} = \frac{1}{2} \|w\|^2 + \frac{1}{2} \gamma \sum_{i=1}^{N} e_i^2 - \sum_{i=1}^{N} \alpha_i \left[w^T \phi(x_i) + b + e_i - y_i \right] \tag{5-9}$$

where α represents a Lagrange multiplier which can be either a positive or negative value, which is proportional to the error of the corresponding training data points.

The optimum point can be obtained using the partial differentiation of the Eq. 5-9 with respect to w, b, e_i, and α_i, as in Eq. 5-10 [22, 42]:

$$\begin{aligned}
&\frac{\partial \mathrm{L}}{\partial w} = 0 \;\rightarrow\; w = \sum_{i=1}^{N} \alpha_i \; \phi(x_i) \\
&\frac{\partial \mathrm{L}}{\partial b} = 0 \;\rightarrow\; \sum_{i=1}^{N} \alpha_i = 0 \\
&\frac{\partial \mathrm{L}}{\partial e_i} = 0 \;\rightarrow\; \alpha_i = \gamma e_i \\
&\frac{\partial \mathrm{L}}{\partial \alpha_i} = 0 \;\rightarrow\; w^T \phi(x_i) + b + e_i - y_i = 0
\end{aligned} \tag{5-10}$$

By eliminating w and e_i, the following linear equation can be achieved (Eq. 5-11):

$$\begin{bmatrix} 0 & 1_N^T \\ 1_N & \Omega + \gamma^{-1} I_N \end{bmatrix} \begin{bmatrix} b \\ \alpha \end{bmatrix} = \begin{bmatrix} 0 \\ y \end{bmatrix} \tag{5-11}$$

in which $\alpha = [\alpha_1 , \ldots, \alpha_N]^T$, $y = [y_1 , \ldots, y_N]^T$, $1_N = [1 , \ldots, 1]^T$, I_N denotes identity matrix of the size $N \times N$, and $\Omega \in R^{N \times N}$ represents a kernel function presented by Eq. 5-12:

$$\Omega_{ij} = \phi(x_i)^T \phi(x_j) = K(x_i, x_j) \quad \text{for} \quad i \text{ and } j = 1, 2, \ldots, N \tag{5-12}$$

where $K(x_i, x_j)$ represents the kernel function. Therefore, the non-linear regression prediction model of the LSSVM can be obtained using kernel function as given by Eq. 5-13:

$$y_i = \sum_{i=1}^{N} \alpha_i K(x_i, x_j) + b \tag{5-13}$$

Based on the literature the kernel equation can be sigmoid, polynomial, linear, and radial basis function (RBF), resulting in different LSSVM results [43, 44].In this research, the RBF is selected to be applied in the LSSVM algorithm as follows:

$$K(x_i, x_j) = \exp\left(-\frac{\|x_i - x_j\|^2}{\sigma^2}\right) \tag{5-14}$$

where σ is the RBF kernel width, which is the regression ability, optimized by an external optimization algorithm in the training phase. Both regularization parameter (γ) and kernel width (σ) need to be optimized to develop the LSSVM model with generalization behavior and highest convergence speed. To this end, we use coupled simulated annealing (CSA) optimization method to achieve the optimum values of two adjustable parameters (σ and γ) of the LSSVM models through trial and error [45].

5.2.3. GEP model

Gene expression programming (GEP) was developed by Ferreria [46] as an AI-based optimization technique; it combines genetic algorithm (GA) and genetic programming (GP). The computer programs in GEP are developed based on Darwin's theory of mutation, crossover, and reproduction [28, 47]. The individuals in the GEP are encoded chromosomes that reform into one or more genes with terminals tails and a head of functions. Finally, they are presented as an expression tree (ET) with different shapes and sizes. Indeed, the chromosomes encode any program for effective solutions through transitioning into an ET, resulting in a model with high precision and reliable performance compared with standalone GA and GP [25]. Figure 5. 2

illustrates a typical example of a two-gene chromosome containing four functions of +, *, /, and Q, and three terminals including a, b, and c. The mathematical expression of the ET illustrated in Figure 5. 2 can be written through Karva notation or K-expression [24, 28] of $(a * b) + (\sqrt{b/c})$.

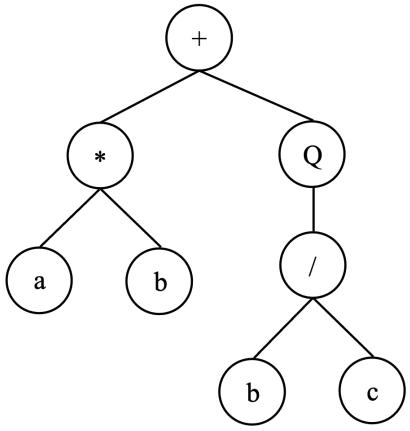

Figure 5. 2. A typical two-chromosome expression tree in Gene expression programming (GEP) approach

5.3. Advantages and limitations of the models

The smart models (black-box models) with higher computational speed result in a higher efficiency compared to the other models (white and grey) without adequate knowledge of the targeted phenomena [13]. Table 5. 1 provides the main advantages and limitations of the applied models in this research work.

Table 5. 1. Advantages and limitations of different models

Models	Advantages	Limitations
ANFIS	• Highly generalization capabilities. • High adaption capability and learning capacity speed.	• Limited application for large datasets due to their complex structure and high computational cost [41].

	• Need fewer adjustable parameters compared to other neural network models [48]. • Handle both numerical and linguistic knowledge. • Provide room for application involving crisp input and outputs [49].	• Difficulty of finding the type and number of membership function, initial rule-base, and clustering input variables. • Balance between accuracy and interpretability [15].
LSSVM	• High prediction accuracy and generalization capabilities. • Does not need a large database and prior knowledge of the network topology. • No under- or over-fitting problem. • Less complex structure in comparison with ANN. • Converges to the global optima, no local minima. • Contains only two variable factors (σ and γ) to predict targets. • High computation speed, easy development, and applicability [13, 34].	• Limited application for large-scale issues due to lack of sparsity. • Using sum square error without regularization might result in less accuracy in predictions [34]. • Difficulty in selecting kernel function among its different types [41].
GEP	• Easy to implement on a personal computer. • High iteration speed. • Can find mathematical function. • Hierarchical prediction method using multigenic chromosomes. • Easy to manipulate genetically due to simple entities chromosomes.	• Needs a considerable data • Higher computational/run time

	• Provides visualization data model and simple result interpretation. • Easy parametric sensitivity analysis. • Greater performance compared to adaptive algorithm [34, 50].	

Generally, the main limitation of all the black-box (data-driven) models is their strong dependency on the data with low capability in extrapolating data. However, there are limited studies in the literature to provide adequate data for further investigation of the emulsified oil adsorption process using MNPs.

5.4. Materials and method

5.4.1. Materials

The iron oxide nanopowder (Fe_3O_4) with a size of 15–20 nm (>99.5% purity) is purchased from US Research Nanomaterials, Inc. Ethanol absolute is obtained locally, while cetyltrimethylammonium bromide (CTAB) is purchased from Millipore Sigma Corporation, USA. Chloroform (HPLC grade, >99.5%) is ordered from Thermo Scientific, and *n*-dodecane (≥ 99%) is bought from Thermo Scientific Alfa Aesar, Canada. The On/Off magnetic welding square is provided by Master Magnetics, Inc. Deionized water with a resistivity of 18.2 MΩ is produced using a SYBRON/Barnstead water purification system, USA.

5.4.2. Adsorption experiments

The synthesis of the functionalized MNPs is described in detail in our previous work [6]. The oil-in-water (o/w) nanoemulsion is prepared by combining dodecane and DI water using a probe sonicator for 5 min. The sonication process involves applying a pulsed sequence (working for 10

s followed by a 5-s break) while maintaining the temperature in a water bath. The resulting emulsion contains 1000 ppm oil concentration. To assess the separation efficiency of the functionalized MNPs, the residual oil content in the liquid phase is analyzed using an Agilent 7890B Gas Chromatography (GC) with Flame Ionization Detector (GC-FID). Therefore, demulsification performance of both bare and coated MNPs are compared. To this end, a specific amount of the functionalized particles (at a concentration of 0.5 g/L) is mixed with freshly prepared nanoemulsion, which has an average oil droplet size of approximately 320 nm. The mixture is subjected to intense vibration at 2000 rpm to evaluate demulsification efficiency of the coated particles [6].

The percentage of oil removal by magnetic particles (separation efficiency, SE%) and the amount of adsorbed oil onto the MNPs (adsorption capacity, q_e) are calculated by Eqs. 5-15 and 5-16 equations:

$$SE\% = \left(\frac{C_0 - C_e}{C_0}\right) 100 \tag{5-15}$$

$$q_e = \left(\frac{C_0 - C_e}{w}\right) V \tag{5-16}$$

where C_0 is the initial oil concentration in emulsion (ppm); C_e is the residual oil concentration after separation (ppm); q_e is the amount of adsorbed oil per unit mass of adsorbent (mg/g adsorbent); V is the total volume of emulsion (L); and w is the weight of adsorbent (g).

5.4.3. Data pre-processing

Identifying the input (independent) and output (dependent) variables is the first step of the modeling process. In this study, oil adsorption capacity (q_e) is considered a response (output)

variable which depends on the oil concentration, MNP dosage, and mixing time as input variables. The experiments generated 149 data points. The input and output experimental data are normalized between +1 and –1 to avoid numerical overflow caused by too large or too small weights and to obtain convergence. The experimental data are normalization using Eq. 5-17.

$$\hat{x} = 2\frac{x_i - x_{min}}{x_{max} - x_{min}} - 1 \tag{5-17}$$

where $\hat{x}$ is the normalized value of x_i, and x_{max} and x_{min} represent the maximum and minimum values of data, respectively.

5.4.4. Model development

Figure 5. 3.shows the basic procedure of model development. First, the 149 experimental data points are randomly divided into two subsets, including training and testing datasets. For this purpose, 80% of the whole database is used for the training process, and the remaining 20% is used for the testing process. The training process stops when the value of R^2 and errors reach a high value (close to one) and a very small value, respectively. The testing process of data is conducted to assess the accuracy and reliability of the developed models.

The ANFIS and LSSVM-CSA modeling are developed using MATLAB software (version R2022a). The GeneXproTools software package version 5 is used to implement the GEP model.

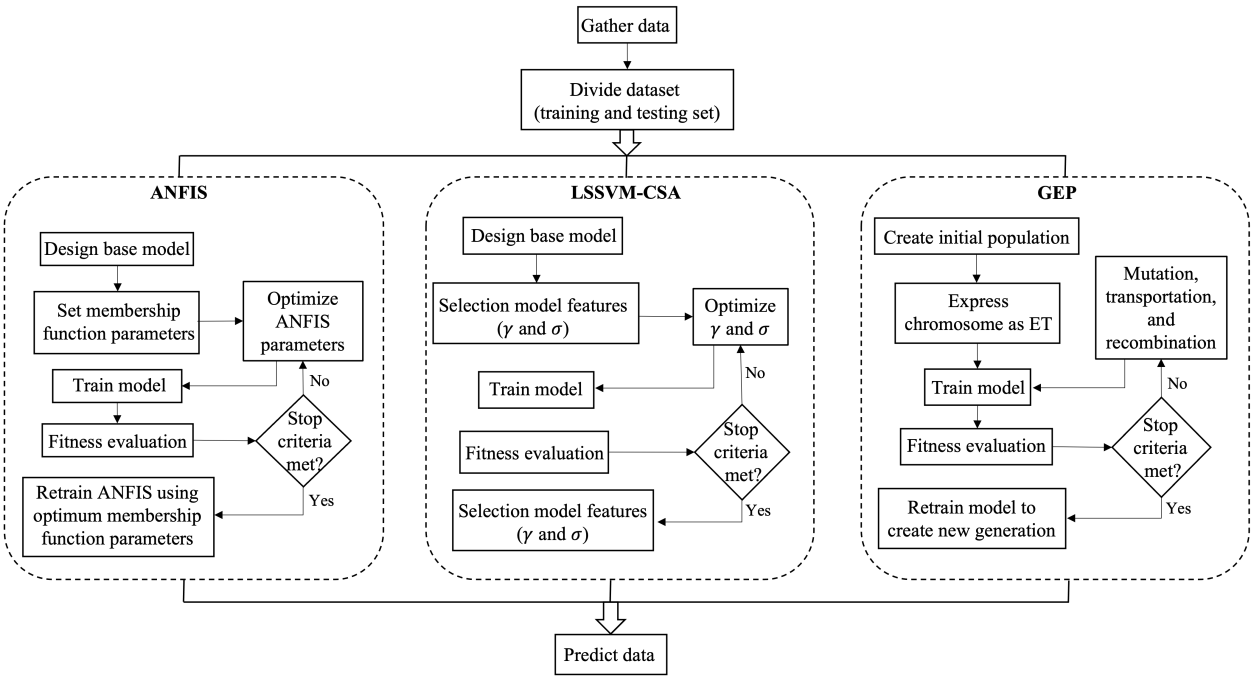

Figure 5. 3. The basic procedure of the modelling approaches

5.4.5. Model evaluation criteria

The reliability and robustness of the developed models are examined based on various statistical analysis, such as coefficient of determination (R^2), mean percentage error (MPE) and mean absolute percentage error (MAPE); Eqs. 5-18, 5-19, and 5-20 calculate these parameters [51, 52].

$$R^2 = 1 - \frac{\sum_{i=1}^{n}[y_i - (y_p)_i]^2}{\sum_{i=1}^{n}[(y_p)_i - \bar{y}_i]^2} \tag{5-18}$$

$$MPE = 100\sum_{i=1}^{n}\left(\frac{y_i - (y_p)_i}{y_i}\right)/n \tag{5-19}$$

$$MAPE = 100\sum_{i=1}^{n}\left|\frac{y_i - (y_p)_i}{y_i}\right|/n \tag{5-20}$$

where y_i is the output value for the data i, $(y_p)_i$ is the predicted output variable achieved by the model, and n represents the number of data points.

The magnitude of R^2 close to 1 indicates how good the models fit the data, while the values of MPE and MAPE should be close to zero for accurate models. The MAPE indicates the absolute magnitude of the prediction error (the difference between the predicted and experimental target values). However, the MPE is obtained using the actual amount of the predicted and experimental target instead of their absolute values to represent the prediction bias (the over- and underestimation of the prediction target) based on the developed models.

5.5. Results and discussion

In this section, oil adsorption data analysis and the modeling results are presented in terms of statistical analyses, and the performance of the three developed models are compared to find the most precise and reliable approach for predicting oil adsorption capacity in our study.

5.5.1. Oil adsorption data analysis

To perform demulsification tests, 0.5 g/L functionalized MNP@CTAB particles are introduced into a freshly prepared nanoemulsion consisting of 1000 ppm dodecane-in-water with an average particles size of approximately 320 nm. The particles are then dispersed within the emulsion using a mixing rate of 2000 rpm for 20 min. The analysis of separation efficiency using GC-FID, which is described in our previous work in more detail [6], indicates that our fabricated amphiphilic particles provide a great potential in emulsified oil capturing with SE of 99.80% and q_e of around 19.98 (mg/g adsorbent). This is attributed to the positive surface charge of CTAB functionalized particles with a zeta potential of (+35.8 ± 0.34) mV, which provides a strong interaction with oil droplets with a zeta potential of (−55.9 ± 2.44) mV via the electrostatic attraction. The superior

demulsification performance of amphiphilic particles, featuring both hydrophilic and oleophilic properties, was also confirmed in the literature [53-56].

The oil adsorption capacity is affected by various parameters such as oil concentration, MNP dosage, and mixing time which are considered dependent (input) variables to optimize the oil adsorption process by developing ANFIS, LSSVM-CSA, and GEP models. Table 5. 2 gives the ranges of input and output variables.

Table 5. 2. The ranges of the input and output parameters

Parameters		Minimum	Average	Maximum	Standard Deviation
Input	Oil concentration (ppm)	1000	5942.45	20000	4981.88
	MNP dosage (g/L)	0.025	0.75	1.5	0.44
	Mixing time (min)	5	17.30	60	11.02
Output	Oil adsorption capacity (mg/g adsorbent)	5.83	90.94	355.16	85.93

5.5.2. ANFIS model performance

The Gaussian membership function is used for all input variables to develop a proper model based on ANFIS algorithm. The type of output membership function is linear. Table 5. 3. presents the optimization parameters and specifications of the developed ANFIS model to predict oil adsorption capacity.

Table 5. 3. Specifications of developed ANFIS model in this study

Parameter	Description/Value
Fuzzy structure	Takagi-Sugeno

Initial FIS for training	genfis2
Membership function type	Gaussian
Output membership function	Linear
Number of inputs	3
Number of outputs	1
Optimization method	Hybrid
Number of fuzzy rules	9
Training maximum epoch number	200
Initial step size	0.1
Step size decrease rate	0.9
Step size increase rate	1.1

The values of R^2 for the training and testing datasets are 0.9914 and 0.9939, respectively (

(a) **Training dataset** **(b) Testing dataset**

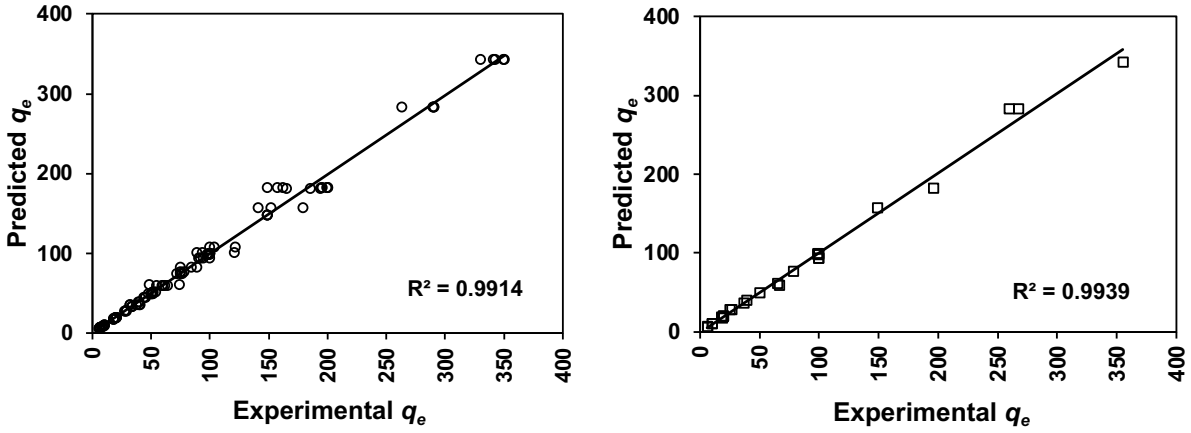

(c) Total dataset

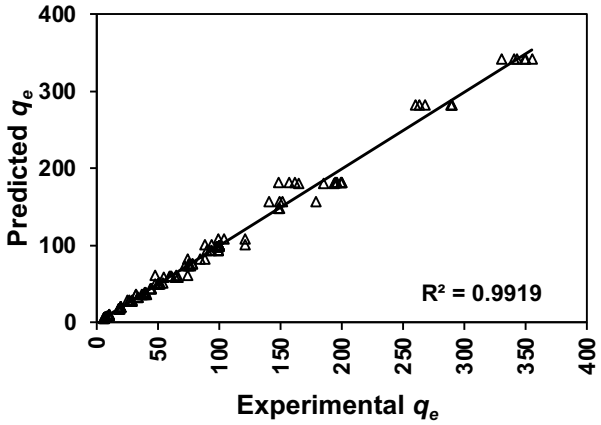

Figure 5. 4), indicating a very good fitness of the developed ANFIS model. Foroutan et al.[31] also claimed that the ANFIS model can be effectively used to predict the chromium removal efficiency using natural clay, Fe_3O_4 magnetic nanoparticle, and chitosan. Their results indicate a good agreement between the ANFIS predictions and the laboratory data with high values of R^2 (close to one) for all adsorbents. Figure 5. 5 shows the unbiased prediction error as the under and overestimated target values, which are almost equally distributed, resulting in MPE values close to zero.

(a) Training dataset **(b) Testing dataset**

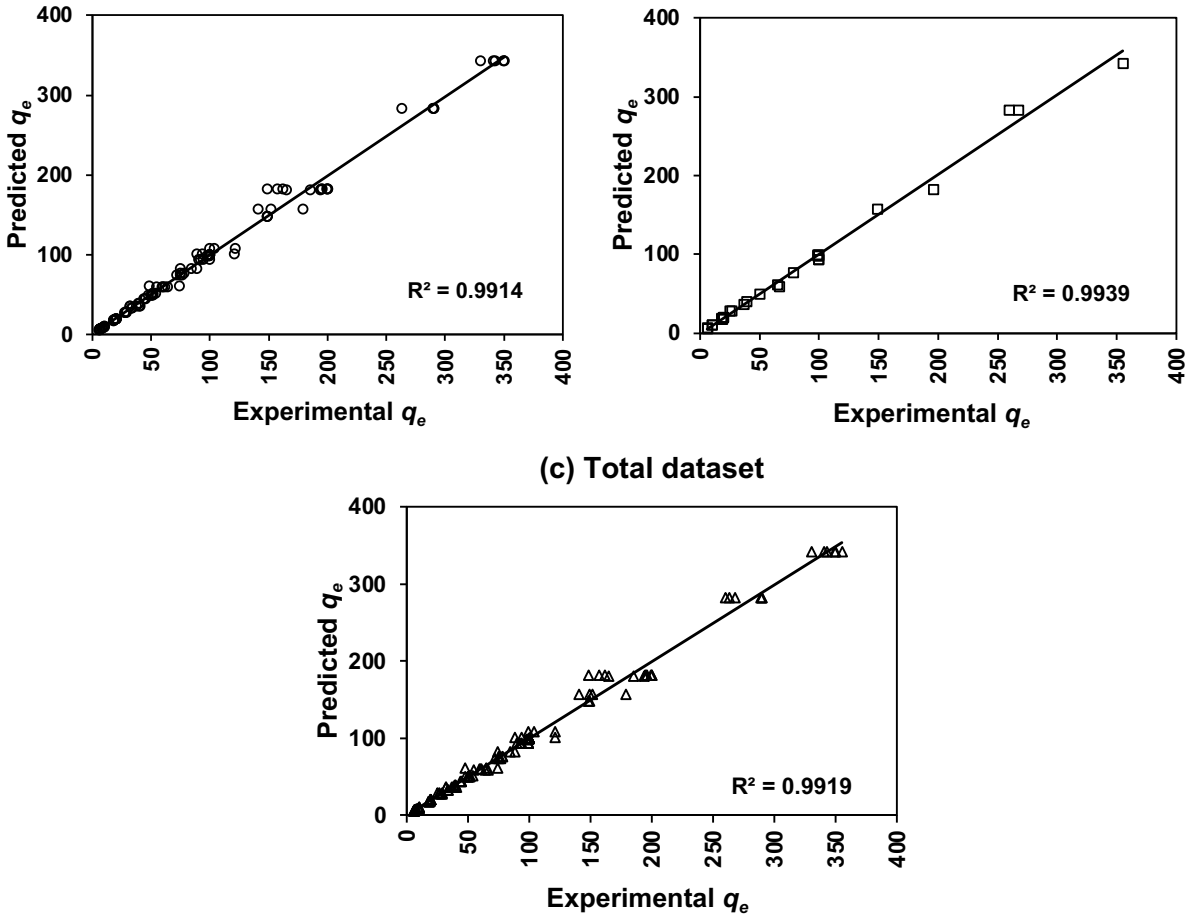

Figure 5. 4. Regression plots of predicted vs. corresponding experimental values of q_e using ANFIS model for the (a) training, (b) testing, and (c) total datasets.

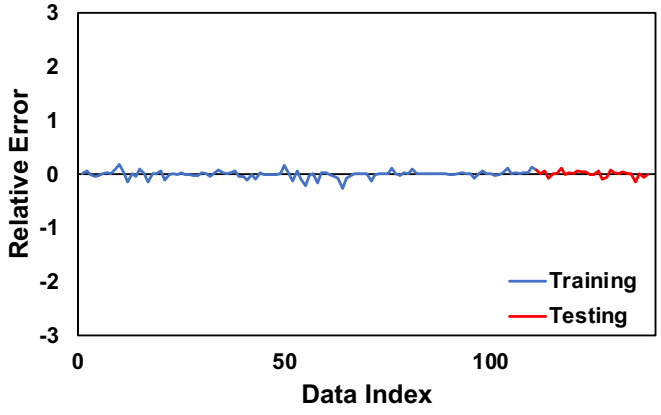

Figure 5. 5. Relative errors of qe predictions in training and testing processes of the ANFIS modelling

5.5.3. LSSVM model performance

Based on the developed LSSVM, the optimum value of kernel parameter (σ) and regularization term (γ) are 0.2517 and 3.25E+05, respectively, achieved with CSA optimization technique. The values of R^2 for the training and testing phase of the LSSVM-CSA model are very close to one (0.9918 and 0.9942, respectively) (Figure 5. 6), implying a very good agreement between q_e predictions and corresponding experimental values. The high accuracy of LSSVM model have also confirmed in other studies to predict methylene blue adsorption onto copper oxide nanoparticle loaded on activated carbon [57], adsorption capacity of methan and carbon dioxide from pure and binary gas mixture [58], removal efficiency of ciprofloxacin from aqueous solution using magnetization of functionalized multiwalled carbon nanotubes [59] with R^2 values of 0.92, 0.99, and 0.97 for testing datasets, respectively. Figure 5. 7 shows the variation of the relative error values of the developed LSSVM-CSA model to indicate deviation between the magnitudes of actual and predicted oil adsorption capacity.

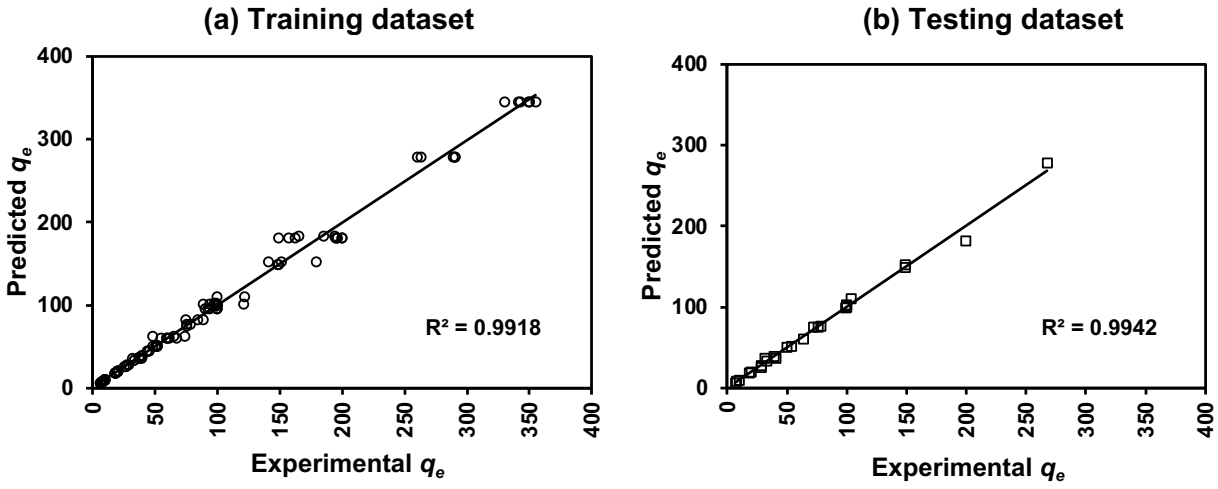

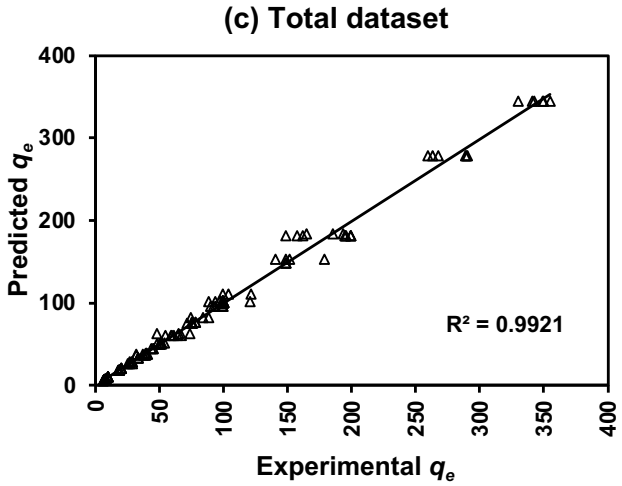

Figure 5. 6. Regression plots of predicted vs. corresponding experimental values of qe using LSSVM-CSA model for the (a) training, (b) testing, and (c) total datasets.

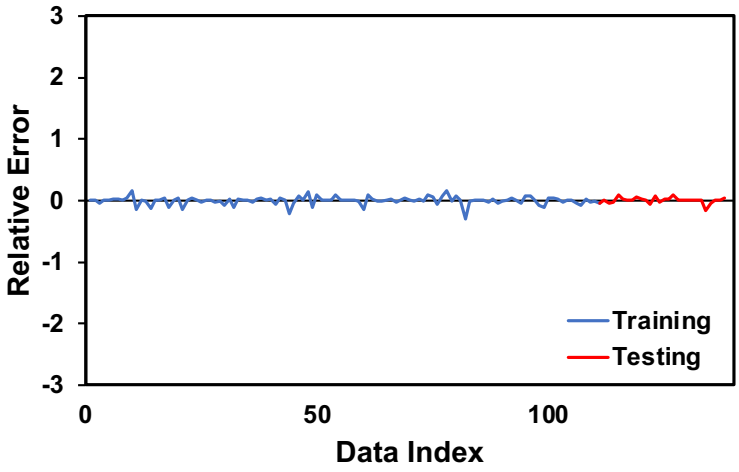

Figure 5. 7. Relative errors of qe predictions in training and testing processes of the LSSVM-CSA modelling

5.5.4. GEP model performance

The prediction performance of GEP model is evaluated for oil adsorption capacity estimation. The performance of this model is influenced by many different factors, such as the number of genes and chromosomes. In this study, the number of genes and chromosomes are set to 3 and 30,

respectively. As Figure 5. 8 depicts, the values of R^2 for training and testing datasets are 0.9547 and 0.9553, respectively, indicating a good agreement between the experimental data and predicted targets of the developed GEP model. Nguyen et al. [60] also confirmed the ability of GEP model to predict cesium adsorption capacity using synthesized soluble and insoluble Prussian blue with R^2 values of 0.79 and 0.88, respectively, for the testing phase. Figure 5. 9 also illustrates the distribution of relative error values of the developed GEP model against the data index, in which there are some points with relative error up to 2.52, making relatively weak model predictions and higher MAPE of the GEP model for training and testing datasets.

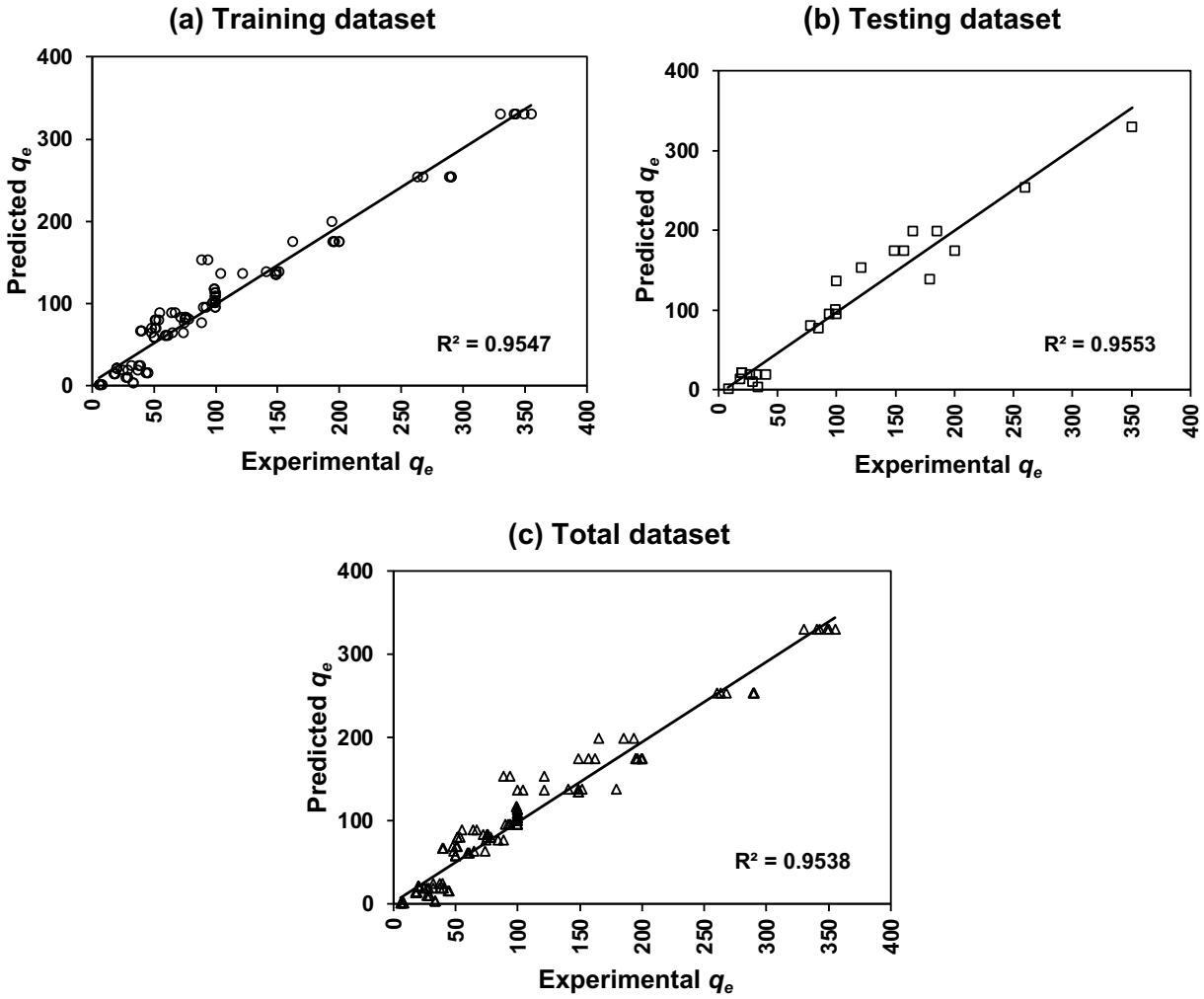

Figure 5. 8. Regression plots of predicted vs. corresponding experimental values of q_e using GEP model for the (a) training, (b) testing, and (c) total datasets.

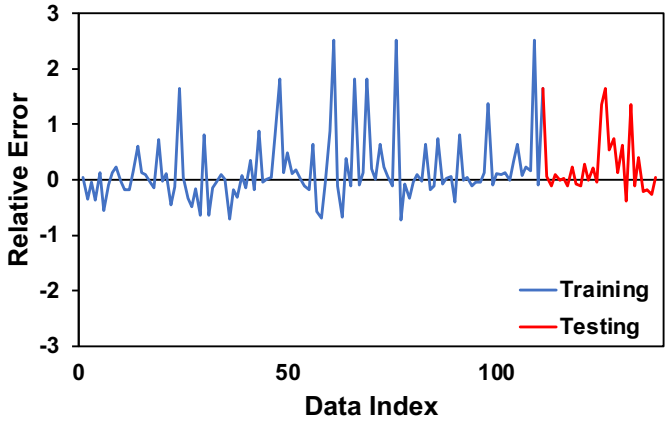

Figure 5. 9. Relative errors of qe predictions in training and testing processes of the GEP modelling

The desired GEP model is developed by considering main operators (+, –, ×, ÷), and also some mathematical functions such as X2, Exp, 3RT, ln, Inv, Atan, and NOT with a combination of genetic operators, including transportation, recombination, and mutation. According to the resultant ETs demonstrated in Figure 5. 10, the objective function relationship for oil adsorption capacity prediction is achieved as follows:

$$y = f(d0, d1, d2) \qquad d0\text{: Oil concentration; } d1\text{: Mixing time; } d2\text{: MNP dosage} \tag{5-21}$$

$$y = A + B + C \tag{5-22}$$

where

$$A = \frac{\sqrt[3]{d1 - 12.7965}}{d2} - \log\left(\frac{1}{d0}\right) \tag{5-23}$$

$$B = \sqrt[3]{\left(\frac{d0}{d2}\right) - (1001.4508 + d0) \times \log(d1)} \tag{5-24}$$

$$C = \left[\left((-4.0702) + (-8.1166)\right) + \sqrt[3]{d0}\right]^2 + \log(d1 \times d0) \quad (5\text{-}25)$$

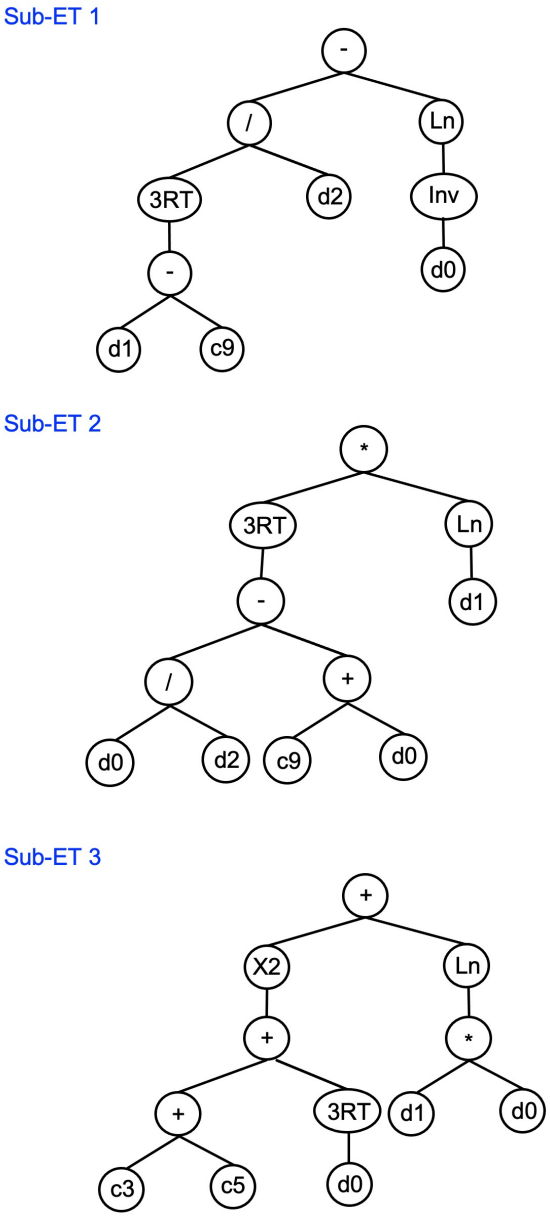

Figure 5. 10. Expression tree on the developed GEP model for qe prediction

5.5.5. Comparative analysis of the models

Table 5. 4 provides a comparison of the performance of developed models using statistical criteria such as R^2, MPE, MAPE, minimum absolute percentage error (APE_{min}) and maximum absolute percentage error (APE_{max}).

Table 5. 4. Comparison of predictive performance of developed models based on the statistical analysis.

Parameter	LSSVM-CSA			ANFIS			GEP		
	Training	Testing	Total	Training	Testing	Total	Training	Testing	Total
R^2	0.991	0.994	0.992	0.991	0.993	0.991	0.954	0.955	0.953
$MPE(\%)$	-0.392	0.215	-0.270	-0.399	0.428	-0.232	17.655	24.894	19.113
$MAPE(\%)$	3.945	3.022	3.759	3.868	3.496	3.793	38.800	36.425	38.322
$APE_{max}(\%)$	29.605	16.957	29.605	26.927	15.194	29.927	252.019	164.548	252.019
$APE_{min}(\%)$	0	0.0064	0	0.0008	0.0073	0.0008	0.0623	1.7096	0.0623

The magnitude of MPE for the LSSVM-CSA, ANFIS, and GEP models in the training process are -0.3924, -0.3994 and 17.6558%, respectively, while in the testing dataset are 0.2153, 0.4288, and 24.8940%, respectively. Also, the R^2 values are 0.9918, 0.9914, and 0.9547 in the training dataset, whereas are 0.9942, 0.9939, and 0.9553 for the testing phase of the developed LSSVM-CSA, ANFIS, and GEP models, respectively.

As it is evident from the statistical parameters (Table 5. 4), all the developed models are well-trained and indicate acceptable performance to predict oil adsorption capacity. However, the higher distribution of relative errors of the GEP model leads to a larger MAPE compared to the other models (Figure 5. 11). The prediction errors of MPE and MAPE for estimating oil adsorption capacity using the LSSVM-CSA and ANFIS models exhibit low values for all datasets. The lowest prediction errors of LSSVM-CSA model indicate a slightly better performance of this model

compared to ANFIS. Moreover, the higher value of R^2 for the developed LSSVM-CSA model predictions indicate the higher accuracy of this model compared to both ANFIS and GEP approaches. The study conducted by Ahangari et al. [61] further confirms the superior prediction performance of LSSVM compared to ANFIS.

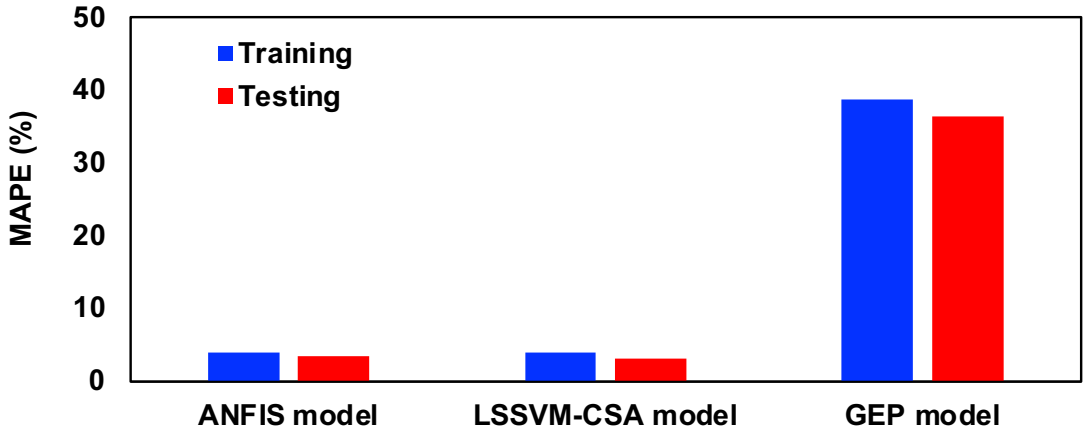

Figure 5. 11. Calculated MAPE values of the three developed models

(a) ANFIS **model**

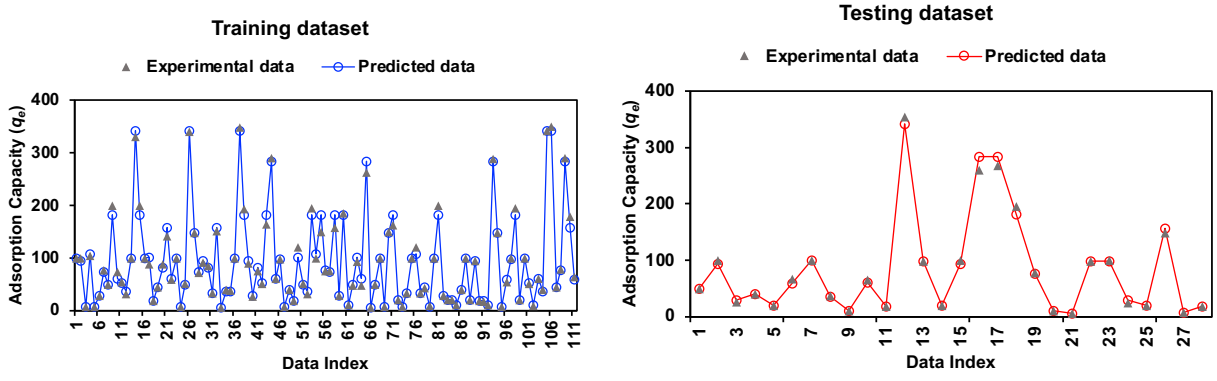

(b) LSSVM-CSA model

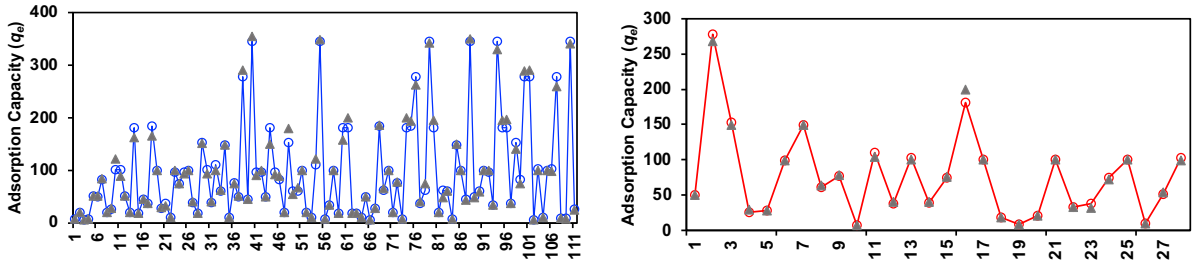

(c) GEP model

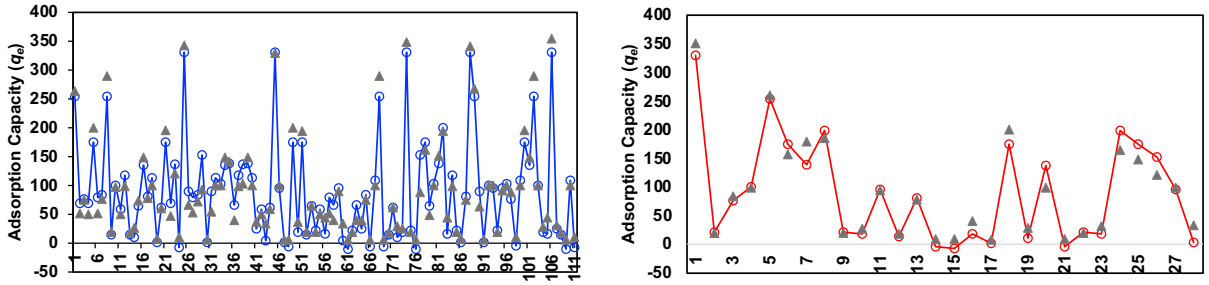

Figure 5. 12 provides better visualization and comparison to investigate the performance of three developed models for predicting oil adsorption capacity, confirming the higher robustness and precision of the LSSVM-CSA model compared to the others.

(a) ANFIS model

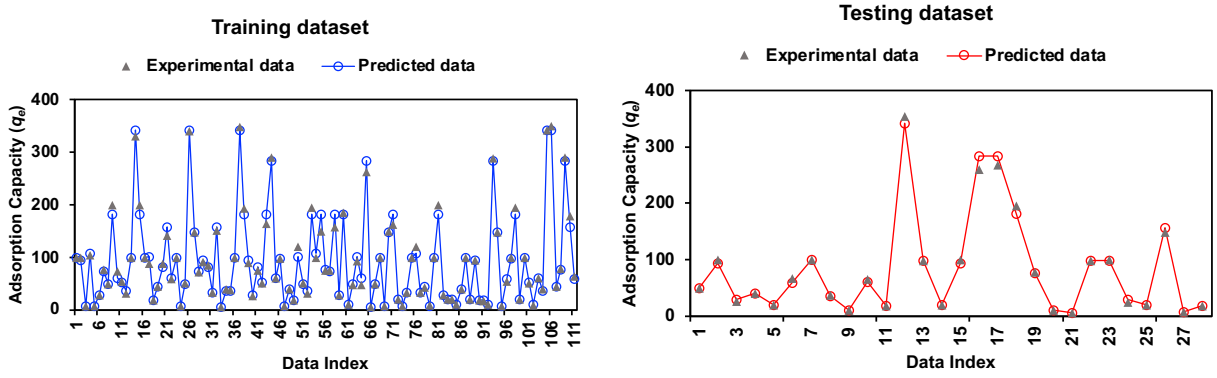

(b) LSSVM-CSA model

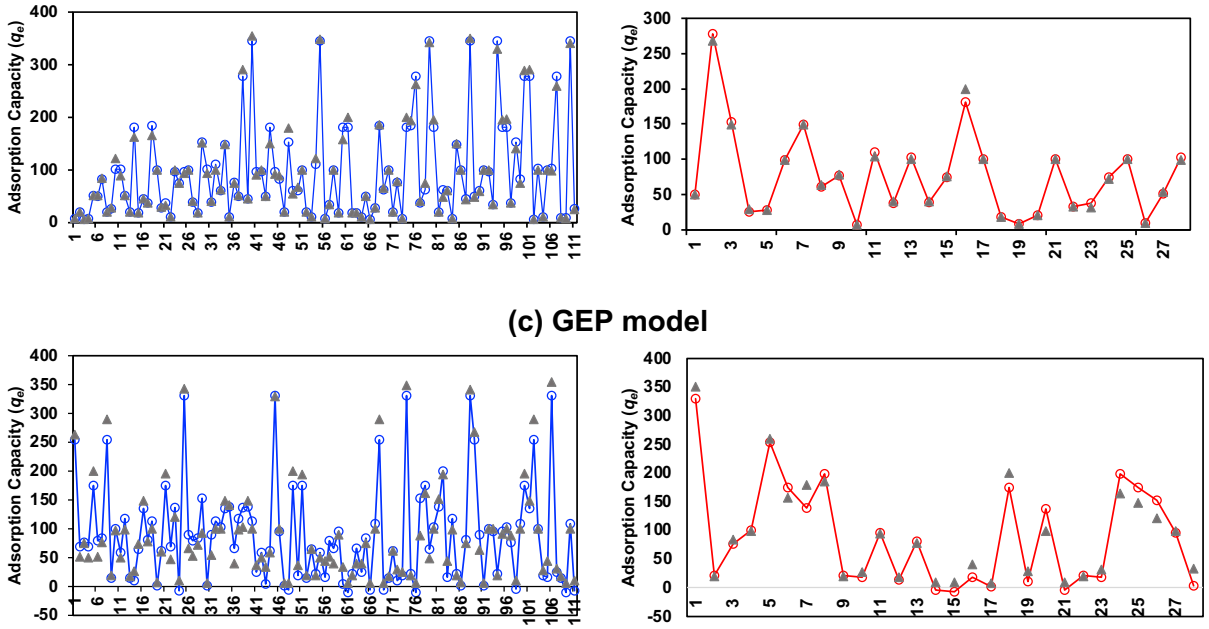

Figure 5. 12. Experimental versus predicted oil adsorption capacity using (a) ANFIS, (b) LSSVM-CSA, and (c) GEP models for training and testing stages.

In addition to the statistical results, the LSSVM-CSA approach is highlighted for more flexibility and generalization, as well as having an optimum convergence owing to a lack of over- and underfitting issues with the LSSVM. Moreover, using CSA optimization algorithm leads to a higher accuracy of the LSSVM-CSA model.

The computational time of developing these three models is another important parameter that should be considered for comparison of their performance, which is less for the LSSVM-CSA model in comparison with the ANFIS model. The GEP is the most time-consuming technique among the models used.

5.5.6. Relative importance of input parameters

In this research, Pearson's correlation (PC) coefficient is employed to determine the impact and relative importance of each input variable on the target parameter. This technique estimates the

strength and direction of a linear correlation between pairs of normally distributed variables. The formula for PC coefficient is as follows [49]:

$$PC = \frac{\sum(X_i - \bar{X})(Y_i - \bar{Y})}{\sqrt{\sum(X_i - \bar{X})^2 \sum(Y_i - \bar{Y})^2}} \quad (5\text{-}26)$$

where X_i and Y_i are the individual data points of X and Y; $\bar{X}$ and $\bar{Y}$ are the means of X and Y, respectively.

PC coefficient is restricted to linear correlation and is too sensitive to outliers. Indeed, a single outlier will decrease the value of the correlation coefficient and weaken the regression relationship [62]. Therefore, we also employed Spearman's correlation (SC) coefficient to evaluate the relative importance of input variables, which is a non-parametric version of the PC coefficient with less sensitivity to outliers. SC coefficient uses a monotonic function to measure the strength and direction relationship between two parameters which is calculated by following equation [63, 64].

$$SC = 1 - \frac{6\sum d_i^2}{n(n^2 - 1)} \quad (5\text{-}27)$$

where d_i is the difference between the ranks of corresponding data points of *X* and *Y*; and n is the number of data points.

Generally, the relative importance is determined based on the magnitude of the calculated correlation coefficient in the range of –1 and +1. If the value of calculated *R* is zero, it indicates there is no linear relationship between the two variables. The positive correlation ($R > 0$) implies a strong linear relationship, while the negative correlation ($R < 0$) shows a negative strong linear relationship between the two parameters. To this end, we used the predicted q_e generated by the LSSVM-CSA model as this research's most accurate developed modeling technique. A higher correlation between input variables (e.g., oil concentration, mixing time, and MNP dosage) and a

target variable (e.g., oil adsorption capacity) shows more importance of the corresponding variables on the predicted value of the target.

Figure 5. 13 demonstrates the relative importance of input variables on the predicted q_e according to the developed LSSVM-CSA approach. Both PC and SC coefficients show the same behavior for all three input variables in our study. The most effective input parameter is oil concentration parameter with R = 0.76 based on PC coefficient and R = 0.63 based on SC coefficient. Holding the second rank, MNP dosage significantly impacts the target variable (oil adsorption capacity) with R = –0.48 based on PC coefficient and R = –0.58 based on SC coefficient. The positive and negative values of the correlation factor are related to the oil concentration and MNP dosage, respectively, as two important operation variables. Therefore, the oil adsorption capacity (mg oil per g of MNP) accelerates at higher oil concentrations and lower MNP dosage. Our study also found that the mixing time has the lowest influence on the oil adsorption capacity.

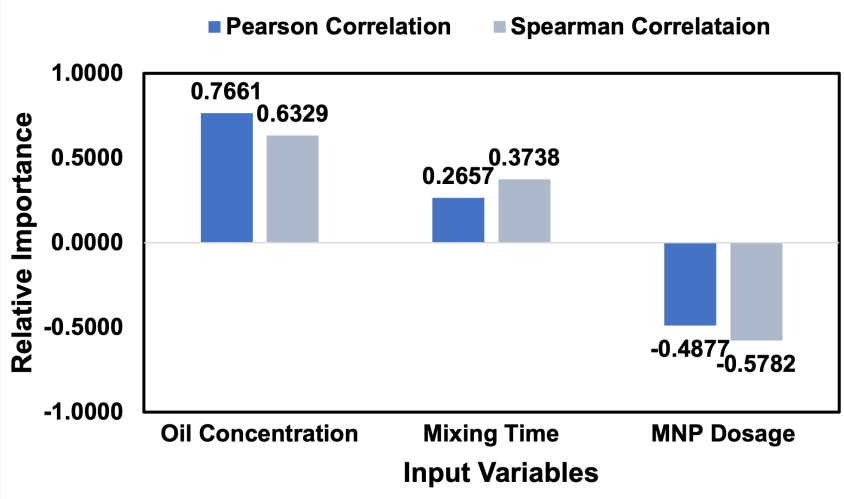

Figure 5. 13. Calculated relative importance of input variables to predict qe using LSSVM-CSA model.

Additionally, we conducted a parametric sensitivity analysis based on the developed GEP model. As indicated in Fig. 5.14. a, there is a strong correlation (R^2=0.99) between oil adsorption capacity

and oil concentration when MNP dosage and mixing time remain unchanged. The influence of MNP dosage and mixing time on the oil adsorption capacity is the next most significant factor, with R^2 values of approximately 0.90. MNP dosage demonstrates an indirect relationship, whereas mixing time exhibits a direct relationship with oil adsorption capacity, all while keeping the other factors constant.

a)

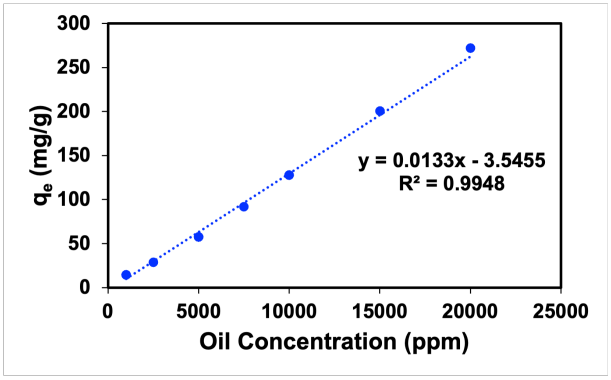

b)

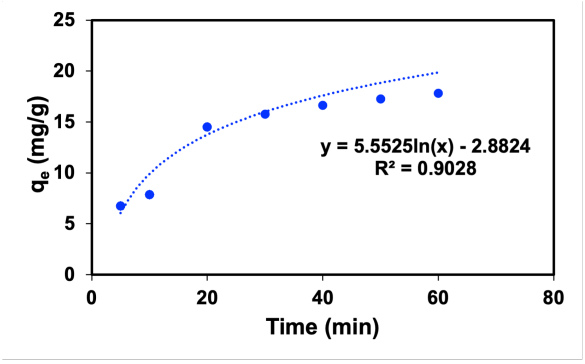

c)

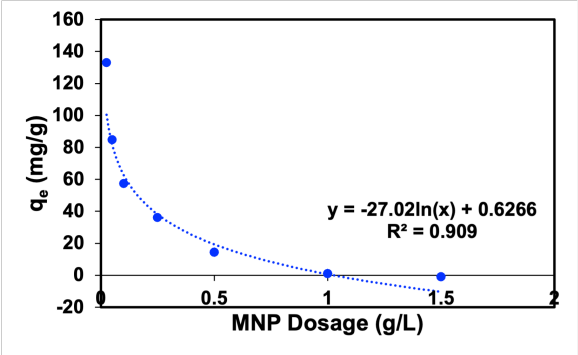

Fig. 5.14. Oil adsorption capacity vs. a) oil concentration, b) mixing time, and c) MNP dosage using the GEP model.

5.6. Summary

Due to the complexity of the adsorption process and non-linear interactions between affecting variables, empirical models appear to be more interesting than mechanistic models with no need for a wide range of experimental data. To our knowledge, there are no studies on optimizing the oil adsorption process using MNPs by machine learning approaches. In this research work, we conduct some experiments to gather adequate reliable data as the first step of modeling. The efficiency of our fabricated MNPs for emulsified oil adsorption is evaluated through oil SE and oil adsorption capacity estimations using GC-FID. The results show that the amphiphilic property of our functionalized particles provides great performance in emulsified oil capturing with SE of 99.80% and q_e of around 19.98 (mg/g adsorbent). Then, oil adsorption capacity predictions using smart models are conducted to optimize the emulsified oil adsorption process using MNPs. The input parameters included some important effective variables such as oil concentration, MNP dosage, and mixing time, whereas the output variable is the oil adsorption capacity. This study developed three types of non-linear data-driven models, including ANFIS, LSSVM optimized with the CSA algorithm, and optimization techniques, such as GEP, to predict the oil adsorption capacity of prepared particles to enhance their efficiency. Then, 80% of all the 149 experimental

data points are used for the training phase and the remaining 20% for the testing step of modeling. The predictive performance of the developed models is evaluated based on statistics such as MPE, MAPE, and R^2. The main conclusions according to the results of this work are:

- All three developed models are well-trained with acceptable performance to predict oil adsorption capacity, while LSSVM-CSA and ANFIS models indicate more accurate predictions with higher values of R^2 (> 0.99) and smaller MPE (close to zero).
- The developed LSSVM-CSA model outperforms the ANFIS model for oil adsorption capacity predictions with the lowest MPE and MAPE for all datasets (training, testing, and total). The optimal magnitude of σ and γ are 0.2517 and 3.25E+05, respectively, to predict oil adsorption capacity.
- The GEP model indicates acceptable target predictions with the R^2 values more than 0.95 for both training and testing datasets; however, the higher distribution of relative errors of the GEP model results in a larger MAPE compared to the other models.
- The relative importance analysis using Pearson's and Spearman's correlation coefficients based on the developed LSSVM-CSA predictions indicates that the most effective input parameters on the oil adsorption capacity predictions are oil concentration and MNP dosage with direct and indirect relationships, respectively. The mixing time has the lowest impact on the target predictions based on both calculated PC and SC coefficients.
- It is recommended to apply molecular dynamics simulation to explore MNPs performance on a molecular scale, to predict the physical and chemical properties of an emulsion system, and to optimize the effectiveness of the entire emulsion separation process using MNPs without conducting conventional experiments for the process design and optimization.

Declaration of competing interest

The authors declare that they have no known competing financial interest or personal relationships that could have appeared to influence the work reported in this paper.

Acknowledgments

The authors would like to acknowledge the financial support offered by Memorial University (NL. Canada), Natural Science and Engineering Research Council of Canada (NSERC), Suncor Energy Inc. /Terra Nova Young Innovator.

Nomenclatures

Acronyms

APE_{max}	-	Maximum absolute percentage error
APE_{min}	-	Minimum absolute percentage error
AI	-	Artificial intelligence
ANFIS	-	Adaptive network-based fuzzy inference system
ANN	-	Artificial neural network
CSA	-	Coupled simulated annealing
CTAB	-	Cetyltrimethylammonium bromide
ET	-	Expression tree
FIS	-	Fuzzy inference system
GA	-	Genetic algorithm
GC-FID	-	Gas Chromatography equipped with Flame Ionization Detector
GEP	-	Gene expression programming
GP	-	Genetic programing

LSSVM	-	Least square support vector machine
$MAPE$	-	Mean absolute percentage error
MNPs	-	Magnetic nanoparticles
MPE	-	Mean percentage error
PC	-	Pearson's correlation
RBF	-	Radial basis function
RSM	-	Response surface methodology
SC	-	Spearman's correlation
SE	-	Separation efficiency
SVM	-	Support vector machine

Variables and Parameters

$(y_p)_i$	-	Predicted output value by the model
C_0	-	Initial oil concentration in emulsion
C_e	-	Residual oil concentration after separation
e_i	-	Regression error
O_i^j	-	Output of the node i in the layer j
q_e	-	Oil adsorption capacity
R^2	-	Coefficient of determination
w_i	-	Firing strength
y_i	-	Output variable for the sample data i
Atan	-	Arctangent
b	-	Bias term

Exp	-	Exponential
Inv	-	Inverse
NOT	-	Complement
T	-	Matrix transpose operation
V	-	Total volume of emulsion
w	-	Weight vector

Greek letters

$\mu_{A_j}^{\ i}$	-	Membership function of A_j^i
α	-	Lagrange multiplier
γ	-	Regularization constant
σ	-	Kernel width
$\phi(x_i)$	-	Non-linear mapping function
Ω	-	Kernel function

References

1. Faisal, W.; Almomani, F., A critical review of the development and demulsification processes applied for oil recovery from oil in water emulsions. *Chemosphere* **2022,** *291*, 133099.

2. Hamedi, H.; Rezaei, N.; Zendehboudi, S., A comprehensive review on demulsification using functionalized magnetic nanoparticles. *Journal of Cleaner Production* **2022,** *380*, 134868.

3. Mi, T.; Cai, Y.; Wang, Q.; Habibul, N.; Ma, X.; Su, Z.; Wu, W., Synthesis of Fe3O4 nanocomposites for efficient separation of ultra-small oil droplets from hexadecane–water emulsions. *RSC Advances* **2020,** *10* (17), 10309-10314.

4. Tang, X.; Si, Y.; Ge, J.; Ding, B.; Liu, L.; Zheng, G.; Luo, W.; Yu, J., In situ polymerized superhydrophobic and superoleophilic nanofibrous membranes for gravity driven oil–water separation. *Nanoscale* **2013,** *5* (23), 11657-11664.

5. Zhou, K.; Zhou, X.; Liu, J.; Huang, Z., Application of magnetic nanoparticles in petroleum industry: A review. *Journal of Petroleum Science and Engineering* **2020,** *188*, 106943.

6. Hamedi, H.; Zendehboudi, S.; Rezaei, N.; Azizi, A.; Shahhoseini, F., Application of Functionalized Fe3O4 Magnetic Nanoparticles Using CTAB and SDS for Oil Separation from Oil-in-Water Nanoemulsions. *Langmuir* **2023,** *39* (23), 7995-8007.

7. Lü, T.; Wu, Y.; Qi, D.; Sun, Y.; Zhang, D.; Zhao, H., Fabrication of alkyl/amino siloxane-modified magnetic nanoparticles for simultaneous demulsification of O/W and W/O emulsions. *Colloids Surf. Physicochem. Eng. Aspects* **2022,** *648*, 129295.

8. Elmobarak, W. F.; Almomani, F., Functionalization of silica-coated magnetic nanoparticles as powerful demulsifier to recover oil from oil-in-water emulsion. *Chemosphere* **2021,** *279*, 130360.

9. Wang, B.; Wei, Y.; Wang, Q.; Di, J.; Miao, S.; Yu, J., Superhydrophobic magnetic core–shell mesoporous organosilica nanoparticles with dendritic architecture for oil–water separation. *Materials Chemistry Frontiers* **2020,** *4* (7), 2184-2191.

10. Fossati, A.; Martins Alho, M.; Jacobo, S. E., Covalent functionalized magnetic nanoparticles for crude oil recovery. *Mater. Chem. Phys.* **2019,** *238*, 121910.

11. Fan, M.; Hu, J.; Cao, R.; Xiong, K.; Wei, X., Modeling and prediction of copper removal from aqueous solutions by nZVI/rGO magnetic nanocomposites using ANN-GA and ANN-PSO. *Scientific Reports* **2017,** *7* (1), 18040.

12. Khan, T.; Mustafa, M. R. U.; Isa, M. H.; Manan, T. S. B. A.; Ho, Y.-C.; Lim, J.-W.; Yusof, N. Z., Artificial Neural Network (ANN) for Modelling Adsorption of Lead (Pb (II)) from Aqueous Solution. *Water, Air, Soil Pollut.* **2017,** *228* (11), 426.

13. Zendehboudi, S.; Rezaei, N.; Lohi, A., Applications of hybrid models in chemical, petroleum, and energy systems: A systematic review. *Applied Energy* **2018,** *228*, 2539-2566.

14. Schmitt, F.; Do, K.-U., Prediction of membrane fouling using artificial neural networks for wastewater treated by membrane bioreactor technologies: bottlenecks and possibilities. *Environmental Science and Pollution Research* **2017,** *24* (29), 22885-22913.

15. Salleh, M.; Talpur, N.; Hussain, K., *Adaptive Neuro-Fuzzy Inference System: Overview, Strengths, Limitations, and Solutions*. 2017; p 527-535.

16. Ameli, F.; Hemmati-Sarapardeh, A.; Tatar, A.; Zanganeh, A.; Ayatollahi, S., Modeling interfacial tension of normal alkane-supercritical CO2 systems: Application to gas injection processes. *Fuel* **2019**.

17. Jang, J. S. R., ANFIS: adaptive-network-based fuzzy inference system. *IEEE Transactions on Systems, Man, and Cybernetics* **1993,** *23* (3), 665-685.

18. Hussain, K.; Salleh, M., *Analysis of techniques for anfis rule-base minimization and accuracy maximization*. 2016.

19. Balabin, R. M.; Lomakina, E. I., Support vector machine regression (LS-SVM)—an alternative to artificial neural networks (ANNs) for the analysis of quantum chemistry data? *PCCP* **2011,** *13* (24), 11710-11718.

20. Kamari, A.; Mohammadi, A. H.; Bahadori, A.; Zendehboudi, S., A Reliable Model for Estimating the Wax Deposition Rate During Crude Oil Production and Processing. *Pet. Sci. Technol.* **2014,** *32*, 2837 - 2844.

21. Suykens, J. A. K.; Vandewalle, J., Least Squares Support Vector Machine Classifiers. *Neural Processing Letters* **1999,** *9* (3), 293-300.

22. Fayazi, A.; Arabloo, M.; Mohammadi, A. H., Efficient estimation of natural gas compressibility factor using a rigorous method. *Journal of Natural Gas Science and Engineering* **2014,** *16*, 8-17.

23. Yu, Z.; Lu, H.; Si, H.; Liu, S.; Li, X.; Gao, C.; Cui, L.; Li, C.; Yang, X.; Yao, X., A Highly Efficient Gene Expression Programming (GEP) Model for Auxiliary Diagnosis of Small Cell Lung Cancer. *PLOS ONE* **2015,** *10* (5), e0125517.

24. Choi, B.; Choi, S.-U., Physical habitat simulations of the Dal River in Korea using the GEP Model. *Ecol. Eng.* **2015,** *83*, 456-465.

25. Tao, Y.; Wang, P.; Wang, J.; Wu, Y.; Han, Y.; Zhou, J., Combining various wall materials for encapsulation of blueberry anthocyanin extracts: Optimization by artificial neural network and genetic algorithm and a comprehensive analysis of anthocyanin powder properties. *Powder Technol.* **2017,** *311*, 77-87.

26. Zare, M.; Zendehboudi, S.; Abdi, M. A., Deterministic tools to estimate induction time for methane hydrate formation in the presence of Luvicap 55 W solutions. *J. Mol. Liq.* **2022,** *348*, 118374.

27. Roy, S.; Ghosh, A.; Das, A. K.; Banerjee, R., Development and validation of a GEP model to predict the performance and exhaust emission parameters of a CRDI assisted single cylinder diesel engine coupled with EGR. *Applied Energy* **2015,** *140*, 52-64.

28. Asadu, C. O.; Ekwueme, B. N.; Onu, C. E.; Onah, T. O.; Sunday Ike, I.; Ezema, C. A., Modelling and optimization of crude oil removal from surface water via organic acid

functionalized biomass using machine learning approach. *Arabian Journal of Chemistry* **2022,** *15* (9), 104025.

29. Ike, I. S.; Asadu, C. O.; Ezema, C. A.; Onah, T. O.; Ogbodo, N. O.; Godwin-Nwakwasi, E. U.; Onu, C. E., ANN-GA, ANFIS-GA and Thermodynamics base modeling of crude oil removal from surface water using organic acid grafted banana pseudo stem fiber. *Applied Surface Science Advances* **2022**.

30. Foroutan, R.; Peighambardoust, S. J.; Mohammadi, R.; Omidvar, M.; Sorial, G. A.; Ramavandi, B., Influence of chitosan and magnetic iron nanoparticles on chromium adsorption behavior of natural clay: Adaptive neuro-fuzzy inference modeling. *Int. J. Biol. Macromol.* **2020,** *151*, 355-365.

31. Debs, K. B.; Cardona, D. S.; da Silva, H. D. T.; Nassar, N. N.; Carrilho, E. N. V. M.; Haddad, P. S.; Labuto, G., Oil spill cleanup employing magnetite nanoparticles and yeast-based magnetic bionanocomposite. *J. Environ. Manage.* **2019,** *230*, 405-412.

32. Yarveicy, H.; Ghiasi, M. M.; Mohammadi, A. H., Determination of the gas hydrate formation limits to isenthalpic Joule–Thomson expansions. *Chemical Engineering Research & Design* **2018,** *132*, 208-214.

33. Hamedi, H.; Ehteshami, M.; Mirbagheri, S. A.; Zendehboudi, S., New deterministic tools to systematically investigate fouling occurrence in membrane bioreactors. *Chem. Eng. Res. Des.* **2019,** *144*, 334-353.

34. Wieland, D.; Wotawa, F.; Wotawa, G., From Neural Networks to Qualitative Models in Environmental Engineering. *Copmut. Aided Civil Infrastruct. Eng.* **2002,** *17* (2), 104-118.

35. Khajeh, A.; Modarress, H., Prediction of solubility of gases in polystyrene by Adaptive Neuro-Fuzzy Inference System and Radial Basis Function Neural Network. *Expert Syst. Appl.* **2010,** *37*, 3070-3074.

36. Ghiasi, M. M.; Arabloo, M.; Mohammadi, A. H.; Barghi, T. S., Application of ANFIS soft computing technique in modeling the CO2 capture with MEA, DEA, and TEA aqueous solutions. *International Journal of Greenhouse Gas Control* **2016,** *49*, 47-54.

37. Onu, C. E.; Nwabanne, J. T.; Ohale, P. E.; Asadu, C. O., Comparative analysis of RSM, ANN and ANFIS and the mechanistic modeling in eriochrome black-T dye adsorption using modified clay. *South African Journal of Chemical Engineering* **2021,** *36*, 24-42.

38. Vapnik, V., Golowich, S.E., Smola, A.,, Support vector method for function approximation, regression estimation, and signal processing. *MIT Press, Cambridge, MA.* **1997**.

39. Suykens, J.; De Brabanter, J.; Lukas, L.; Vandewalle, J., Weighted Least Squares Support Vector Machines: robustness and sparse approximation. *Neurocomputing* **2002,** *48*, 85-105.

40. Seyyedattar, M.; Ghiasi, M. M.; Zendehboudi, S.; Butt, S., Determination of bubble point pressure and oil formation volume factor: Extra trees compared with LSSVM-CSA hybrid and ANFIS models. *Fuel* **2020,** *269*, 116834.

41. De Brabanter, J., De Moor, B., Suykens, J.A., Van Gestel, T., Vandewalle, J.P., , Least Squares Support Vector Machines. *World scientific* **2002**.

42. Müller, K. R.; Mika, S.; Rätsch, G.; Tsuda, K.; Schölkopf, B., An introduction to kernel-based learning algorithms. *IEEE Trans Neural Netw* **2001,** *12* (2), 181-201.

43. Gunn, S. R. In *Support Vector Machines for Classification and Regression*, 1998.

44. Ghiasi, M. M.; Yarveicy, H.; Arabloo, M.; Mohammadi, A. H.; Behbahani, R. M., Modeling of stability conditions of natural gas clathrate hydrates using least squares support vector machine approach. *J. Mol. Liq.* **2016,** *223*, 1081-1092.

45. Ferreira, C., Gene Expression Programming: A New Adaptive Algorithm for Solving Problems. *Complex Syst* **2001,** *13*.

46. Bhowmik, S.; Paul, A.; Panua, R.; Ghosh, S. K.; Debroy, D., Artificial intelligence based gene expression programming (GEP) model prediction of Diesel engine performances and exhaust emissions under Diesosenol fuel strategies. *Fuel* **2019,** *235*, 317-325.

47. Kondori, J.; Miah, M. I.; Zendehboudi, S.; Khan, F.; Heagle, D., Hybrid connectionist models to assess recovery performance of low salinity water injection. *Journal of Petroleum Science and Engineering* **2021,** *197*, 107833.

48. Afzali, S.; Zendehboudi, S.; Mohammadzadeh, O.; Rezaei, N., Hybrid Mathematical Modelling of Three-Phase Flow in Porous Media: Application to Water-Alternating-Gas Injection. *Journal of Natural Gas Science and Engineering* **2021**, 103966.

49. Zendehboudi, S.; Ahmadi, M. A.; James, L.; Chatzis, I., Prediction of Condensate-to-Gas Ratio for Retrograde Gas Condensate Reservoirs Using Artificial Neural Network with Particle Swarm Optimization. *Energy & Fuels* **2012,** *26* (6), 3432-3447.

50. Hauke, J.; Kossowski, T., Comparison of Values of Pearson's and Spearman's Correlation Coefficients on the Same Sets of Data. *Quaestiones Geographicae* **2011,** *30* (2), 87-93.

51. Chok, N. S. In *PEARSON'S VERSUS SPEARMAN'S AND KENDALL'S CORRELATION COEFFICIENTS FOR CONTINUOUS DATA*, 2010.

52. Tatar, A.; Moghtadaei, G. M.; Manafi, A.; Cachadiña, I.; Mulero, Á., Determination of pure alcohols surface tension using Artificial Intelligence methods. *Chemometrics Intellig. Lab. Syst.* **2020**.

6. CHAPTER SIX

Conclusions and Recommendations for Future Work

This thesis focuses mainly on the application of functionalized MNPs for capturing emulsified oil from nanoemulsions, as well as the modelling and optimization of the adsorption process. In the experimental phase of the research, amphiphilic compounds are employed to stabilize MNPs through utilization of cationic and anionic surfactants. Oil separation efficiency and oil adsorption capacity are examined using GC-FID analysis to identify the most effective functionalized MNPs with higher separation performance. In the modelling phase of the study, isotherm and kinetic models are investigated to obtain a better understanding of the adsorption process. Moreover, we use smart connectionist models based on artificial intelligence strategies to optimize the adsorption process. This thesis includes six chapters: Introduction and overview (chapter one), literature review (chapter two), experimental phase (chapter three), adsorption kinetic and isotherm investigation (chapter four), and optimization using smart models (chapter five). The current chapter (chapter six) includes the summary and recommendations.

6.1. Literature Review (Chapter 2)

The literature review is accomplished to achieve a comprehensive understanding of theory and background related to MNPs, recent advancements in modifying the surfaces of MNPs, their applications, and the mechanisms involved in separating oil and water. The primary conclusions drawn from this review are as follows:

- The stability of emulsion is influenced significantly by various factors such as droplet size, zeta potential, and properties of the interfacial film between oil and water.
- Droplet size is the most important factor in controlling emulsion stability. Smaller droplets with smaller interfacial area cause increasing emulsion stability due to less energy exchange by reducing flocculation and coalescence.

- The interfacial film thickness impacts the emulsion stability; a thicker film extends the film drainage time and reduces the rate of demulsification. Lowering the IFT by enhancing the similarities of oil and water reduces droplet flocculation and coalescence rate.
- Lower zeta potential values indicate less emulsion stability, resulting from a decline in the electrostatic repulsion between droplets, leading to flocculation rate enhancement.
- Demulsification using chemical demulsifiers occurs through increasing IFT, reducing droplets elasticity and viscosity, and decreasing the interfacial film thickness through film drainage. However, demulsifiers also create secondary pollution.
- MNPs, as chemical demulsifiers, have high oil adsorption capacity and reusability without causing secondary pollution. Effective reuse of MNPs requires good dispersivity in the continuous phase through changing surface wettability with coating. More importantly, a protective coating layer is essential to overcome the inherent instability of MNPs by preventing their agglomeration, precipitation, oxidation, and loss of magnetism.
- The demulsification using MNPs is based on the physical and chemical adsorption, involving electrostatic attraction (between the negatively charged oil droplets and positively charged MNPs) and interfacial activity between the oil droplets and MNPs.
- The desirable MNPs wettability is amphiphilic with both hydrophilic and oleophilic properties for effective dispersivity. This results in high interfacial activity, leading to better demulsification efficiency.
- Demulsification using MNPs is directly influenced by temperature, mixing time, and salt concentration, while it is inversely affected by the pH and surfactant concentration in the emulsions.

- The effect of MNPs size on demulsification is controversial as the larger MNPs with a higher settling velocity enhance the separation efficiency, while smaller ones provide larger contact area, leading to improvement of separation performance. Smaller MNPs boost up the surface and interfacial effects due to increased surface area per unit.
- Optimal MNPs dosage directly affects demulsification efficiency, beyond which can have a negative impact on the oil/water separation performance.

6.2. Experimental Phase of the Research (Chapter 3)

The application of functionalized MNPs using CTAB as a cationic and SDS as an anionic surfactant with different coating to MNP mass ratios, are investigated for emulsified oil adsorption from 1000 ppm dodecane-in-water nanoemulsion. The main findings can be summarized as follows:

- The results of oil-water separation demonstrate that the highest oil SE of around 99.8% is achieved using smaller size of CTAB coated particles (MNP-S@CTAB) with a lower surfactant to MNP mass ratio of 0.4. This superior SE is attributed to the more positive surface charge on CTAB compared to SDS, confirmed by the zeta potential measurements. Additionally, the CTAB-coated MNPs exhibit better hydrophilicity compared to those coated with SDS, as revealed from WCA analysis, and SEM and TEM images indicate less aggregation of MNP@CTAB.
- For the bare MNPs, it becomes evident that smaller particles indicate lower stability compared to the larger particles, exhibiting denser aggregation which is supported by the observations from TEM and SEM images and their less dispersibility in the O/W emulsion. However, the smaller functionalized particles exhibit higher stability and SE compared to the larger ones, attributed to their higher surface energy and charge density.

- The functionalized MNP-S@CTAB demonstrates favorable reusability with high performance over 10 cycles. It is worth noting that the adsorption capacity is reduced gradually during the 10^{th} cycle; but it is still significant, indicating the efficient usability of the particles in the following cycles.
- With an increase in MNPs concentration, SE enhances until it reaches an optimal dosage. However, the adsorption capacity decreases due to adsorption sites saturation or particle aggregation, resulting in a reduction of the available surface area of the MNPs.
- Increasing the concentration of salt (NaCl) in the emulsion leads to an increase in the IFT, while it decreases the zeta potential of each particle due to the electrostatic screening effect. Therefore, the lowered electrostatic repulsion between the MNPs and oil facilitates a higher SE%. Conversely, the addition of surfactant (e.g., SDS) to the emulsion reduces the IFT; thus, it reduces oil adsorption. Increasing surfactant dosage beyond the CMC leads to an increase in SE% by enhancing the number of accessible active sites on MNPs. This is achieved by reducing steric hindrance and enhancing accessibility through formation of SDS micelles.

6.3. Kinetic and Isotherm Studies (Chapter 4)

The adsorption behavior and the capacity of MNP@CTAB to adsorb emulsified oil droplets from nanoemulsion are examined by employing adsorption isotherm and kinetic models. The equilibrium oil adsorption capacity is determined using GC-FID analysis. The key findings drawn from this research are summarized as follows:

- Both linear and non-linear regression analyses indicate that the adsorption process is properly described in the order of Freundlich > Temkin > Langmuir isotherm models. This suggests that Freundlich isotherm can better simulate the experimental equilibrium data.

- The obtained Freundlich model's constant value of $1/n$, which is equal to 0.24 ($n = 4.156$), suggests the favorable physical adsorption of emulsified oil droplets onto MNP@CTAB. This value implies strong interactions between the adsorbents and adsorbate.
- The maximum oil adsorption capacity obtained from the Langmuir model is 327.647 mg/g. According to the Langmuir model, the estimated R_L value is in the range of 0.005–0.04, indicating favorable oil adsorption onto the MNP@CTAB.
- Based on the non-linear regression analysis of the kinetic models, it is evident that the PFO model (with a higher R^2 value of 0.99) outperforms the PSO and IPD models in describing the kinetics of the oil adsorption process. This indicates that the adsorption process involves physical adsorption through van der Waals forces and physical bonding. This is also confirmed by the zeta potential measurements.
- The predicted adsorption capacity (q_e) by the PFO model is approximately 99.99 mg/g, verifying an excellent match with the experimental equilibrium value of q_e (99.90 mg/g).

6.4. Smart Modelling (Chapter 5)

Optimization of the emulsified oil adsorption process using MNPs is conducted through application of smart models for oil adsorption capacity predictions. Some important variables such as oil concentration, MNP dosage, and mixing time are considered as the input parameters and oil adsorption capacity as the output variable. In this study, three types of non-linear data-driven models, namely ANFIS, LSSVM optimized with the CSA algorithm, and an evolutionary algorithm called GEP are developed to predict oil adsorption capacity of prepared particles to enhance their efficiency. For the modelling process, 149 experimental data points are used, with 80% of the data allocated for the training phase and the remaining 20% for the testing step of the

deterministic approach. The predictive performance of the developed models is assessed based on the statistical parameters of MPE, MAPE, and R^2. The following conclusions can be drawn according to the results of this work:

- Based on the statistical analysis, all three developed models are accurate (and reliable) in predicting oil adsorption capacity, while LSSVM-CSA and ANFIS models exhibit greater accuracy with higher values of R^2 (above 0.99) and smaller MPE (close to zero).
- The developed LSSVM-CSA model indicates superior performance compared to the ANFIS model for oil adsorption capacity predictions with the lowest MPE and MAPE for all datasets (training, testing, and total). The optimal values of σ and γ are determined to be 0.2517 and 3.25×10^5, respectively, to predict oil adsorption capacity.
- The GEP model results in acceptable target predictions with the R^2 values more than 0.95 for both training and testing phases; however, the higher distribution of relative errors of the GEP model results in a higher MAPE compared to the other models. Moreover, the computational time of this modeling strategy is much more than that of the other deterministic approaches.

6.5. Recommendation for Future Work

The following suggestions and recommendations are given for future studies:

- The performance and stability of MNPs can be assessed for oil adsorption in practical applications through conducting tests under realistic conditions that mimic real-world scenarios, such as different temperature, pH values, and the presence of other contaminants.

- Additionally, investigating adsorption of different types of oil, and applying various coating materials can be beneficial to achieve a better understanding of adsorption process and enhance the practical applicability of the research findings.
- It is suggested to compare the performance of MNPs with other commonly used adsorbents, such as activated carbon, graphene, carbon nanotube, and metal and metal oxide nanoparticles. This will provide valuable insights into the advantages and limitations of MNPs and help identify their properties.
- The potential environmental impact of MNPs for oil adsorption can be systematically studied to ensure the overall sustainability and safety of the technology. This evaluation can be performed by assessing the possible leaching of nanoparticles and their long-term effects on ecosystem.
- It would be useful to perform a comprehensive economic analysis of using MNPs for oil adsorption compared to other available methods such as activated carbon and membrane technology, considering the cost of MNP synthesis, scalability, energy consumption, and disposal or regeneration costs.
- We also recommend conducting further experimental and modelling studies to scale up the production and application of MNPs for oil adsorption. This can involve investigating the feasibility of using MNPs in large-scale remediation projects or developing continuous flow systems for efficient oil capturing.
- Use of molecular dynamics simulation and lattice Boltzmann methods to explore MNPs performance in small (e.g., molecular and atomic scales) is recommended for future work to predict physical and chemical properties of an emulsion system, and to optimize the

effectiveness of the entire emulsion separation process using MNPs without conducting conventional experiments for the process design and optimization.